Fall 11-15-2016

Approaches For Capturing Time-Varying Functional Network Connectivity With Application to Normative Development and Mental Illness

Barnaly Rashid
University of New Mexico, Mind Research Network

Barnaly Rashid

Candidate

Electrical and Computer Engineering

Department

This dissertation is approved, and it is acceptable in quality and form for publication: *Approved by the Dissertation Committee:*

Dr. Vince D. Calhoun, Chair

Dr. Marios S. Pattichis , Member

Dr. Erik B. Erhardt, Member

Dr. Meeko Oishi, Member

Approaches For Capturing Time-Varying Functional Network Connectivity With Application to Normative Development and Mental Illness

by

Barnaly Rashid

B.S., Electronic and Telecomm. Engineering, North South University, 2010
M.S., Electrical Engineering, University of New Mexico, 2014

DISSERTATION
Submitted in Partial fulfillment of the
requirements for the degree of

Doctor of Philosophy
Engineering

The University of New Mexico
Albuquerque, New Mexico
December, 2016

Dedication

I dedicate this work to my parents, Dr. Harun-or-Rashid and Nargis Akhter, for their unconditional love and unforgettable sacrifice, my brother, Ishtiaque Rashid, for his great support and encouragement, and my uncle, Mamunur Rosid, who has always been there and strongly supported me.

Acknowledgements

I would like to express my deepest gratitude to my advisor, Dr. Vince Calhoun, for his continuous support and guidance over the past five years. I would also like to express my appreciation to my committee members, Dr. Marios S. Pattichis, Dr. Erik B. Erhardt, and Dr. Meeko Oishi for their insightful comments and feedback on my research work. I would like to thank Eswar Damaraju for his contribution to this work. My extended gratitude goes to all outside collaborators who contributed to the studies presented in this dissertation: Dr. Godfrey D. Pearlson at Olin Neuropsychiatry Research Center and Dr. Tonya White and her group at Erasmus Medical Center, the Netherlands. Also, I would like to thank my sister-in-law, Raisa Tareen, for her support, and Dr. Anupam Aich for his encouragement.

Approaches For Capturing Time-Varying Functional Network Connectivity With Application to Normative Development and Mental Illness

By

Barnaly Rashid

B.S., Electronic and Telecomm. Engineering, North South University, 2010
M.S., Electrical Engineering, University of New Mexico, 2014
Ph.D., Engineering, University of New Mexico, 2016

ABSTRACT

Since the beginning of medical science, the human brain has remained an unsolved puzzle; an illusive organ that controls everything- from breathing to heartbeats, from emotion to anger, and more. With the power of advanced neuroimaging techniques, scientists have now started to solve this nearly impossible puzzle, piece by piece. Over the past decade, various in vivo techniques, including functional magnetic resonance imaging (fMRI), have been increasingly used to understand brain functions. fMRI is extensively being used to facilitate the identification of various neuropsychological disorders such as schizophrenia (SZ), bipolar disorder (BP) and autism spectrum disorder (ASD). These disorders are currently diagnosed based on patients' self-reported experiences, and observed symptoms and behaviors over the course of the illnesses. Therefore, efficient identification of biological-based markers (biomarkers) can lead to early diagnosis of these mental disorders, and provide a trajectory for disease progression. By applying advanced machine learning techniques on fMRI data, significant differences in brain function among patients with mental disorders and healthy controls can be identified. Moreover, by jointly estimating information from multiple modalities, such as, functional brain data and genetic factors, we can now investigate the relationship between brain function and genes.

Functional connectivity (FC) has become a very common measure to characterize brain functions, where FC is defined as the temporal covariance of neural signals between multiple spatially distinct brain regions. Recently, researchers are studying the FC among functionally specialized brain networks which can be defined as

a higher level of FC, and is termed as functional network connectivity (FNC, defined as the correlation value that summarizes the overall connection among brain networks over time). Most functional connectivity studies have made the limiting assumption that connectivity is stationary over multiple minutes, and ignore to identify the time-varying and reoccurring patterns of FNC among brain regions (known as time-varying FNC).

In this dissertation, we demonstrate the use of time-varying FNC features as potential biomarkers to differentiate between patients with mental disorders and healthy subjects. The developmental characteristics of time-varying FNC in children with typically developing brain and ASD have been extensively studies in a cross-sectional framework, and age-, sex- and disease-related FNC profiles have been proposed. Also, time-varying FNC is characterized in healthy adults and patients with severe mental disorders (SZ and BP). Moreover, an efficient classification algorithm is designed to identify patients and controls at individual level. Finally, a new framework is proposed to jointly utilize information from brain's functional network connectivity and genetic features to find the associations between them. The frameworks that we presented here can help us understand the important role played by time-varying FNC to identify potential biomarkers for the diagnosis of severe mental disorders.

CONTENTS

LIST OF FIGURES

LIST OF TABLES

CHAPTER 1

INTRODUCTION

Over the past two decades, expansions in neuroimaging techniques have helped us unravel various mysteries of the human brain. One of the fastest growing techniques, functional magnetic resonance imaging (fMRI), has since been extensively applied to study development of brain functions, effects of long term abuses of tobacco, alcohol and drugs. These studies have enlightened our understanding of the brain functions, as well as the important factors that impact the critical functions of the brain. Above all, the major field of research that immensely relies on fMRI technique is discriminating various mental and neurodevelopmental disorder with the help of neuroimaging features. By applying advanced machine learning techniques on fMRI data, significant differences in brain functions among patients with mental disorders and healthy controls can be identified. Moreover, by jointly estimating information from multiple modalities, for example, fMRI and structural magnetic resonance imaging (sMRI), we can now investigate the relationship between brain functions and structures.

There is a growing interest in studying imaging measures related to the brain. Functional neuroimaging is extensively being used to facilitate the identification of various neuropsychological disorders as schizophrenia (SZ), bipolar disorder (BP) and autism spectrum disorder (ASD). These disorders are currently diagnosed based on patients' self-reported experiences, and observed symptoms and behaviors over the course of the illnesses.

fMRI is used to measure indirect level of brain activity associated with a physical or mental action, where brain activity refers to transfer of electrical and chemical energy between neurons in different regions of the brain. fMRI measures changes in deoxygenated hemoglobin levels in blood vessels located nearby to neurons. This process is known as blood oxygenation level-dependent or BOLD activity (Ogawa et al., 1990b).

Functional connectivity (FC, defined as the temporal correlation between a seed region and individual brain voxels (Cordes et al., 2002; Fox and Raichle, 2007) shows promising predictive power to differentiate between patients with mental illnesses and healthy subjects. Also, it has been shown that a set of distant and functionally specialized brain regions demonstrates strong FC among them as they interact and exchange information while performing a certain cognitive task or during rest. Collectively these regions form a functional network of the brain, and the connectivity among these functional networks is known as functional network connectivity (FNC, defined as the correlation value that summarizes the overall connection between independent brain maps over time (Arbabshirani et al., 2013a; Jafri et al., 2008).

In this dissertation, we demonstrate the use of FNC features as potential biomarkers to differentiate between patients with mental disorders and healthy controls.

An efficient classification algorithm is designed to identify patients and controls at individual level. Moreover, a new framework is proposed to jointly utilize information from brain's functional network connectivity and genetic features to find the associations between them. Also, the developmental characteristics of FNC with respect to age and sex in children with typically developing brain and autism spectrum disorder have been extensively studies in a cross-sectional framework, and age- and sex-related FNC profiles have been proposed.

1.1 Functional Connectivity of the Brain

Human brain is a complex network that consists of spatially distributed but functionally connected regions that continuously communicate and share information with each other. Recent improvements in the acquisition and analysis of functional neuroimaging data have given a boost to the investigation of brain's functional connectivity. The conventional way to study FC is by measuring the statistical dependencies in terms of correlations among neuronal activation patterns of anatomically separated brain regions across the time domain. More formally, FC is defined as the temporal covariance of neural signals between multiple spatially distinct brain regions (Friston et al., 1993). fMRI technique can be used to first identify the functionally specialized regions, and then evaluation of FC can be done through computation of the correlations between the activities of these regions. FC analysis captures interactions among different brain regions either during a specific task or resting state.

Recently, FC has been used to examine the functional organization of brain networks in various psychiatric illnesses. Different analytic tools have been applied to

resting-state fMRI data to describe brain functional connectivity, including seed-based analysis (Biswal et al., 1995; Greicius et al., 2003), data-driven methods, such as independent component analysis (ICA) (Hyvärinen and Oja, 2000; Calhoun et al., 2001c; Damoiseaux et al., 2006; Fox and Raichle, 2007; Calhoun et al., 2009b; Calhoun and Adali, 2012), clustering (Cordes et al., 2002), multivariate pattern analysis (MVPA) (Norman et al., 2006; Zhu et al., 2008; Zeng et al., 2012), graph theory (Achard et al., 2006; Buckner et al., 2009) and centrality Lohmann et al. (2010). In seed-based approach, the connectivity patterns are based on a selected seed region of interest (ROI), while ICA-based methods do not require prior knowledge of brain activity or seed ROI selection (Erhardt et al., 2011a). ICA-based FC is also widely known as FNC analysis, which is considered as a higher level of FC.

1.2 Motivation for Time-Varying Connectivity

FNC of the brain has been proven to be substantially useful for differentiating between patients and healthy controls. Identification of typical connectivity patterns, both in developing children and adult subjects, can lead us to finding potential biomarkers for diagnosis of mental illness. Thus, the optimum utilization of the features from brain's FNC is highly required.

1.2.1 Unpacking the 'Mean'

Studies on functional connectivity using fMRI data have shown to capture aberrant connectivity in various mental disorders. One of the highly investigated brain

networks is the default mode network (DMN), which is consists of a set of brain regions known to be activated during internally focused tasks and may be involved in processes such as attention to internal emotional states, self-referential processing or task- independent thoughts (Buckner et al., 2008). DMN data may distinguish between mental disorders such as SZ and BP (Öngür et al., 2010; Calhoun et al., 2011).

There are numerous studies suggesting abnormal default network connectivity in SZ and BP (Zhou et al., 2007; Calhoun et al., 2008b; Zhou et al., 2007; Calhoun et al., 2011). However, these studies have focused on the mean or average FNC by assuming spatial and temporal stationarity throughout the whole scanning period. This representation of mean FNC fails to capture spontaneous fluctuations of activity and connectivity at different scanning time points. Time-varying FNC approach efficiently unpacks the 'mean' of the connectivity into different meaningful connectivity states. By learning about various mental states experienced during fMRI scans and how transitions between the states have occurred, we can get the broader scenario of FNC. Therefore, looking beyond the mean FNC and assessing dynamic changes in connectivity are necessary.

1.2.2 Dynamic Changes: Brain Connectivity is not stationary

The majority of FNC studies are primarily based on the assumption that FNC is stationary throughout the entire scan session (or at least stationary during a given task or resting-state condition) (Greicius, 2008; Camchong et al., 2011; Meda et al., 2012; Sorg et al., 2013). Static FNC (sFNC) analysis overlooks the fact that

individual subjects are likely to engage in slightly different mental activities at different instances in time (Arieli et al., 1996; Makeig et al., 2004). The assumption of stationarity was challenged in a recent work focused on time-varying multivariate connectivity patterns (Sakoğlu et al., 2010). The evidence of dynamic fluctuation in FNC from several studies supports the idea of dynamic changes in FNC during the experimental period. Recent studies have demonstrated the utilization of the powerful information contained within the temporal features of spontaneous fluctuation of BOLD signals (Hutchison et al., 2013a). These studies provide results that cannot be detected with static functional connectivity analyses.

1.2.3 Quantitative Summary Measures

In sFNC analysis, node-level patterns of connectivity across a massive matrix of information are identified and assessed. In contrast, in time-varying FNC analysis where have the FNC states, we are able to define the state transition matrix, mean dwell time (MDT), fraction of time (FT) spent in a specific state, and the group-wise occupancy rate, allowing for a quantitative interpretation of a given state as a whole (Allen et al., 2012a). These quantitative summary measures could potentially aid in simplifying interpretations of the complex networks' information, which historically are often subjectively evaluated.

1.3 Research Aims and Contributions

Researchers have recently started to look beyond the mean connectivity, and more into different aspects of time-varying properties of FNC. The aims of this doctoral work are to identify and characterize specific properties of time-varying

FNC that will help differentiate between patients with various mental disorders and healthy controls, and develop new algorithms to further classify subjects at individual level based on these features of dynamic FNC. In addition, an imaging-genetics framework based on parallel independent component analysis (parallel-ICA, an extension of the conventional ICA algorithm that is used in analyzing multiple modalities) algorithm is proposed that offers new insights, and can potentially become a strong tool for exploring the relationships between genetic features and dynamic FNC markers. The major contributions of this doctoral study are briefly discussed as follows:

1. The first aim of this project is to advance the application of time-varying FNC approach to a large, population-based resting-state fMRI (rsfMRI) data on children with normal development, as well as with autism spectrum disorder. Autism spectrum disorder is often studied with little context of typical brain development. In addition, most functional connectivity studies have made the limiting assumption that connectivity is static over multiple minutes. In this work, we employ a 'chronnectomic' approach (i.e., identifying time-varying and reoccurring patterns of connectivity among brain regions) to evaluate transient states of connectivity among brain networks. We investigate age-related aspects of functional maturation during childhood with both modularized and disconnected dynamic states. In addition, we characterized the "chronnectopathy" (i.e. dysfunctional chronnectivity) associated with autistic traits.

2. Many of the severe mental disorders such as SZ and BP share significant overlap in clinical symptoms, brain characteristics, and risk genes, and both are associated with dysconnectivity among large-scale brain networks. rsfMRI data facilitates studying macroscopic connectivity among distant brain regions. Standard approaches to identifying such connectivity include seed-based correlation

and data-driven clustering methods such as ICA, but typically focus on average connectivity. In this study, we utilize ICA on rsfMRI data to obtain intrinsic connectivity networks (ICNs) in cohorts of healthy control (HC) and age matched SZ and BP patients. Subsequently, we investigated difference in FNC. Disease-specific differences were identified in connectivity within different dynamic states. Our results provide new information about these illnesses and strongly suggest that state-based analyses are critical to avoid averaging together important factors that can help distinguish these clinical groups.

3. A third aim is to develop efficient classification algorithms based on the time-varying features of dynamic FNC (dFNC). Recently, FNC has been used to examine the functional organization of brain networks in various psychiatric illnesses. dFNC is a recent extension of the conventional FNC analysis that takes into account FNC changes over short periods of time. While such dFNC measures may be more informative about various aspects of connectivity, there has been no detailed head-to-head comparison of the ability of sFNC and dFNC to perform classification in complex mental illnesses. This study proposes a framework for automatic classification of SZ, BP and HC subjects based on their static and dynamic FNC features. Also, we compare cross-validated classification performance between static and dynamic FNC. Results show that dFNC has significantly higher predictive accuracy than sFNC. A three-way classification methodology based on static and dynamic FNC features discriminates individual subjects into appropriate diagnostic groups with high accuracy. Our proposed classification framework is potentially applicable to additional mental disorders.

4. The fourth and final contribution of this work is to assess the impact of genetics on brain's functional network connectivity by developing an imaging-genetics

framework. Recently, resting-state studies have shown evidence of disrupted connectivity between functional networks of the brain to underlie SZ. However, its genetic basis is not well studied. In this work, we propose a framework to explore the genetic underpinnings of the dFNC in SZ and HC subjects by using a multivariate approach, parallel-ICA. Here, we combine the power of neuroimaging to characterize time-varying FNC with genetic data, and link the genetic variants to imaging traits. Our framework provides evidence for genetic effects on time-varying connectivity in the human brain, and also enables the identification of genetic risk factors mediating specific dynamic states for complex brain behavior and psychiatric disease.

1.4 Organization of Dissertation

The rest of this dissertation describes concepts, techniques, and results that we have implemented and analyzed in the course of application and development of the time-varying FNC related framework. The dissertation will be organized as follows:

Chapter 2 provides a brief description of the some of the basic conceptual backgrounds on the conducted research, including BOLD fMRI mechanism, principle and common implementation of ICA, group independent component analysis (GICA) and parallel-ICA approaches, various aspects of FNC, and concept of imaging-genetics and single nucleotide polymorphism (SNP).

Chapter 3 demonstrates the underlying maturational properties of time-varying FNC in a large, population-based cohort study with typically developing children, and compared the results with respect to autistic traits and ASD.

Chapter 4 presents the application of time-varying FNC or dFNC analysis in adult subjects, including both HC subjects and patients with severe mental disorders (SZ and BP), and characterizes the group differences in terms of dFNC. This chapter also outlines group-specific properties and group-wise differences between controls and patients, as well as between the two patient groups.

Chapter 5 provides a novel classification framework based on the sFNC and dFNC features to differentiate the subjects at individual level. A comparison among the proposed classification algorithms developed using sFNC, dFNC and combined FNC features is also presented in terms of classification accuracy.

Chapter 6 presents a novel imaging-genetics framework using parallel-ICA algorithm, to explore the association between time-varying FNC and genetic features (SNP). Also, the preliminary results showing how genetics features may influence brain's time-varying FNC are provided in this chapter.

Chapter 7 summarizes and concludes the project, and provides some scopes for future work.

CHAPTER 2

BACKGROUND

2.1 BOLD fMRI

fMRI, a noninvasive imaging technique, is considered as one of the most thrilling success stories in the field of modern neuroimaging. This powerful technique has enhanced diagnostics of clinical data, as well as provided us insight into basic understanding on brain functions and dysfunctions. fMRI is widely employed study brain functions and corresponding cognitive systems by measuring the BOLD signal (Ogawa et al., 1990a,b, 1993) by extending the use of magnetic resonance imaging (MRI) technique. In MRI imaging technique, the magnetic moments related to the nuclear spin properties of the atom are utilized as the target object is placed align a strong static magnetic field. This influences the randomly oriented nuclear spins to be aligned with the direction of the external magnetic field, where the alignment can either be at a low-energy state or parallel, or high-energy state or antiparallel to the magnetic field. These aligned nuclear spins are then perturbed by an excitation pulse or radio wave at the resonant frequency. Once the

excitation pulse is turned off, the perturbed atoms naturally realign back to their initial orientation after different relaxation time depending on the tissue properties the atoms belong to. This difference can be captured into a MRI structural image. By changing the resonant frequencies using magnetic field gradients, the spatial and structural information can be obtained from MRI. In addition to all the steps involved in MRI imaging, fMRI records the hemodynamic response in different brain regions that has occurred due to neural activity as described next

The basis of all hemodynamic-based neuroimaging techniques can be traced back to an experiment that took place over a century ago. In 1890, Roy and Sherrington experimentally showed that regional cerebral blood flow (CBF) could reflect the neuronal activity in the brain (Roy and Sherrington, 1890). An increase in CBF is considered to relate directly to the neuronal activities as the metabolic rate of glucose and changes in CBF are tightly coupled. This has been the concept behind mapping brain functions by measuring the changes in CBF that are induced by stimulation. The coupling between glucose metabolism rate and changes in CBF has led researchers to the assumption that cerebral metabolic rate of oxygen and changes in CBF are also coupled. After more than a century later since the experiment by of Roy and Sherrington took place, in 1990, Ogawa and colleagues first reported that mapping of the brain functions is possible by utilizing the BOLD contrast (defined above) of MRI (Ogawa et al., 1990a,b). The fact that deoxygenated hemoglobin is paramagnetic while oxygenated hemoglobin is not paramagnetic makes the BOLD imaging technique work. The signal-producing atom spins tend to dephase at an expedite rate in the presence of paramagnetic deoxyhemoglobin as they are influenced by the local magnetic field gradients produced by paramagnetism. Higher concentration of oxygenated blood can be observed as a result of increased blood flow to the active brain regions, which ultimately leads

to a higher level of MRI signal in those active brain regions.

2.2 Independent Component Analysis (ICA)

ICA is a data-driven, blind source separation technique, which is widely used in fMRI-based neuroimaging research for both task-related (Calhoun et al., 2001a,c,d, 2004b; McKeown et al., 1997) and resting-state data (Beckmann et al., 2005; Biswal et al., 1995; Calhoun et al., 2008a; Damoiseaux et al., 2006; Sorg et al., 2007). ICA treats the observed data as a linear mixture of unknown independent sources, and decomposes the observed data to extract the underlying sources while maximizing the independence among them. Mathematical model for ICA is as follows:

$$X = AS \tag{2.1}$$

Where, $X = [x_1, x_2, x_3, ...x_M]^T$ is a M-dimensional observed vector , and $S = [S_1, S_2, S_3, ...S_M]^T$ is a N-dimensional vector of independent sources. A is the M-by-N unknown mixing matrix. ICA tries to estimate the N-by-M unmixing matrix, W, and approximates the independent sources, Y, as follows:

$$Y = WX \tag{2.2}$$

Note that, this estimation process of unmixing matrix W is typically performed iteratively by updating W based on an objective function in order to optimize the independence among the source components.

FMRI data is four-dimensional (4D) with a series of three-dimensional (3D) matrices collected over time. The MRI signal from the brain at each of these time

points are sampled over voxels, which defines the discrete grid of volume-related elements. For a given time point, the entries from the data matrix represent the magnitudes of the measured MRI signals for the corresponding voxels. These signals are considered as a linear contribution of signals generated by various biological processes, many of which are assumed to be related to specific functional brain activities. During ICA approach, the spatial activation maps and corresponding time courses related to the activities of the function.

Many ICA algorithms have been developed and implemented including Infomax, fast ICA, eigen-value decomposition (EVD), joint diagonalization of eigen-matrices (JADE) and algorithm for multiple unknown signals extraction (AMUSE) (Bell and Sejnowski, 1995; Cardoso and Souloumiac, 1993; Georgiev and Cichocki, 2001; Hyvärinen and Oja, 1997; Tong et al., 1990). Among these algorithms Infomax (Amari, 1998; Bell and Sejnowski, 1995) is a popular choice for neuroimaging data given its high reliability (Correa et al., 2007). It is possible to perform ICA and estimate independent signals over space (special ICA or SICA) or over time (temporal ICA or TICA), as the fMRI data contain both spatial and temporal information (Calhoun et al., 2001d). However, in practice, spatial ICA is the most common choice for fMRI data. Figure 2.1 and Figure 2.2 show illustrations of SICA and TICA.

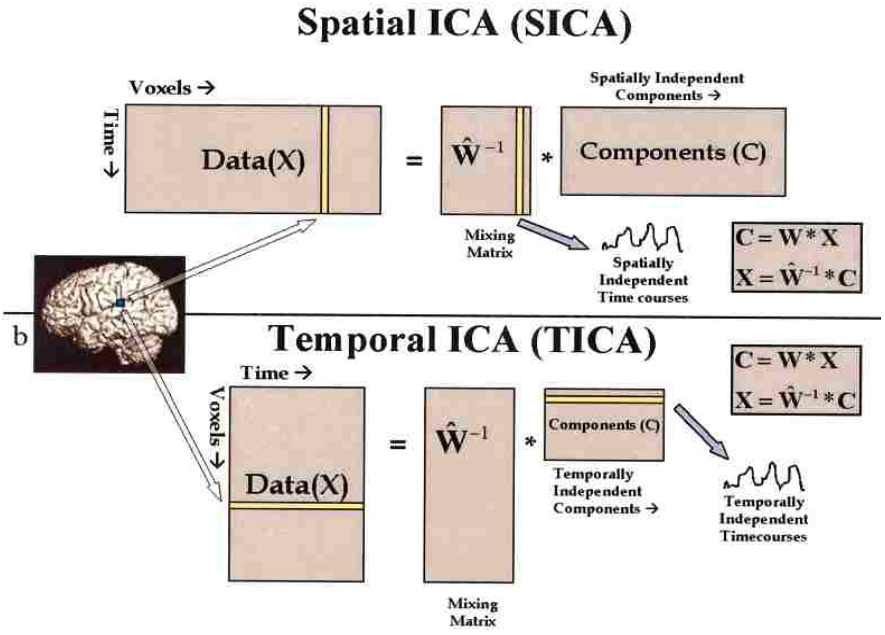

FIGURE 2.1: Illustration of two types of ICA on fMRI data: (a) Spatial ICA (SICA) and (b) Temporal ICA (TIC) (Calhoun et al., 2001d).

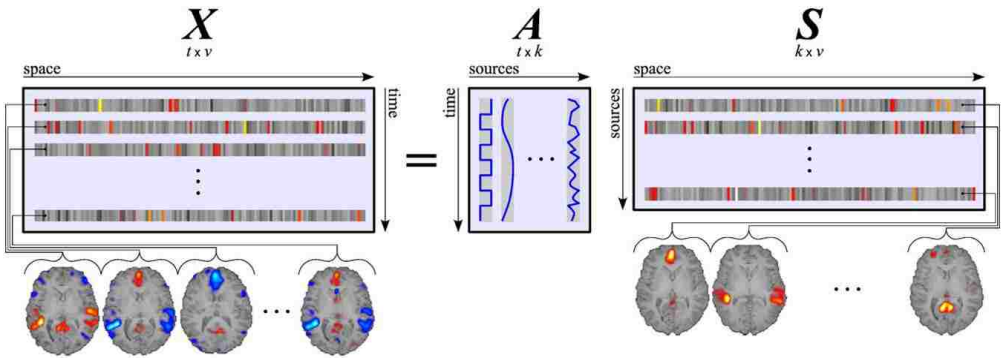

FIGURE 2.2: Spatial ICA for fMRI data. Data matrix, is decomposed into independent sources that are rows of matrix and corresponding time-courses that are columns of the mixing matrix, A (Ylipaavalniemi and Vigário, 2008).

2.2.1 Group Independent Component Analysis (GICA)

Application of ICA analysis can also be executed at the group level, by finding the activation maps containing voxels with higher correlation among them, but show maximum independence with all other set of voxels. See Figure 2.3 for an

illustration of GICA approach. In GICA approach, first principle component analysis (PCA) is applied to reduce the dimensionality of each subject's data matrix, which reduces the computational burden for ICA (McKeown et al., 2002). Then, all of these reduced matrices are stacked, and another PCA is performed prior to applying ICA. Finally, ICA is performed on the data to estimate independent component commonly found among all the subjects. The subject-specific spatial maps (SMs) and time-courses (TCs) can be obtained from the aggregate data using a back-reconstruction technique as shown in Figure 2.4 (Erhardt et al., 2011b). More details of GICA approach can be found in (Calhoun et al., 2001c).

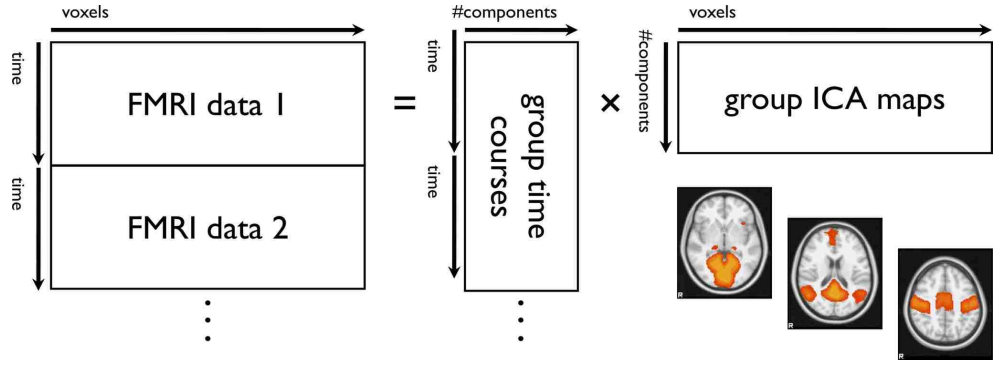

FIGURE 2.3: An illustration of Group ICA approach (Cole et al., 2010).

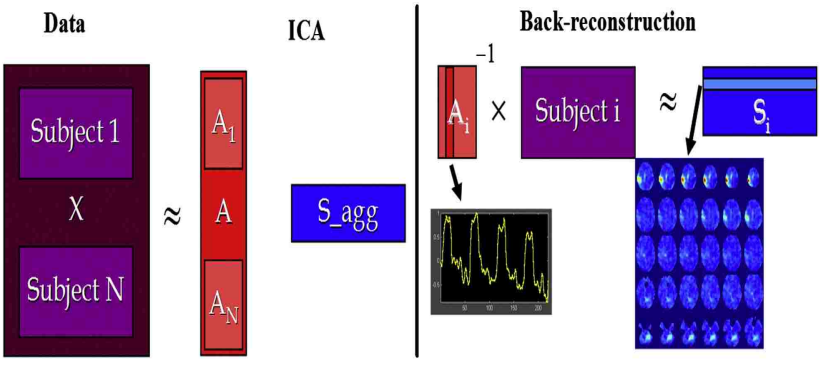

FIGURE 2.4: Forward and backward estimation for ICA analysis (Calhoun et al., 2009b).

2.2.2 Parallel Independent Component Analysis

ICA can also be extended to examine the combined information from multiple modalities by jointly analyzing and estimating the numerical data. One of the data fusion approaches is parallel-ICA, which finds the hidden factors from both modalities and the correlations between them, by estimating the independent components of both modalities as well as their correlation (Liu et al., 2009). To date parallel ICA has been applied in fusion of various modalities including fMRI-electroencephalography (EEG) (Liu and Calhoun, 2007; Wu et al., 2010), fMRI-Gene (SNP) (Liu et al., 2009; Meda et al., 2010) and gray matter - Gene (SNP) (Jamadar et al., 2011; Jagannathan et al., 2010).

Parallel-ICA assumes that the data set from two modalities are mixed in a similar manner (but not identical). The main focus of parallel ICA is to find individual linked components and their correlations.

2.3 Functional Network Connectivity (FNC)

In section 1.1, we have briefly discussed about FC of the brain. It has been shown that a set of distant and functionally specialized brain regions interact and exchange information while they perform a certain cognitive task. This set of regions demonstrates strong FC among them, and collectively form a functional network of the brain. This type of connectivity among brain's functional networks is known as FNC, which is indeed a higher level of FC (Jafri et al., 2008). Figure 2.5 illustrates an example of functional network connectivity among different brain networks. FNC quantifies the statistical dependencies among functional brain networks, which is commonly measured as the pairwise correlations among

the independent brain networks (Arbabshirani et al., 2013a; Jafri et al., 2008). A functional network can be comprised of several brain regions that are anatomically distant. Both within-network FNC (defined as the connectivity within the functionally specialized brain regions or components that belong to the same functional network) and among-network FNC (defined as the connectivity among the brain regions or components that belong to different functional networks) can be observed.

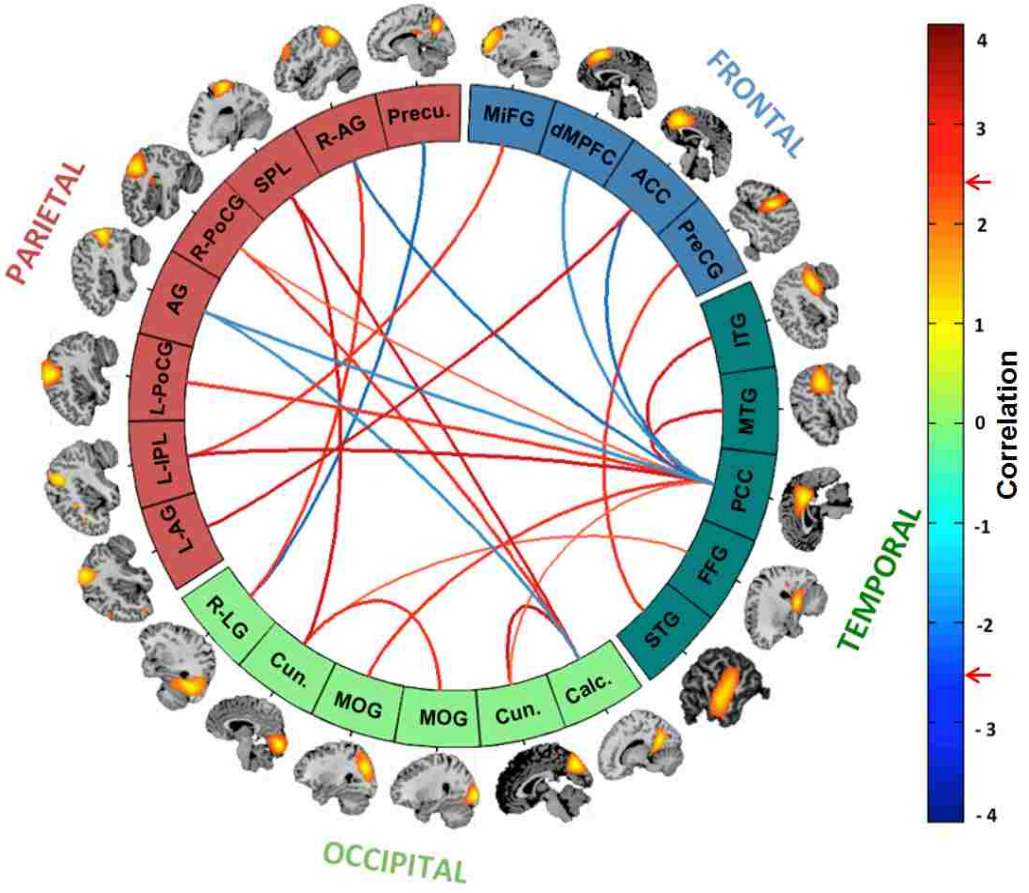

FIGURE 2.5: Example of functional network connectivity among different brain regions.The FDR threshold (q< 0.05) is depicted on the color bar with red arrows.

2.3.1 Functional Specialization and Integration

There are two fundamental principles to explain the functional organization of the brain: functional specialization and functional integration (Friston, 2011; Tononi et al., 1998). The term functional specialization implies that a cortical region is responsible for and specialized for some aspects of perceptual or motor processing, where the specialization can be anatomically separated within the cortex. The cells with common functional properties are grouped together to form a functionally specialized region. Since the beginning of anatomical theories of the brain, researchers had been focusing on identifying particular brain regions related to specific function. After so many inconclusive studies and experiments, scientists have only begun to successfully separate and understand localized functions of the brain. In case of functional integration, these specialized functional areas unite and integrate to perform higher-level cognitive and behavioral tasks. Note that, functional specialization and integration are complementary to each other, where they are only meaningful given the context of each other.

2.3.2 Resting-state Connectivity

Resting-state BOLD studies have proven useful recently to investigate abnormal functional connectivity, as the absence of a specific task complements task-specific study by measuring intrinsic functional brain organization without any differential behavioral performance and task activity between diagnostic groups, and thus makes it easier for cognitively compromised patients to participate in such studies. Resting-state fMRI connectivity has been used to identify differences in multiple patient groups including SZ (Calhoun et al., 2009b; Sakoğlu et al., 2010; Calhoun

et al., 2011), BP (Calhoun et al., 2011), Alzheimer's disease (Greicius et al., 2004; Sorg et al., 2007), ASD (Starck et al., 2013), and others.

Recent studies showed consistent existence of most of the resting-state networks (RSNs), also known as ICNs, not only during the resting-state but also during performance of a task (Calhoun et al., 2008a; Harrison et al., 2008; Laird et al., 2009; Smith et al., 2009). Also high reproducibility and reliability of the RSNs have been demonstrated in several recent resting-state studies (Allen et al., 2011; Franco et al., 2009). The absence of any specific task in rsfMRI studies makes it less likely to show variability across different data acquisition sites, allowing reproducibility of the findings at different laboratories. This also allows a wider range of subjects including healthy controls, patients and young children to be examined, and make it possible to study multiple cortical systems from one dataset (Fox and Greicius, 2010). Moreover, connectivity maps with higher accuracy can be identified using rsfMRI data compared to task-based fMRI data (Xiong et al., 1999).

The significance of RSNs can be linked to the fact that the topography of these networks closely corresponds to responses that are stimulated by a variety of sensory, visual, motor and cognitive tasks. These RSNs are present even during eyes-open or eyes-closed conditions, during sleep or drowsiness and general anesthesia (Fukunaga et al., 2006; Vincent et al., 2007). Given the evidence of robustness of these resting-state spontaneous fluctuations, it has been suggested that this phenomenon related to intrinsic neuronal activity is a fundamental property to maintain the functional integrity of the brain. However, the exact functions of these RSNs are still not fully understood.

DMN is one of the most widely studied RSNs, which is defined by its unique

property to be more active at rest than during performance of a specific task. Greicius and colleagues (Greicius et al., 2003) first identified the DMN using rsfMRI data, which was than successfully identified and replicated in many other studies using different analysis methods.

2.3.3 Static and Dynamic Connectivity

Brain connectivity has become a major research area in both clinical and cognitive neuroimaging. As discussed in section 1.1, different analytic tools such as seed-based methods or data-driven approaches have been applied to resting-state fMRI data to describe brain functional connectivity. Until recently, most functional connectivity approaches characterized the interaction among different brain regions in terms of stationarity by measuring the temporal correlation or global data decomposition. Such static-like approaches collapsed the data across their temporal domain, and ignored any transient and non-stationary nature of the interactions among these brain regions. This stationarity approach restricts our ability to fully comprehend the spatio-temporal dynamics of the interconnected brain regions in terms of transient resource allocations as well as the dependencies of connectivity in the brain across the temporal domain. Such dynamics of the connectivity can occur at both short and long temporal scales. Therefore, to get a more dynamic understanding of functional connectivity, it is necessary to obtain a broader view on spatio-temporal non-stationarity, in addition to linking hemodynamic measurements to electrophysiological activities. Recent studies showed that connectivity dynamics could capture uncontrolled but reoccurring patterns of interactions among ICNs during task or at rest (Sakoğlu et al., 2010; Calhoun et al.,

2014). A recent approach for studying dynamic connectivity is the sliding-window correlation technique (Allen et al., 2012a; Hutchison et al., 2013b).

2.4 Classification of Mental Disorders

Advances in neuroimaging technologies in the past two decades have opened a new scope into the structure and function of the healthy human brain as well as enlightening many brain disorders such as SZ. SZ is a devastating, chronic heterogeneous disease, which is usually characterized by disintegration in perception of reality, cognitive problems and chronic course with lasting impairment (Heinrichs and Zakzanis, 1998). Multiple structural and functional brain abnormalities are widely reported in patients with SZ (Calhoun et al., 2009a; Shenton et al., 2001). Most neuroimaging-based studies of SZ focus on showing abnormalities of some features (structural or functional) in a patient group by comparing them with a control group. While many of these findings are statistically significant in the average sense, discrimination ability of those features is questionable for classification purposes on a individual basis. Since classification provides information for each individual subject, it is considered a much harder task than reporting group differences. In the case of classifying SZ patients, a small number of training samples (subjects) and high dimensional data make it a challenging task to design an accurate, robust classifier for such a heterogeneous brain disorder.

There is an increasing interest in designing robust and accurate techniques to classify subjects into groups using functional imaging data. For example, previous studies showed the use of functional connectivity-based features for classification of SZ and BP patients at the individual level (Shen et al., 2010; Arbabshirani et al., 2013b; Su et al., 2013). Shen et al. (2010) used an atlas-based method to

extract mean time-courses of 116 brain regions in the resting-state for both HC and SZ subjects. The correlation between these time-courses made the feature vector for each subject. By applying feature selection and dimensionality reduction methods, they reduced the dimensionality down to three where they classified patients from controls with a high accuracy. (Shinkareva et al., 2006) proposed a classification approach for SZ patients based on fMRI time-series from the voxels showing between-group temporal dissimilarity using leave-one-out cross-validation method. Another study combined both structural and functional MRI data for classification of SZ patients and created a training set by projecting the high dimensional data onto a lower dimensional space using the PCA, achieving a high classification accuracy (Ford et al., 2002a). A recent study performed automatic classification of SZ using both structural and functional MRI features, and showed that better classification accuracy could be achieved by using both MRI features, compared to using only a single feature (Silva et al., 2014). However, only a few studies have focused on classification analyses of both SZ and BP patients (Calhoun et al., 2008b; Arribas et al., 2010; Costafreda et al., 2011). In (Calhoun et al., 2008b), temporal lobe and default mode networks were used as features using a leave-one-out cross-validation framework, and classified SZ and BP patients at individual level. In another classification study (Costafreda et al., 2011), a support vector machine (SVM) was applied on the verbal fluency task-based patterns of regional brain responses to identify SZ and BP patients at the individual level. To our best knowledge, no such study has provided a detailed comparison of both static and dynamic FNC features in a cross-validated classification analysis.

2.5 Imaging Genetics

Recently a growing interest has been emerged in studying the role of genetic variation in brain anatomy and function (Scharinger et al., 2010). As a recent emerging field, imaging genetic studies aim to identify and characterize the genetic variants (eg. SNP) that may influence the brain features as measured by functional (eg. fMRI) or structural (eg. sMRI) neuroimaging techniques. It has now become possible to examine the combined information from multiple modalities by jointly analyzing and estimating the multimodal data using data fusion approaches. Findings from these imaging genetics studies have shed more light on the biological mechanisms involved in cognition and emotion. Mapping the influence of certain polymorphisms for brain activation can ultimately help us understand more about the underlying characteristics of different brain disorders.

2.5.1 Single Nucleotide Polymorphism

The fundamental structural units of the gene are nucleotide. The four nucleobases are guanine (G), Adenine (A), Thymine (T) and Cytosine (C). A single nucleotide can show variation in deoxyribonucleic acid (DNA) sequences among the members of a species. This type of genetic mutation is known as single nucleotide, and called an allele. The more frequently observed from of nucleotide or base pair in a population is denoted as the major allele. The more frequently observed form of nucleotide or base pain in a population is denoted as major allele, whereas the alternative form is termed as minor allele. DNA sequences can display genetic variation among members of a species at a single nucleotide known as SNP, as shown in Figure 2.6. In general, SNP is referred to as the genetic variation in nucleotide where the minor allele frequency should be greater than 1%, which

leads to at least 10 million common SNPs out of the 3 billion bases for the whole human genome (Gibbs et al., 2003).

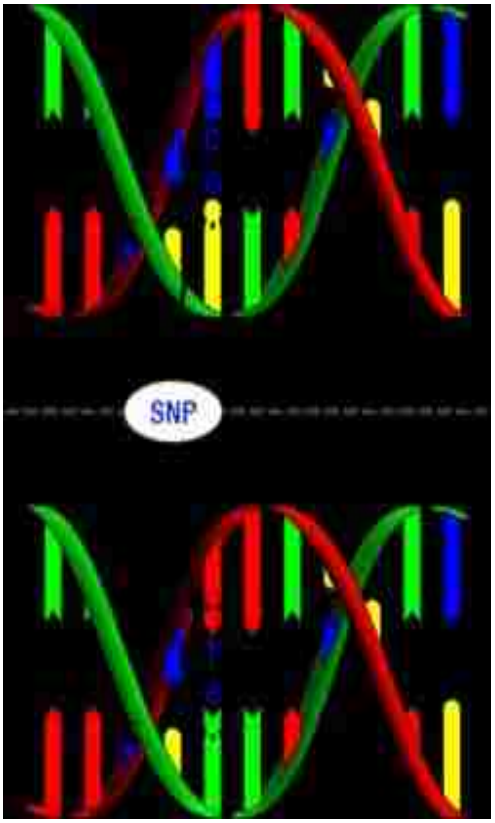

FIGURE 2.6: Illustration of a SNP with C/T polymorphism(from Wikipedia).

SNPs can occur at both coding and non-coding regions of the DNA, with a variety of impacts at the phenotypic level. The structure or functions of the encoded proteins can be affected by polymorphisms occurring in coding regions, which may further lead to disease (Ferreira et al., 2011). However, the majority of the SNPs fall into non-coding regions.

CHAPTER 3

TIME-VARYING CONNECTIVITY OF TYPICAL DEVELOPMENT AND AUTISTIC TRAITS

3.1 Motivation

A number of developmental disorders, including ASD, have demonstrated abnormal FC (Uddin et al., 2013b). Further, atypical development of neural interactions has been considered a major basis in theoretical models of neuropsychiatric disorders (Geschwind and Levitt, 2007). Evidence suggests that short-range or intra-network FC is more dominant during infancy (Fransson et al., 2007; Gao et al., 2011) and decreases with age during childhood and adolescence, with long-range or inter-network connectivity becoming more dominant in early adulthood (Dosenbach et al., 2010; Fair et al., 2009). The majority of existing models applied to the connectome operate under the assumption that the brain's functional architecture is static over a period of multiple minutes. This has been shown to

be a major limitation, as important transient patterns of connectivity could be overlooked (Calhoun et al., 2014). To our knowledge, no study has provided a baseline to understand how the brain's dynamic FC (i.e. chronnectivity) matures with age during childhood, and compared this baseline with the dysfunctional chronnectopathy of emerging mental illness. In this work, we address these limitations by performing chronnectivity analyses of typical development and autistic traits.

Over the past decade, various *in vivo* techniques, including fMRI, have been increasingly used to study patterns of functional connectivity in the developing brain, particularly during rest (rs-fMRI). A wide array of methods has been used to categorize the brain into functionally interconnected parcels, or ICNs, such as the DMN. Most recently, chronnectomic approaches relaxing traditional stationarity assumptions aim to more accurately model the brain's ICNs, avoiding the omission of transient, yet potentially relevant, patterns of functional connectivity (Allen et al., 2012a). dFNC has already been shown to offer unique chronnectomic information (Allen et al., 2012a; Hutchison and Morton, 2015) and is sensitive to neurobiological features of normal brain development (Hutchison and Morton, 2015) and psychopathology (Rashid et al., 2014).

ASD is a heterogeneous neurodevelopmental condition, with central features of impairment in reciprocal social interactions, as well as restricted, stereotypical behaviors. With an estimated prevalence between 1-3%, ASD is generally recognized in early childhood and is accompanied by severe burden, both for the affected individual as well as for caregivers (Baxter et al., 2015). Despite the presence of an extensive and expanding literature, the neurobiological etiology of autism spectrum disorder remains elusive. Along with most psychiatric disorders, ASD has traditionally been conceptualized categorically, but is increasingly recognized as

the severe end of a continuum of traits that extend into the general population (Constantino and Todd, 2003). While not strictly pathological, such variation in autistic traits in the general population serves as an important dimensional behavioral phenotype for clinical autism. Thus, imaging studies using this phenotype of quantitative social impairment can complement case-control studies to better understand the underlying neurobiology of ASD. Irrespective of the classification approach, one of the prominent hypotheses on the origins of ASD is an aberrant development of neuronal connections throughout the brain [i.e., "developmental disconnection syndrome", (Geschwind and Levitt, 2007)].

Within this context, we utilized resting-state fMRI scans from a large, population-based cohort study of children (Jaddoe et al., 2012; White et al., 2013), to search for both underlying maturational and sex-specific properties of chronnectivity, and an underlying neurobiological substrate of ASD traits in the general population. We hypothesized the presence of dynamic connectivity states in children that are similar to those already reported in adults, given many static connectivity networks are present at a young age (Gao et al., 2011). Specifically, a mean, 'static-like' state, a hypo-connected state, and a hyper-connected state that have all previously been observed in dynamic connectivity studies of adults. Further we hypothesized age-related correlates of dynamic connectivity to resemble adult-like patterns, where increasing age is associated with states previously reported in adults. Lastly, as previous work has shown aberrant connectivity dynamics in psychopathology, we hypothesize to see an association between aberrant dynamic connectivity and features of autism. As the static connectivity literature has uncovered widespread patterns of both hyper- and hypo-connectivity in ASD, we hypothesize multiple regions throughout the brain to associate with autistic traits along a continuum. In particular, given numerous reports of the DMN have shown

attenuated within- and between network connectivity in ASD, we hypothesize dynamic (hypo-)connectivity in this network to be of particular relevance. Results showed that multiple ICNs that are widely recognized in studies of adults (e.g., sub-cortical, default-mode and sensorimotor), are also identified in this large group of young children. Results also reveal that the dynamic properties of connectivity vary with both age and sex. Specifically, stronger inter-network connectivity was associated with age in the more mature, "adult-like" dFNC states; states in which older children also demonstrated longer MDT (average time within a given state) compared to younger children. Interestingly, children with more autistic traits showed higher MDT in a globally disconnected state, which resembled the connectivity dynamics observed in younger children. These results show a link between the typical and atypical developmental trajectories as captured by dynamic FNC, where individuals with more autistic traits show both a delayed and muted transition to spending time in the globally modularized or more heavily connected states. Taken together, the present study provides a conceptual framework to support further investigations of typical and atypical brain development in the general population using novel neuroimaging methodology and clinical insight.

3.2 Method

3.2.1 Participants

The current study is embedded in the Generation R Study, which is a large, population-based birth cohort in Rotterdam, the Netherlands (Jaddoe et al., 2012). One thousand seventy children, ages 6-to-10 years, were scanned between September 2009 and July 2013 as part of a sub-study within the Generation R Study

(White et al., 2013). General exclusion criteria for the current study include severe motor or sensory disorders (deafness or blindness), neurological disorders, moderate to severe head injuries with loss of consciousness, claustrophobia, and contraindications to MRI. Raw fMRI data from 964 subjects were available for our study, and after excluding children with bad data (e.g., motion, for details see below) 774 datasets were available for statistical analysis. Informed consent was obtained from the parents, and all procedures were approved by the Medical Ethics Committee of the Erasmus Medical Center. For more information on participant see Tables A.6 and A.7).

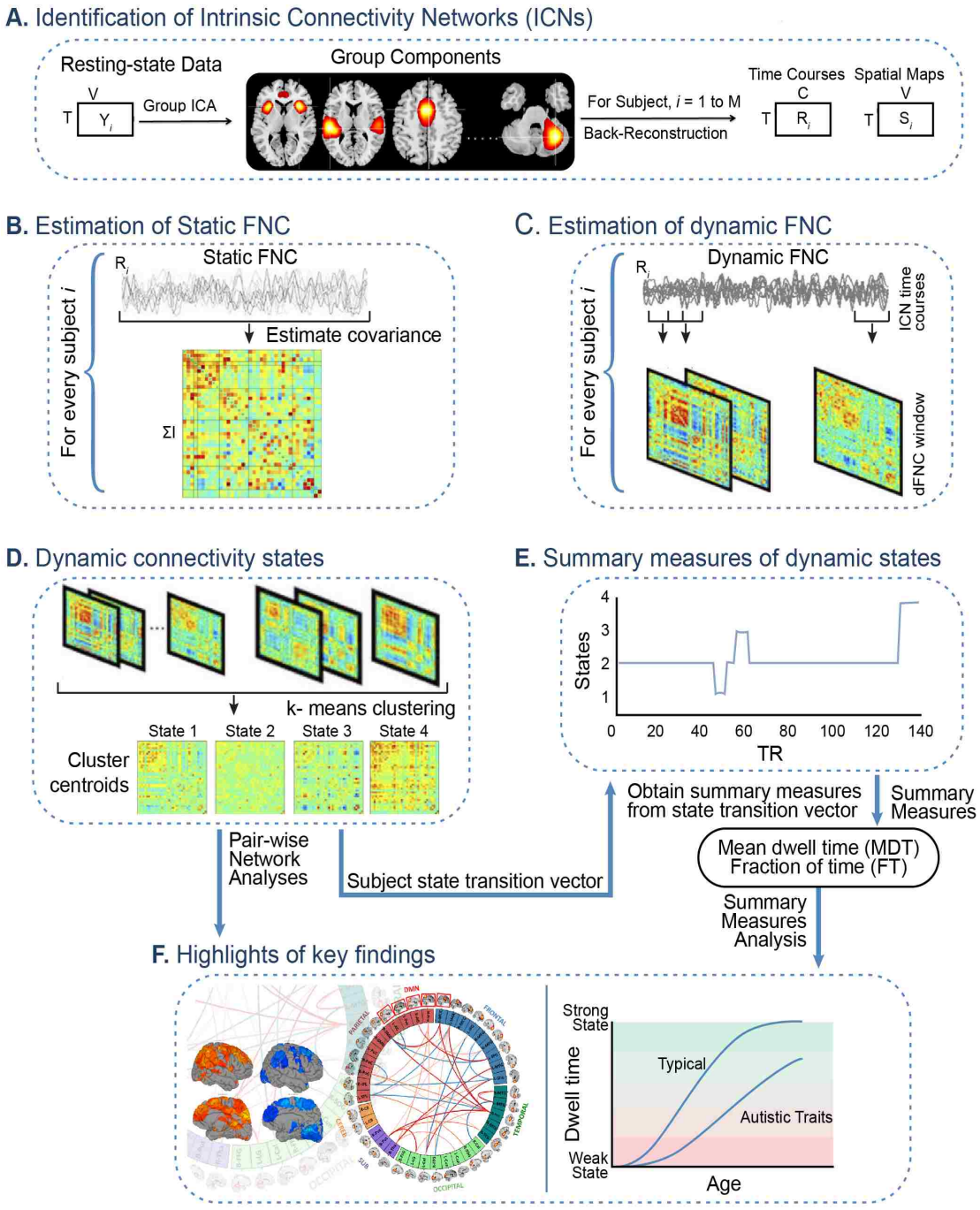

FIGURE 3.1: Graphical depiction of the analysis method and key findings.

3.2.2 Autistic Traits and Autism Spectrum Disorder

The Social Responsiveness Scale (SRS) was administered when children were roughly age 6 years (range: 4.89-8.90 years) to measure autistic traits based on

parental observation during the last six months (Constantino et al., 2013). The Social Responsiveness Scale provides a valid, quantitative measure of subclinical and clinical autistic traits, where higher scores indicate more symptoms related to ASD (Constantino et al., 2013). We utilized the total score derived from the abbreviated, 18-item short-form of the scale, which shows correlates of 0.93 and higher with the full scale in three different large studies (Blanken et al., 2015). Cutoffs used in sensitivity analyses (described below) were based on recommendations for screening in population-based settings (consistent with weighted scores of 1.078 for boys and 1.000 for girls) (Constantino et al., 2013).

3.2.3 Autism Spectrum Disorder diagnoses

At approximately age 7 years, children who scored in the top 15th percentile on the Child Behavior Checklist (CBCL)-1.5-5 total score and those who scored in the top 2nd percentile on the Pervasive Developmental Problems sub-scale underwent a screening procedure for ASD using the Social Communication Questionnaire (SCQ), a 40-item parent-reported screening instrument to assess characteristic autistic behavior. SCQ scores $\geq$15 are considered positive for screening (Berument et al., 1999). We approached the general practitioners of children who scored screen-positive on the SRS, SCQ or for whom the mother reported a diagnosis of ASD in order to confirm this diagnosis with medical records. In the Netherlands, the general practitioner holds the central medical records, including information on treatment by (medical) specialists. In this sample, 22 children with usable MRI data also had a confirmed diagnosis of ASD.

3.2.4 MRI Data Acquisition

Magnetic resonance imaging data were acquired on a 3 Tesla scanner (Discovery 750, General Electric, Milwaukee, WI) using a standard 8-channel, receive-only head coil. A three-plane localizer was run first and used to position all subsequent scans. Structural T1-weighted images were acquired using a fast spoiled gradient-recalled echo (FSPGR) sequence (TR = 10.3 ms, TE = 4.2 ms, TI = 350 ms, NEX = 1, flip angle = 16^o, matrix = 256 × 256, field of view (FOV) = 230.4 mm, slice thickness = 0.9mm). Echo planar imaging was used for the rs-fMRI session with the following parameters: TR = 2000 ms, TE = 30 ms, flip angle = 85^o, matrix = 64 × 64, FOV = 230 mm × 230 mm, slice thickness = 4 mm. In order to determine the number of TRs necessary for functional connectivity analyses, early acquisitions acquired 250 TRs (acquisition time = 8min 20sec). After it was determined fewer TRs were required for these analyses, the number of TRs was reduced to 160 (acquisition time = 5min 20sec) (White et al., 2014). Children were instructed to stay awake and keep their eyes closed during the rs-fMRI scan. Further details on the entire scanning protocol can be found elsewhere (White et al., 2013).

3.2.5 Image Preprocessing

Data preprocessing was performed using a combination of toolboxes (AFNI, http://afni.nimh.nih.gov, SPM, http://www.fil.ion.ucl.ac.uk/spm, GIFT, http://mialab.mrn.org/software/gift), and custom scripts were written in Matlab. As mentioned above, some scans were collected with 250 volumes, which were first trimmed at the end of the acquisition to match the majority of scans with 160 volumes. We performed rigid body motion correction using the INRIAlign (Freire

and Mangin, 2001) toolbox in SPM to correct for subject head motion followed by slice-timing correction to account for timing differences in slice acquisition. Then the fMRI data were despiked using AFNI's 3dDespike algorithm to mitigate the impact of outliers. The fMRI data were subsequently nonlinearly warped to a Montreal Neurological Institute (MNI) template *(http://www.mni.mcgill.ca)* and resampled to 3 mm^3 isotropic voxels. The data were then smoothed with a Gaussian kernel to 5 mm full width at half maximum (FWHM). Each voxel TC was variance normalized prior to performing GICA as this has shown to better decompose subcortical sources in addition to cortical networks. In order to limit the impact of severe head motion, we excluded subjects' data with a maximum translation of $>$ 5 mm and/or with signal-to-noise fluctuation ratio (SFNR) $<$200 from our analyses, resulting in a final dataset with 774 subjects.

3.2.6 Group Independent Component Analysis (ICA)

After preprocessing the data, functional data were analyzed using spatial GICA framework as implemented in the GIFT software (Calhoun et al., 2001b; Calhoun and Adali, 2012). Spatial ICA decomposes the subject data into linear mixtures of spatially independent components that exhibit a unique time TC profile. A subject-specific data reduction step was first used to reduce 160 time point data into 100 directions of maximal variability using principal component analysis. Then subject-reduced data were concatenated across time and a group data PCA step reduced this matrix further into 100 components along directions of maximal group variability. One hundred independent components were obtained from the group PCA reduced matrix using the infomax algorithm (Bell and Sejnowski, 1995). To ensure stability of estimation, we repeated the ICA algorithm 20 times

in ICASSO (http://www.cis.hut.fi/projects/ica/icasso), and aggregated SMs were estimated as the modes of component clusters (Himberg et al., 2004). Subject specific SMs and TCs were obtained using the spatiotemporal regression back reconstruction approach (Calhoun et al., 2001c; Erhardt et al., 2011b) implemented in GIFT software.

3.2.7 Post-ICA processing

Subject specific SMs and TCs underwent post-processing as described in our earlier work (Allen et al., 2012a). Briefly, we obtained one sample t-test maps for each SM across all subjects and thresholded these maps to obtain clusters of voxels with higher intensities for that component; we also computed mean power spectra of the corresponding TCs.

The criteria for identifying independent components as ICNs were implemented in a semi-automated framework. We identified a subset of the independent components to be classified as ICNs (as opposed to physiological artifacts and motion-related noisy components) in two steps. First, we used AFNI software to automatically extract the peak MNI coordinates of each component and their corresponding MNI regions. Next, we inspected the aggregate SMs and average power spectra of each of the independent components (Figure 3.2 and Figure A.9). Three viewers were provided with the MNI regions as extracted by AFNI, and they rated the components from 0 (definite artifact) to 1 (definite ICN) based on expectations that ICNs should exhibit cluster of voxels with higher intensities in gray matter, low spatial overlap with known vascular, ventricular, motion, and susceptibility artifacts, and TCs dominated by low frequency fluctuations (Cordes et al., 2001). To facilitate evaluation, power spectra of the components were characterized with two

previously used metrics to classify components (Robinson et al., 2009): dynamic range, defined by the difference between the peak power and minimum power at frequencies to the right of the peak, and low frequency to high frequency power ratio, the ratio of the integral of spectral power below 0.10 Hz to the integral of power between 0.15 and 0.25 Hz (Figure A.9). Combined votes from the three raters were used to separate components into three broad classes: artifact (score equal to zero), mixed (score between zero and three), and RSN (score of three or greater and no votes equal to zero). This selection procedure resulted in 38 ICNs out of the 100 independent components obtained. Figures highlighting the dynamic range (Figure A.9) and low frequency to high frequency power ratio (Figure A.10) are provided in **Appendix A**.

The subject-specific TCs corresponding to the ICNs selected from the back-reconstructed data were detrended, orthogonalized with respect to estimated subject motion parameters, and then despiked. The despiking procedure involved detecting spikes as determined by AFNI's 3dDespike algorithm and replacing spikes by values obtained from third order spline fit to neighboring clean portions of the data. The despiking process reduces the impact/ bias of outliers on subsequent FNC measures (**see Supplemental Fig. 1** in (Allen et al., 2012a)). Lastly, single-subject post-ICA motion parameters regression from time-series at the voxel level was performed. This step, in combination with despiking and the ability of GICA to remove signals attributable to noise and artifact (including motion) ensures the data are suitable for statistical analysis.

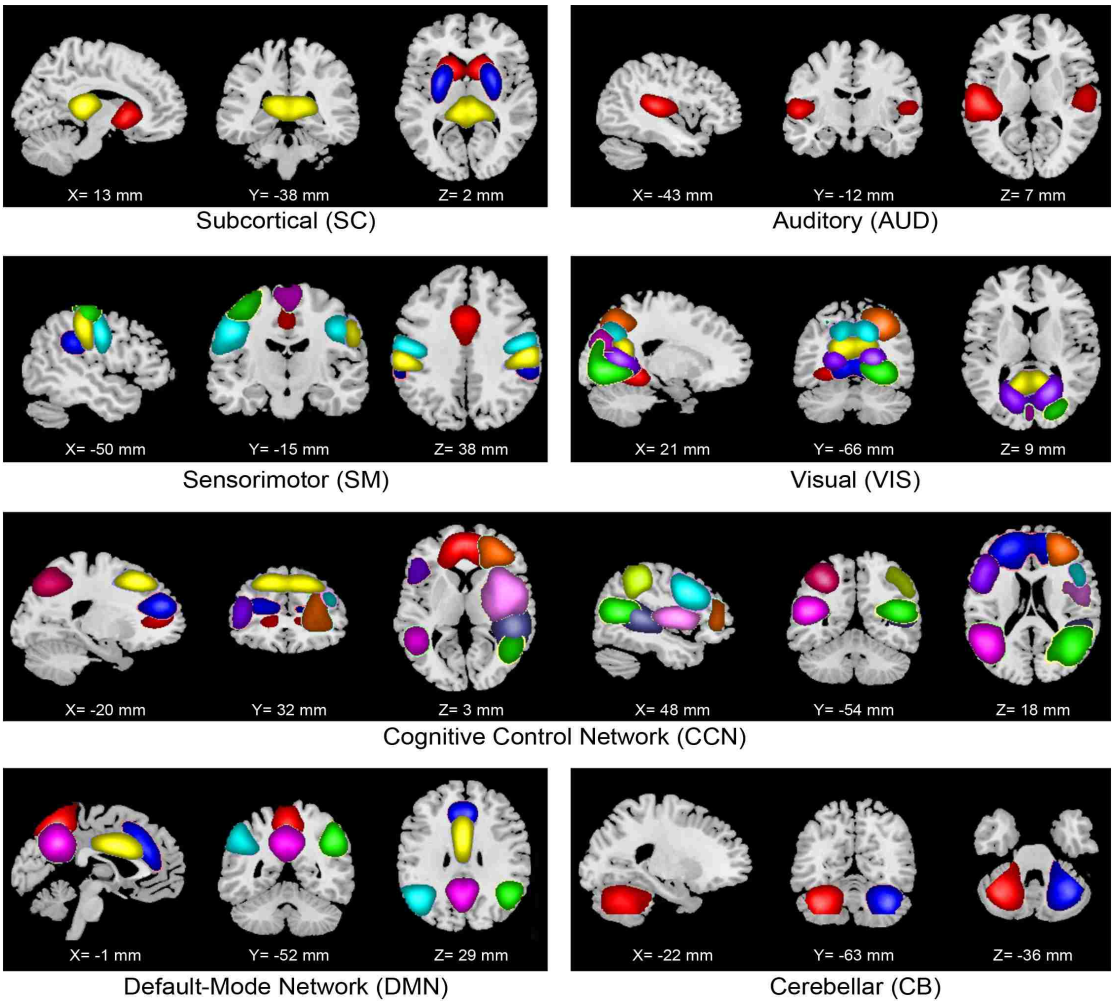

FIGURE 3.2: Non-artifactual intrinsic connectivity networks (ICNs).

3.2.8 Static Functional Network Connectivity (sFNC)

We computed sFNC, defined as pairwise correlation between ICN TCs, as a measure of average connectivity among different ICNs during the scan duration. In this work, the FNC computed using the whole ICN TCs is referred to as stationary or sFNC. Since correlation among brain networks is primarily shown to be driven by low frequency fluctuations in BOLD fMRI data (Cordes et al., 2001), we band pass filtered the processed ICN TCs between [0.01 – 0.15 Hz using 5th order Butterworth filter prior to computing FNC between ICNs. The

mean sFNC matrix was computed over subjects. For partitioning sFNC matrix based on modularity, we followed our prior work (Allen et al., 2012a) to identify the main modules (sub-cortical, auditory, visual, sensorimotor, cognitive control, DMN and cerebellum), and using those same partitioned modules as our main modules, rather than partitioning the frontal and attention-networks as seen in some of the prior published work. For organization of the ICNs inside these main modules, we applied the Louvain algorithm of the brain connectivity toolbox (https://sites.google.com/site/bctnet), and arranged the ICN components accordingly. To address the stochastic nature of the Louvain algorithm, we ran the Louvain algorithm 100 times and compared the number of times we got the same arrangement of ICNs. Finally, we used the arrangement that occurred maximum number of times. The rows of sFNC matrix were partitioned into sub-cortical (SC), auditory (AUD), visual (VIS), sensorimotor (SM), a broad set of regions involved in cognitive control (CC) and attention, DMN regions, and cerebellar (CB) components as shown in Figure A.1.

3.2.9 Dynamic Functional Network Connectivity (dFNC)

As recent studies both in animals and humans have highlighted the nonstationary nature of functional connectivity in BOLD fMRI data (Hutchison et al., 2013b), we sought to determine whether the observed sFNC differences were primarily driven by certain connectivity configurations (Hutchison et al., 2013b). dFNC between two ICA TCs was computed using a sliding window approach with a window size of 22 TR (44 s) in steps of 1 TR (Figure 3.1). The window constituted a rectangular window of 22 time points convolved with Gaussian of sigma 3 TRs to obtain tapering along the edges (Allen et al., 2012a). Since estimation of covariance using

time series of shorter length can be noisy, we estimated covariance from regularized inverse covariance matrix (ICOV) (Smith et al., 2011; Varoquaux et al., 2010) using the graphical LASSO framework (Friedman et al., 2008). We imposed an additional L1 norm constraint on the inverse covariance matrix to enforce sparsity. The regularization parameter was optimized for each subject by evaluating the log-likelihood of unseen data of the subject in a cross-validation framework. After computing dFNC values for each subject, these covariance values were Fisher-Z transformed to stabilize variance prior to further analysis.

3.2.10 Clustering and Dynamic States Detection

Based on our observation that patterns of dFNC connectivity reoccur within subjects across time and also across subjects, we used a k-means algorithm to cluster these dFNC windows, subdividing the data into a set of separate clusters so as to maximize the correlation within a cluster to the cluster centroid. Instead of clustering all of the dFNC windows across all subjects, initial clustering was performed on a subset of windows from each subject, called subject exemplars hereafter, corresponding to windows of maximal variability in correlation across component pairs. To obtain the exemplars (see Figure A.11), we first computed variance of dynamic connectivity across all pairs at each window. We then selected windows corresponding to local maxima in this variance TC. The optimal number of centroid states was estimated using the elbow criterion, defined as the ratio of within cluster to between cluster distances (see **Appendix A.4** and Figure A.8 for detailed information). A k of 4 was obtained using this method in a search window of k from 2 to 9. The correlation distance metric was chosen as it is more sensitive to the connectivity pattern irrespective of magnitude.We repeated the

clustering method using different distance functions (cosine and L1-norm, rather than the correlation function) and also found very similar results. These sets of initial group centroids were used as a starting point to cluster all of the dFNC windows from all subjects. Information on validation of the clustering approach with respect to a null model can be found in **Appendix A.7** and Figure A.12 and Figure A.13.

Also, summary measures such as MDT and FT were computed from the state transition vector. Using the following equations 3.1 and 3.4, we computed MDT and FT for each subject:

$$MDT^{\text{state(k)}} = \text{mean}(\text{end\_}t - \text{start\_}t) \tag{3.1}$$

where,

$$\text{start}_t = \text{count}(\text{difference}(\text{state\_vectorsubject(i)}, \text{state}) == 1) \tag{3.2}$$

$$\text{end}_t = \text{count}(\text{difference}(\text{state\_vectorsubject(i)}, \text{state}) == -1) \tag{3.3}$$

$$FT^{\text{state(k)}} = \frac{\text{sum}(\text{state\_vector}^{\text{subject(i)}}) == \text{state}}{\text{Number of Windows}} \tag{3.4}$$

The pseudo code for computing MDT using equation 3.1 is as follows:

For each subject i and for each dynamic state k

1. Compute *start_t* by first taking the difference between the adjacent elements of the state vector for that particular subject, and then by finding the differences that are equal to 1.

2. Compute end_t by first taking the difference between the adjacent elements of the state vector for that particular subject, and then by finding the differences that are equal to -1.

3. If the first value of the state vector is equal to the current state k, store $start\_t$ as [0; $start\_t$].

4. If the last value of the state vector is equal to the current state k, store end_t as [end_t, $Number\_of\_windows$].

5. subtract the $start\_t$ vector from the end_t vector, and take the mean of the resulting vector to compute MDT of that subject on that particular state.

6. Repeat step 1 to step 5 for all subjects i and all states k.

3.2.11 Statistical Analyses

Statistical analyses were carried out in Matlab (version R2011b) using the statistics toolbox and linear model class. Multiple linear regression was used to examine associations between connectivity metrics and explanatory variables (i.e., age, sex, and autistic traits). Two separate models were used to investigate associations with sFNC, dFNC and summary metrics from dFNC such as MDT and FT: first, a model where age and sex were entered as independent (predictor) variables and main effects for each were examined, and a second model where autistic traits (SRS) was entered as the independent variable and age and sex were added as covariates. All of the results reported correspond to a false discovery rate multiple comparison correction threshold $p < 0.05$.

Note that, we also started with a full model that included interaction terms (age-sex and SRS-age and SRS-sex), and the backward model selection led us to a

first-order model. In the backward model selection procedure, unimportant or less significant variables are eliminated one at a time. The process starts from the full model, and isolates the least important predictor left in the model, and checks its significance. We used the Akaike information criterion (AIC), a penalized-likelihood criteria of the relative goodness-of-fit of a statistical model to the observed data. A 0.10 significant level has been used for this strategy while dropping the less significant variables. Final results were corrected for false discovery rate (FDR) at p <0.05 level. We have used step( ) function to employ this approach.

After backward model selection, the following models were used for investigating associations with sFNC matrices:

$$Model1_{sFNC} : sFNC \sim \beta_0 + \beta_1 age_i + \beta_2 sex_i + \varepsilon_i \tag{3.5}$$

$$Model2_{sFNC} : sFNC \sim \beta_0 + \beta_1 SRS_i + \beta_2 age_i + \beta_3 sex_i + \varepsilon_i \tag{3.6}$$

For dFNC analyses, we computed a subject median (computed element-wise) for each subdivision from the subject windows that were assigned to that subdivision as a representative pattern of connectivity of the subject for that state. To investigate if the observed effects of age, sex and SRS on sFNC are primarily driven by certain dynamic FNC states, we used these subject medians for each state, as well as the summary matrices for each state, and evaluated the associations using two separate models as mentioned above, and are adapted for the dFNC below:

$$Model3_{dFNC} : dFNC_i^{state(k)} \sim \beta_0 + \beta_1 age_i + \beta_2 sex_i + \varepsilon_i \tag{3.7}$$

$$Model4_{dFNC} : dFNC_i^{state(k)} \sim \beta_0 + \beta_1 SRS_i + \beta_2 age_i + \beta_3 sex_i + \varepsilon_i \tag{3.8}$$

Similar to sFNCs, we started with a full model that included interaction terms (age-sex, age-SRS and sex-SRS), and the backward model selection led us to a first-order model. Pair-wise associations from the above mentioned models are depicted in connectivity matrices and in connectograms (Langen et al., 2015).

The following models were used for investigating associations with summary metrics of dFNC (MDT and FT):

$$Model5_{MDT} : MDT_i \sim \beta_0 + \beta_1 age_i + \beta_2 sex_i + \varepsilon_i \tag{3.9}$$

$$Model6_{MDT} : MDT_i \sim \beta_0 + \beta_1 SRS_i + \beta_2 age_i + \beta_3 sex_i + \varepsilon_i \tag{3.10}$$

$$Model7_{FT} : FT_i \sim \beta_0 + \beta_1 age_i + \beta_2 sex_i + \varepsilon_i \tag{3.11}$$

$$Model8_{FT} : FT_i \sim \beta_0 + \beta_1 SRS_i + \beta_2 age_i + \beta_3 sex_i + \varepsilon_i \tag{3.12}$$

In order to ensure linear terms were the best fit for the data, quadratic and cubic age terms were also tested, however model fits were not improved when these higher order terms were added. This has also been evaluated using several residual plots, which showed linear trend of the data.

Several sensitivity analyses were run in order to ensure results were not influenced various confounding factors, and are reported in **Appendix A.3**. First, to ensure behavioral problems did not influence age- and sex-related associations, analyses were run where children with high levels of behavioral problems were excluded. Similarly, to test whether continuous associations between autistic traits and connectivity were truly along a continuum and not driven by extreme cases, analyses were run after excluding children scoring above the screening threshold on the SRS and those with a clinical ASD diagnosis. In order to disentangle the effects of SRS

and age, an SRS-by-age interaction term was added to MDT and FT models for the sensitivity analysis. Further, for SRS models examining MDT and FT, the sample was refined into an age-restricted sample (ages 8-to-9 years only) to minimize the residual confounding effects of age. Lastly, to ensure motion-related artifacts were not responsible for any age-related or SRS-related associations, children with more than 3mm maximum translation during rsfMRI acquisition were dropped from analyses, and common motion parameters (e.g., frame-wise displacement) were added to the models. Note that, the motion parameters were only added to the models for the sensitivity analyses as presented in **Appendix A.3**.

3.3 Results

3.3.1 Characterizing static and dynamic functional network connectivity in children

Our first goal was to characterize the connectivity in typical development through age associations in a large sample of 774 school-age children. This was accomplished by evaluating the properties of both static and dynamic connectivity (Figure 3.1(A-D)) of the developing brain using 38 ICNs (extracted from a 100 component group independent component analysis (Calhoun et al., 2001b)) grouped into brain networks according to their anatomical and functional properties (Figure 3.2). The static FNC of the developing brain showed similar patterns as previous large-scale analyses of adults (Allen et al., 2012a; Damaraju et al., 2014a) for both intra- and inter-network connectivity. The default mode network was strongly connected within itself, and less connected to other brain networks (Figure A.1).

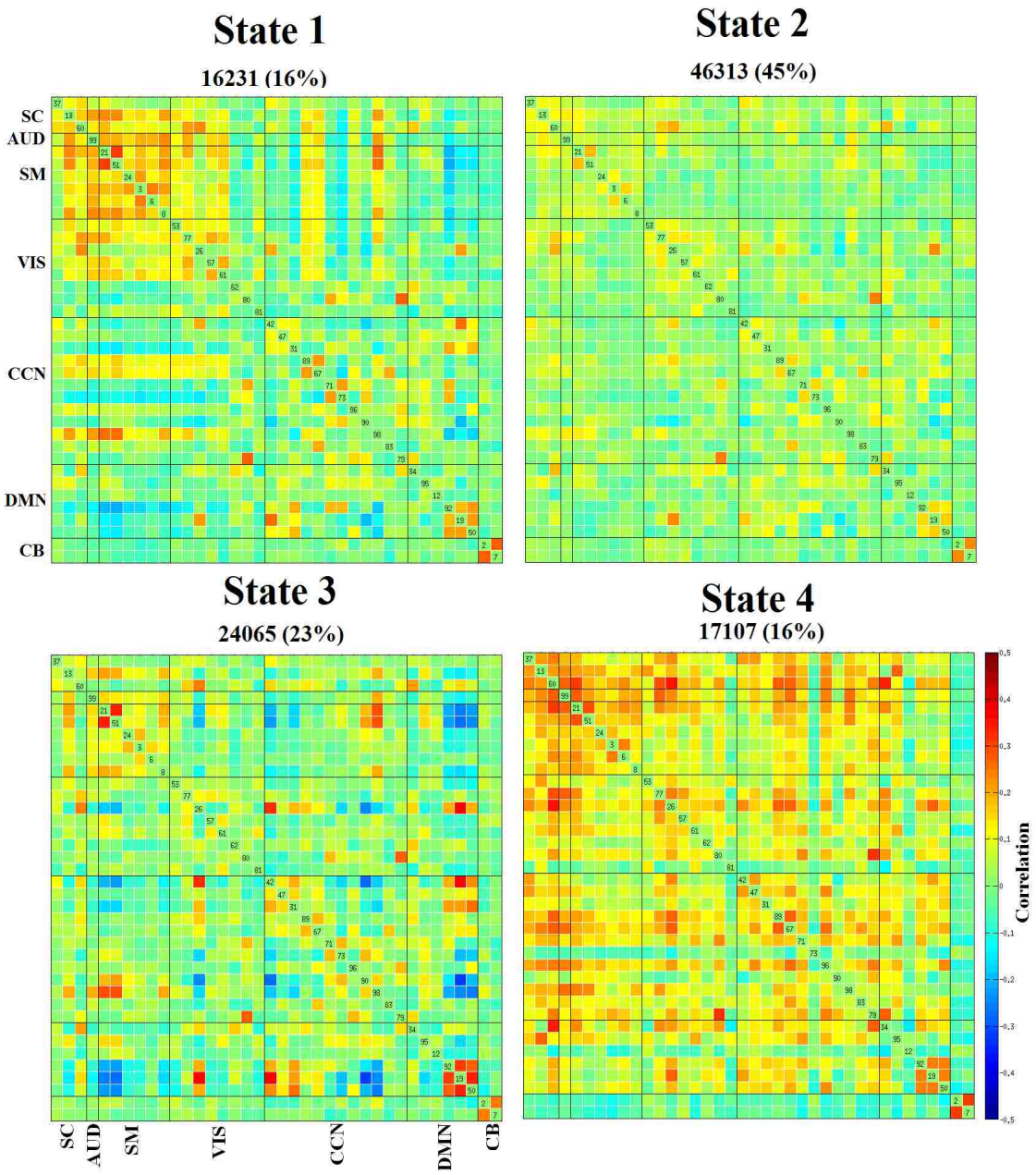

FIGURE 3.3: Dynamic functional network connectivity (FNC) states.The total number and percentage of occurrences is listed above each centroid.

Dynamic connectivity analyses (Figure 3.3) identified two modularized (i.e., bearing resemblance to previously reported static connectivity configurations): State-1: globally modularized, static-like, i.e., FNCs were present globally in intra- and inter-network connectivity, and State-3: default-mode modularized, i.e., strong intra-network positive connectivity and inter-network negative connectivity in

DMN. In addition, a globally disconnected state was identified (State-2: globally loosely connected intra- and inter-network connectivity) and one globally hyper-connected state (State-4: high positive connectivity found globally). Previous dynamic connectivity studies in adults reported each of these dynamic states, except for State-2, the globally disconnected state (Allen et al., 2012a).

3.3.2 Development of dynamic FNC states

Next, we evaluated the relationship of age and sex with the discrete dynamic states to evaluate the development of transient states from less-to-more mature representations of FNC (Equation (3.7) and Figure 3.4). Age-related associations were mostly localized in (but not limited to) State-1, the globally modularized dynamic state. In particular, positive age-related associations among frontal-temporal components, and both positive and negative age-related associations among frontal-parietal and temporal-parietal components were observed in State-1. Also, sex differences were mostly localized in (but not limited to) State-3, a state characterized by a modularized DMN. This particular dynamic state showed greater connectivity among frontal-temporal and frontal-occipital components in girls, and greater connectivity between a parietal component (right angular gyrus (AG), also a DMN component) and a temporal component (right middle temporal gyrus (MTG)) in boys. In other dynamic states, the age- and sex-specific effects were mostly localized to the DMN. Specifically, the left middle cingulate cortex (MCC) DMN component showed stronger inter-network connectivity with age in all FNC states, and stronger intra-network connectivity with age in State-4. Lastly, the left MCC showed higher inter-network connectivity for girls in all FNC states, and higher intra-network connectivity for boys in State-3.

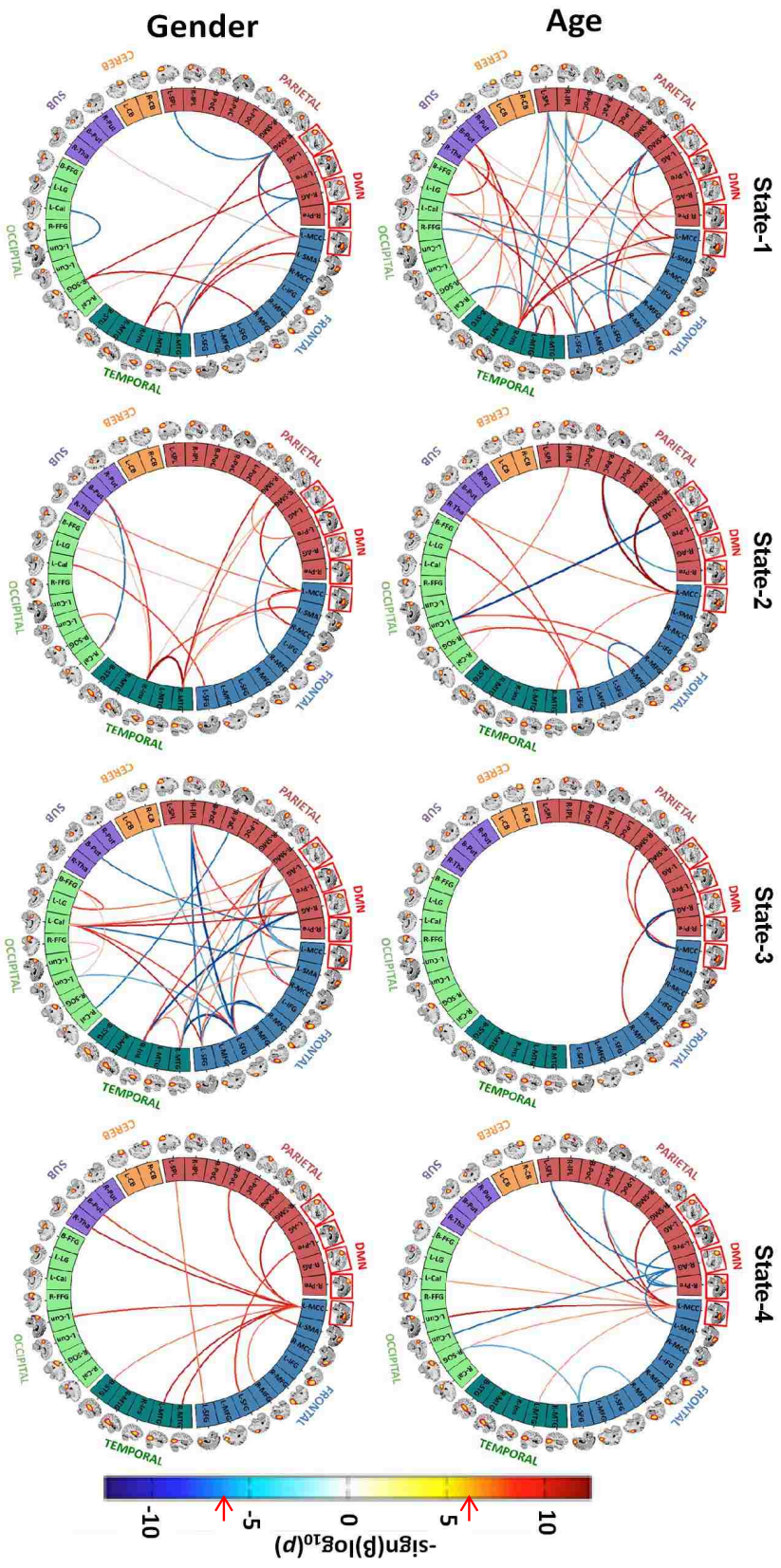

FIGURE 3.4: Connectograms showing age and sex associations across the dynamic connectivity states.The FDR threshold (q<0.05) is depicted on the color bar with red arrows.

3.3.3 Dwell time in dynamic states: age associations and sex differences

Next, we explored how different quantitative summary metrics of dynamic connectivity, such as MDT and FT, change as functions of age and sex (Equations (3.9), (3.11) and Figure 3.5). For each of the dynamic FNC states, we computed the MDT (how long an individual spends in a given state on average) and FT (total time spent in a given state). We found that older children showed longer MDT and FT in the globally modularized dFNC state (State-1). Conversely, younger subjects showed longer MDT and FT in the globally disconnected state (State-2). We also investigated sex differences in MDT and FT in the dynamic states and found that boys showed higher FT in the disconnected state (State-2), whereas girls showed higher MDT and FT in the DMN-modularized state (State-3). The other two dynamic states, the globally modularized state (State-1) and the globally hyperconnected state (State-4) showed trend-level sex effects, where boys had higher MDT and FT compared to girls in States-1 and -4.

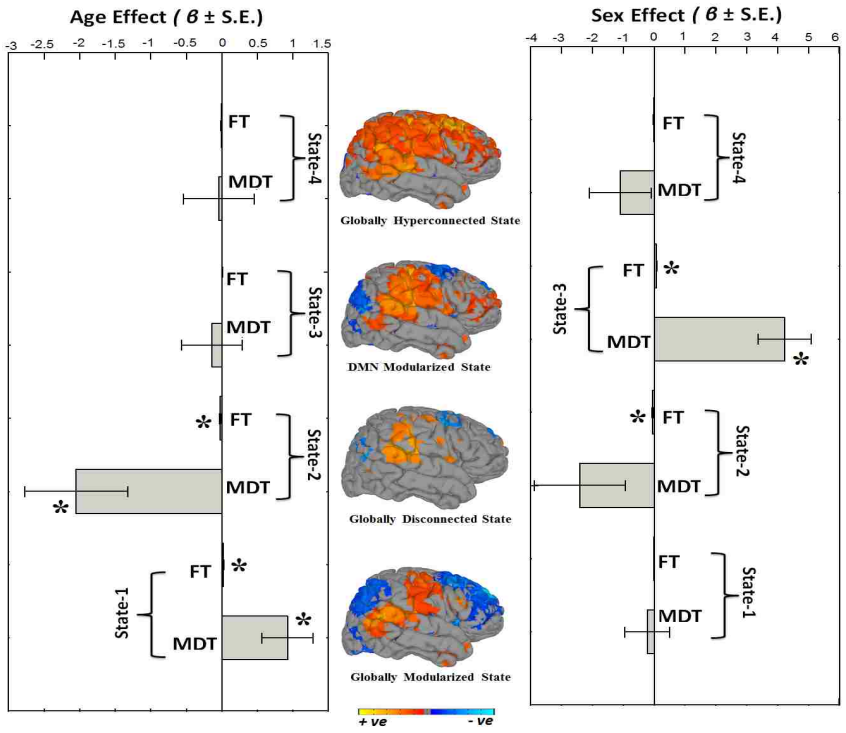

FIGURE 3.5: Summary metrics and age- and sex- effects. Here, MDT=mean dwell time, FT=fraction of time

3.3.4 Characterization of dynamic chronnectopathy: autistic traits and autism spectrum disorder

In addition to characterizing static and dynamic FNCs in typical development, we also studied the chronnectopathy, or disruption of the typical dynamic connectivity patterns, through autistic traits in the general population as well as in clinical autism spectrum disorder. We assessed autistic traits using the SRS score (Constantino et al., 2003) in a subset of children in the original sample (n=560). For static connectivity, one component pair (the left supplementary motor area, i.e. SMA, and the right supramarginal gyrus, i.e. SmG), showed an association with autistic traits. Specifically, children with more autistic traits showed weaker static connectivity. Interestingly, for dFNC State-3, children with more autistic traits showed higher connectivity in three component pairs (right insula and left

superior frontal gyrus (SFG), right SmG and left precuneus i.e. preC, and right insula and left preC) and lower connectivity in two component pairs (right-insula and right SmG, and left SMA and right SmG). Next, we assessed how MDT and FT vary with respect to autistic trait scores (Equations (3.10), (3.12) and Figure 3.6). In the globally disconnected state (State-2), autistic traits showed a positive association with MDT. In the DMN-modularized state (State-3), autistic traits were negatively associated with MDT. Thus, children with high levels of autistic traits had longer dwell times in the globally disconnected state (State-2) and children with fewer traits had longer dwell times in the DMN-modularized state (State-3). Results remained highly consistent when models were additionally adjusted for non-verbal IQ. Further, a similar pattern of effects was observed at the severe end of the spectrum, when a sub-sample of 22 children with clinical ASD were compared to 88 age, sex and IQ matched controls (Figure A.6). In order to assess whether the above-mentioned associations are a core feature of the trait-continuum or if the associations were driven by the most severely affected children, sensitivity analyses were run. When children with clinical ASD or an autistic traits score above the screening threshold were excluded, results remained consistent (Figure A.7), demonstrating that underlying neurobiological features covary with sub-clinical and clinical autistic traits.

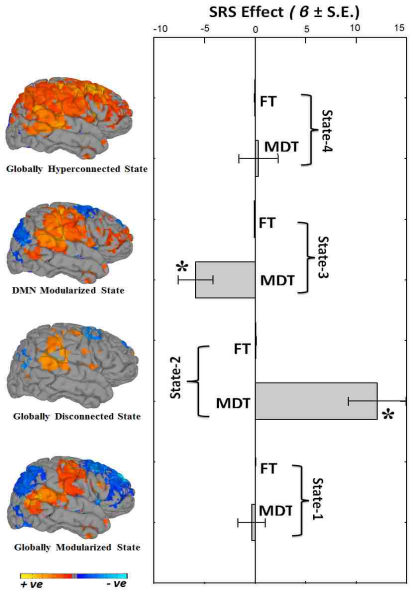

FIGURE 3.6: Summary metrics and autistic trait effects. Here, MDT=mean dwell time, FT=fraction of time.

3.4 Discussion

Here we apply a novel approach to the study of brain connectivity, both in typical and atypical child development. Complementing the existing static functional connectivity literature, we show age-related associations with discrete dynamic states that illustrate higher order maturational effects on chronnectivity. We also provide additional support for a disconnection construct in children with autistic traits and clinical ASD using dynamic functional connectivity. Lastly, we demonstrate the utility and potential clinical relevance of quantitative metrics that summarize large amounts of complex chronnectomic information.

3.4.1 The development of whole-brain dynamic connectivity in young children

In a large group of young children with a narrow age-range, we demonstrate that older children on average have longer dwell times in dynamic states typically observed in healthy adults. Age-related associations with static connectivity were consistent with previous reports, including increased integration and decreased segregation of control networks (Fair et al., 2007). This validation of the existing static connectivity literature is nicely complemented with new information where assumptions of network stationarity are relaxed, and quantitative summary metrics, such as MDT, are examined (Hutchison and Morton, 2015). Interestingly, evidence for sexual dimorphism in dynamic connectivity was also observed with girls showing longer dwell times in the modularized default-mode state and boys showing longer dwell times in the globally disconnected state. While no age-by-sex interaction was observed, given the narrow age range, this could complement existing evidence showing neuromaturational processes begin earlier in girls (Simmonds et al., 2014; Lenroot and Giedd, 2006).

3.4.2 Functional connectivity, autistic traits and autism spectrum disorder

Novel neuroimaging findings in combination with a characteristic early onset have brought momentum to ASD being conceptualized as a developmental disconnection syndrome (Geschwind and Levitt, 2007). Previous studies of static FNC in ASD have revealed mixed patterns of increased and decreased connectivity strength Uddin et al. (2013b). Similarly, within the discrete dynamic FNC states,

we found local patterns of stronger as well as weaker connection strength. Specifically, we observed decreased connectivity between the right SmG and the right insula, which is consistent with findings of lower insula activation in subjects with ASD in a large number task-based neuroimaging studies, covering a range of social processing tasks (Di Martino et al., 2009a). However, we also found hyperconnectivitity in the right insula, with the preC and the left SFG. Hyperconnectivity of the salience network, in which the insula is a key region, is particularly well replicated in the context of childhood ASD (Uddin et al., 2013a). Our findings in children in a similar age range suggest that the hyperconnectivity of the insula may also extend beyond regions of the salience network. Further, divergent findings of hypo- and hyperconnectivity in this region across studies, which have been previously attributed to developmental differences between samples (Uddin et al., 2013b), may be in fact be present at the same developmental stage, but across different dynamic states, and thus only be revealed simultaneously when using dynamic connectivity approaches.

Here, for the first time, we demonstrate that children with higher levels of autistic traits have longer dwell times in a globally disconnected state during rest, whereas children with lower levels of autistic traits have longer dwell times in a globally modularized state that more resembles an adult-like pattern of connectivity. Interestingly, in SZ, another disorder frequently classified as a disconnection syndrome, patients also spend more time in weakly connected dynamic states compared to HC (Rashid et al., 2014; Damaraju et al., 2014a). This also potentially fits with previous work in adults showing that, at the individual level, those with ASD may have distinct, noisy patterns of connectivity that may even mask 'typical' patterns of connectivity (Hasson et al., 2009). Higher levels of autistic traits were also associated with lower dwell times in a default-mode modularized state; a state where

nodes from the well-documented default-mode network were prominent. Despite heterogeneity in much of the functional connectivity literature, there is a growing body of evidence suggesting that the default mode network is more weakly connected in individuals with ASD (Jung et al., 2014; Stigler et al., 2011). Interestingly, task-based data examining the effect of a cognitive load on the DMN has previously suggested the DMN does not 'deactivate' during a task in ASD (Kennedy et al., 2006). However, in the context of our findings and other reports of weaker connectivity in the DMN, it is possible that rather failing to deactivate, the DMN actually fails to 'activate' in individuals with ASD; an alternative interpretation that could be made from task-rest contrasts of BOLD activation. We also demonstrated that, in the absence of clinically relevant cases, autistic symptoms in the general pediatric population are related to dynamic aspects of network connectivity. This is further evidence that aspects of the neurobiology of autistic traits, similar to the symptomatology, indeed lie on a continuum (Constantino and Todd, 2003; Blanken et al., 2015; Di Martino et al., 2009b). In addition to the dimensional trait approach, children with clinical ASD were compared to a group of age- and sex-matched controls, revealing similar patterns of longer dwell time within the globally disconnected state. Thus, we show that these dynamic functional connectivity features of autistic traits are also present in the most severely affected children. We propose the label "chronnectopathy" where patterns of dynamic functional connectivity in clinical groups deviate from those observed in the reference group without the disorder. While autistic traits in the general population are by no means pathological, this dimensional behavioral phenotype for clinical autism, which is considered pathological, serves as the basis for the term chronnectopathy. Interestingly, the longer mean dwell time in a less connected state observed in children with autistic traits and ASD which mimics the patterns

in younger, typically developing children, potentially indicative of a delayed or halted trajectory (Di Martino et al., 2014).

3.5 Conclusion and Additional Considerations

Strengths of this study include the large, population-based sample of children in a narrow age range, enabling us to show subtle age effects during a crucial, pre-adolescent period of development. Further, the age-range included in the current study is particularly under-studied in the context of ASD (Uddin et al., 2013b). Another major strength is the use of a dynamic approach to resting-state connectivity combined with an efficient and interpretable presentation of a wealth of data. While there is some consistency in the expansive static connectivity literature in ASD, it is unfortunately plagued by heterogeneity in clinical characteristics of the subjects, image acquisition, analysis strategy, and ultimately the core findings (Uddin et al., 2013b; Hernandez et al., 2015). The quantitative summary measures presented here could potentially aid in simplifying interpretations of complex network information, which historically are often subjectively evaluated. For instance, specific and isolated features of large (e.g., 80x80) connectivity matrices are often summarized when undoubtedly more complex patterns are present. While the present study also assigned labels to the four dynamic states, most of the interpretation comes from quantitative metrics, such as MDT. The subjects were all scanned on the same MRI scanner, which reduces vendor- and hardware-dependent differences. Finally, the study of ASD is approached dimensionally as well as from a traditional case-control perspective, revealing dynamic connectivity features of ASD that lie along a continuum in the general population. While many studies of ASD include only boys, our sample was sex-balanced and also

presented in the context of typical brain development. However, some limitations deserve mention. While increased scan duration is likely to reveal the complexity of dynamic connectivity states and their temporal aspects more accurately, our rsfMRI scan was limited to just over 5 minutes to ensure high quality data given the scale of the study and to minimize the burden on our young participants (White et al., 2014). Further, our study was cross-sectional and all participants were of school-age, so the interpretation of our results can not be extended to other stages of development. Longitudinal studies are warranted to reveal trajectories of dynamic connectivity in typical and atypical development.

In conclusion, our approach suggests that a hallmark of childhood is not limited to the under-development of the frontal lobe, but also about the efficient utilization of vast interconnections; in essence, younger children are less frequently tapping into the resources that they have. Also, children with higher levels of autistic traits are even less likely to efficiently use such connections and may have less capacity in this regard. This study revealed novel aspects of psychopathology and future studies should evaluate the utility of this methodology in, for example, the classification, evaluation and treatment response prediction of conditions like ASD.

CHAPTER 4

CONNECTIVITY DYNAMICS OF HEALTHY ADULTS AND PATIENTS WITH SCHIZOPHRENIA AND BIPOLAR

4.1 Connectivity and Dysconnectivity: Comparing Healthy and Diseased Brain

SZ and BP are two common psychiatric conditions characterized by gray and white matter abnormalities and disrupted connectivity across large-scale brain networks (Mohamed et al., 1999; Kubicki et al., 2007). Such dysconnectivity includes disruption of both structural (Kubicki et al., 2007; Rotarska-Jagiela et al., 2008, 2009) and FC (Meyer-Lindenberg et al., 2001; Uhlhaas and Singer, 2006; Calhoun et al., 2008a) that may be related to clinical symptoms, including cognitive dysfunction. SZ is often referred to as a dysconnection syndrome, where the term "dysconnection" refers to over- or under-connection of neural circuits with respect to a HC

group (Friston et al., 1993). Because changes in the function of a single brain region cannot explain the range of impairments observed in SZ or BP (Achim and Lepage, 2005; Van Snellenberg et al., 2006; Minzenberg et al., 2009; Ragland et al., 2009; Wang et al., 2009; Chepenik et al., 2010) researchers need to identify altered connectivity in relevant core brain networks.

Previous studies show both similarities and differences in static functional connectivity between SZ and BP. Most prior studies focused on quantifying the underlying characteristics of sensory, auditory, cognitive control and emotional processes of the brain. For example, the DMN network, consists of a set of brain regions known to be activated during internally focused tasks and may be involved in processes such as attention to internal emotional states, self-referential processing or task-independent thoughts (Buckner et al., 2008). DMN data may distinguish between SZ and BP (Calhoun et al., 2011; Öngür et al., 2010). There are numerous studies suggesting abnormal DMN connectivity in SZ and BP (Calhoun et al., 2011; Zhou et al., 2007; Calhoun et al., 2008b; Zhou et al., 2008), although both increased and decreased connectivity have been reported. Different analytical techniques could account for these inconsistent findings, as seed-based and data-driven analyses and varying preprocessing steps do not necessarily produce the same results. Also each intrinsic brain network comprises a collection of multiple network components, only a few of which might be affected throughout a specific period of illness. Here, we implement a recently published approach to assess functional network connectivity dynamics between HC and SZ and BP patients, which includes spatial GICA, dFNC via sliding time window correlation, and k-means clustering of windowed correlation matrices (Allen et al., 2012a). We hypothesized that disrupted functional integration in SZ and BP patients can be

found in several brain regions including temporal, frontal, visual, and DMN networks as suggested by previous studies. To test our hypothesis we conducted group difference analyses in connectivity using independent two sample t-tests. The results show that dynamic FNC captured by sliding time window analysis can reveal significant differences between patients and controls that cannot be found using conventional stationary FNC analysis.

4.2 Analysis Methods

4.2.1 Participants

We assessed 159 total subjects comprising 61 screened healthy subjects [HC, age 35.44 ± 11.57 (range), 28 females], 60 patients diagnosed with SZ or schizoaffective disorder (SZ, age 35.85 ± 12.01, 13 females) and 38 bipolar subjects (BP, age 38.96 ± 10.90, 20 females), matched for age with no significant differences among three groups, where age: p= 0.303, F= 1.2031, DF=2. Significant differences in sex among three groups were found, where sex: p= 0.002, $\mathbf{X}^2$= 11.81, DF=2. Diagnoses were based on detailed medical and psychiatric history, chart reviews, and the Structured Clinical Interview for DSM Disorders (First et al., 1997). None were acutely ill at the time of scanning. BP patients were a mixture of psychotic and non-psychotic by history.

4.2.2 Data Acquisition

rsfMRI scans were acquired at the Institute of Living, Hartford, CT, USA on a 3T Siemens Allegra head-only scanner with 40mT/m gradients and a quadrature head coil. T2*-weighted functional images were acquired using gradient echo planar imaging (EPI) method with repetition time (TR)=1.5 s, echo time (TE)=27ms, field of view=24 cm, acquisition matrix 64 $\times$ 64, flip angle=700, voxel size=3.75mm $\times$ 3,75mm $\times$ 4mm, slice thickness=4 mm, gap=1 mm, number of slices=29, 210 frames and ascending acquisition. Subjects were instructed to keep their eyes open, look at a fixation cross on a monitor display and to rest quietly during the scan session.

4.2.3 Data pre-processing

Functional images were pre-processed using an automated pipeline based around SPM 5. Pre-processing included the removal of the first four image volumes to avoid T1 equilibration effects, realignment using INRIalign (Freire et al., 2002), slice-timing correction using the middle slice as the reference frame, spatial normalization into MNI space, reslicing to 3 mm $\times$ 3 mm $\times$ 3 mm voxels, and smoothing with a Gaussian kernel (FWHM = 5 mm). Voxel timeseries were z-scored to normalize variance across space, minimizing possible bias in subsequent variance-based data reduction steps (Allen et al., 2012a).

In order to limit the impact of motion we excluded from analysis subject data with a maximum translation of $>$ 2 mm or with SFNR $<$ 275. Patient and control groups were age matched. Additional processing steps were taken to mitigate against residual motion effects as described later.

4.2.4 Group ICA and post-processing

Imaging data were decomposed into functional networks using a group-level spatial ICA (Calhoun et al., 2001b; Calhoun and Adali, 2012). Group ICA was performed using the GIFT toolbox (Calhoun et al., 2004a). In order to obtain functional parcellation, we used a high model order ICA (number of components, C=100) to decompose the functionally homogeneous cortical and subcortical regions exhibiting temporally coherent activity (Kiviniemi et al., 2009; Smith et al., 2009; Abou-Elseoud et al., 2010). In the subject-specific data reduction PCA step, 120 principal components were retained (retaining $> 99\%$ of the variance of the data). Group data reduction retained C= 100 PCs using the expectation-maximization (EM) algorithm as implemented in the GIFT toolbox. The Infomax group ICA (Calhoun et al., 2001c) algorithm was repeated 20 times in ICASSO (Himberg and Hyvarinen, 2003) and the resulting components were clustered to estimate the reliability of the decomposition (Himberg et al., 2004). Subject-specific SMs and TCs were estimated using the GICA1 back-reconstruction method based on PCA compression and projection (Calhoun et al., 2001c; Erhardt et al., 2011b). Out of the 100 components obtained, we characterized 49 components as ICNs that depicted peak cluster locations in gray matter with minimal overlap with white matter, ventricles and edges of the brain and also exhibit higher low frequency temporal activity. Subject specific TCs and SMs were obtained via back reconstruction.

Additional post-processing steps including linear, quadratic and cubic detrending, multiple regression of the six realignment parameters and their temporal derivatives, removal of detected outliers, and low-pass filtering with a high frequency cutoff of 0.15 Hz were applied to the component TCs in order to remove trends associated with scanner drift and movement-related artifacts. We have detected the

outliers based on the median absolute deviation, as implemented in 3D DESPIKE (Cox, 1996). Outliers were replaced with the best estimate using a third-order spline fit to the clean portions of the TCs.

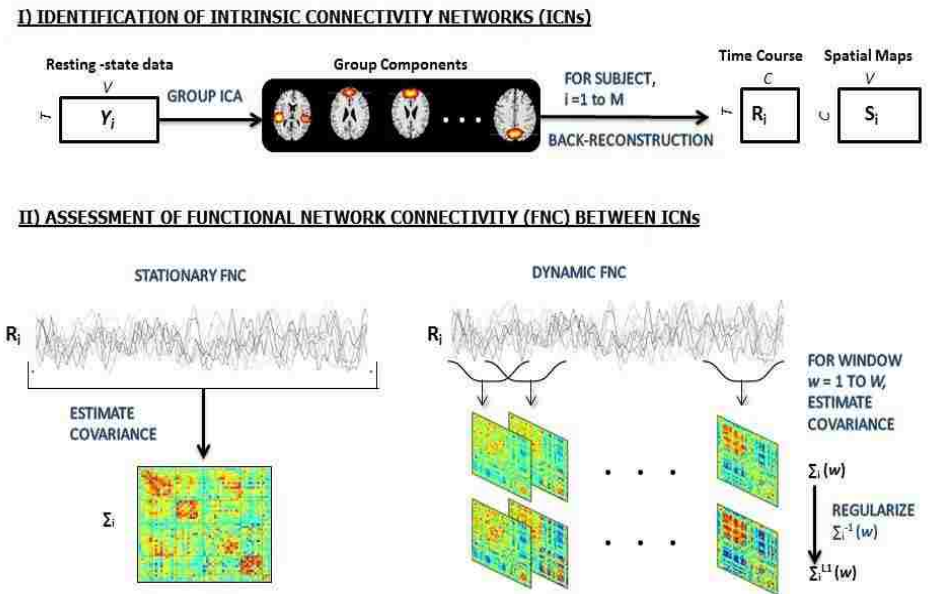

FIGURE 4.1: An overview of the sliding window analysis (Allen et al., 2012a).

4.2.5 FC estimation

The static FNC for each subject was estimated from the TC matrix, as the C × C sample covariance matrix (see Figure 4.1(I)). In addition to the standard FNC analyses, we computed correlations between ICN TCs using a sliding temporal window (Tukey window (see Figure 4.1(II)) having a width of 22 TRs=33 s; sliding in steps of 1 TR), resulting in W=180 windows to capture the variability in connectivity. To characterize the full covariance matrix, we estimated covariance from the regularized precision matrix or the inverse covariance matrix (Smith et al., 2011). Following the graphical LASSO method of (Friedman et al., 2008), we placed a penalty on the L1 norm of the precision matrix to promote sparsity. The regularization parameter lambda was optimized separately for each subject by

evaluating the log-likelihood of unseen data (windowed covariance matrices from the same subject) in a cross-validation framework. Final dynamic FC estimates for each window, were concatenated to form a C × C × W array representing the changes in covariance (correlation) between components as a function of time.

4.2.6 Dynamic states and clustering

From all of the dynamic windowed FNC matrices, we selected windows of higher variability as subject exemplars and used K-means clustering to obtain group centrotypes(see section 3.2.9 for details). We repeated the clustering method using different distance functions (correlation, cosine, rather than the L1-norm) and also found very similar results. We determined the number of clusters to be 5 using the elbow criterion of the cluster validity index. These centrotypes are then used as starting points to cluster all of the dynamic FNC data. Group specific centrotypes were computed. Subject specific centrotypes were used to perform independent sample t-tests to probe for group differences.

4.3 Results

4.3.1 Intrinsic Connectivity Networks (ICNs)

ICA was successfully used to identify the iICNs in HC and patients with SZ and BP, and to identify differences in functional network connectivity among these ICNs. The SMs of 49 ICNs identified with group ICA are shown in Figure. 4.2(A). Intrinsic connectivity networks are grouped by their anatomical and functional properties, which include the following: SC, AUD, SM, VIS, CC, DMN and CB

components. The observed ICN networks are very similar to those found in previous studies with low model order ICA (Calhoun et al., 2008a) as well as high model order ICA (Kiviniemi et al., 2009; Smith et al., 2009; Allen et al., 2011).

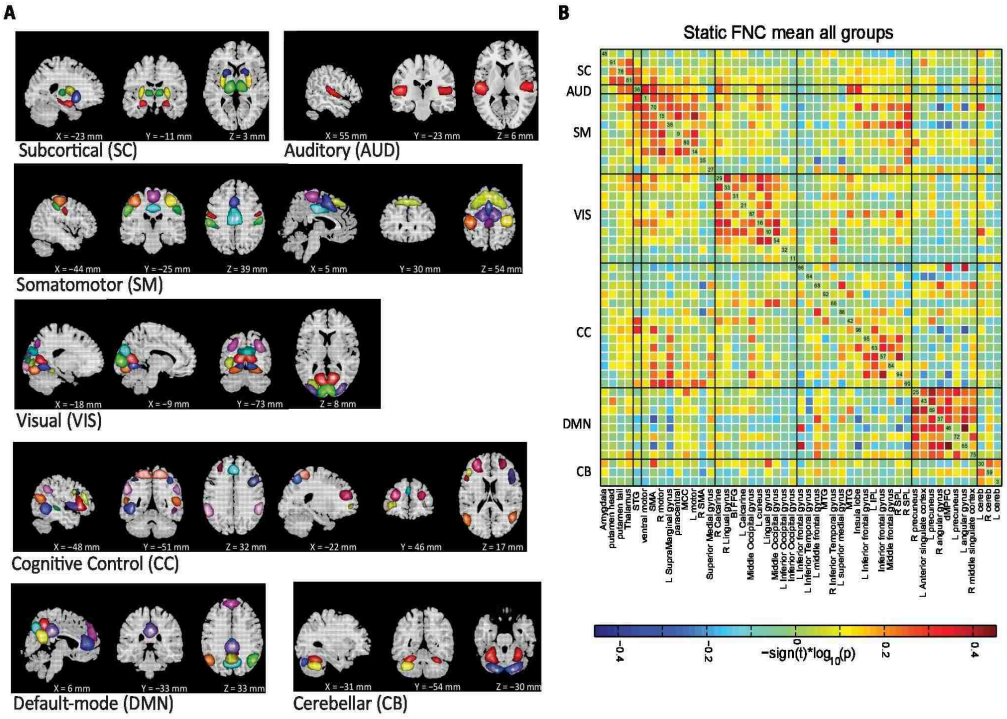

FIGURE 4.2: (A) Non-artifactual ICNs and (B) Group mean static FNC between ICN timecourses.

4.3.2 Static FNC

Group mean functional connectivity or sFNC between ICN TCs is shown in Figure.4.2(B). The ICN components in the static FNC matrix were initially ordered using algorithms in the brain-connectivity toolbox (Rubinov and Sporns, 2010) that maximize modularity of the connectivity matrix. These were manually partitioned into subgroups as in our earlier work (Allen et al., 2012a). The average connectivity matrix demonstrates strong positive connectivity within subcortical, visual, sensorimotor, default-mode and cerebellar networks. A set of CC regions also shows this positive connectivity among themselves and are also connected to

certain visual networks. These CC and visual regions show anti correlation to default-mode regions.

Two sample t-tests did not reveal any group differences in static or overall connectivity. Previous studies have found differences in FNC in similar groups, but not with such a high model order that produces more focus brain regions, but also more comparisons. In our case, several FNC pairs showed a trend level of significance, but did not quite reach a corrected level of significance for the static FNC analysis.

However, we also computed an analysis of FNC differences within groups of components (e.g. DMN components re-combined), called a network group (NG). To do this we computed, for each NG, the average connectivity between it and all other NGs (Repovs et al., 2011). We then applied an FDR correction for multiple comparisons of the between- NG connectivity. Several between-NG pairs showed significant group SZ/control differences, including sub-cortical and sensory-motor, sub-cortical and cognitive control, and default mode and cerebellum. One pair, sub-cortical and cognitive control, showed a significant difference between SZ and BP patients. No between-NG connectivity difference was found between HC and BP.

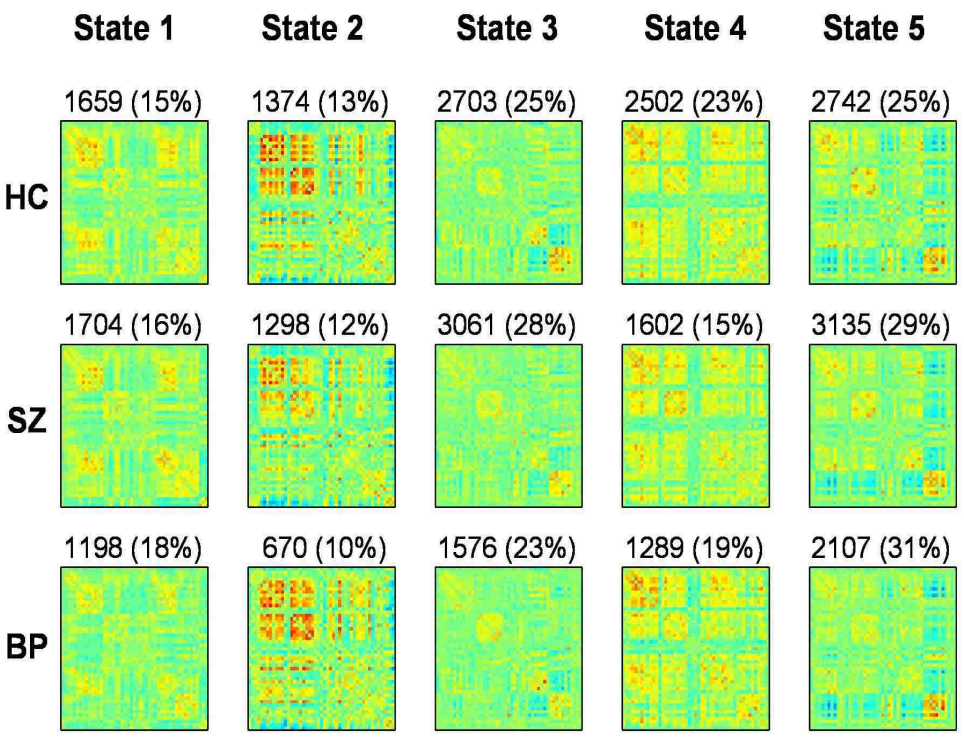

FIGURE 4.3: Group-specific dynamic FNC states obtained from clustering approach for k=5.The total number and percentage of occurrences is listed above each centroid.

4.3.3 Dynamic connectivity states and group differences

We use k-means clustering method to identify re-occurring pattern of FC states (Figure 4.3). We used the common states for all the groups to estimate differences in dynamic FNC. Dynamic FNC analysis suggests that patients make fewer transitions to some states (States 1, 2 and 4) compared to HC. Significant differences were found between groups in dynamic FNC states 1, 2, 3 and 4, between HC and patient groups as well as between SZ and BP patients.

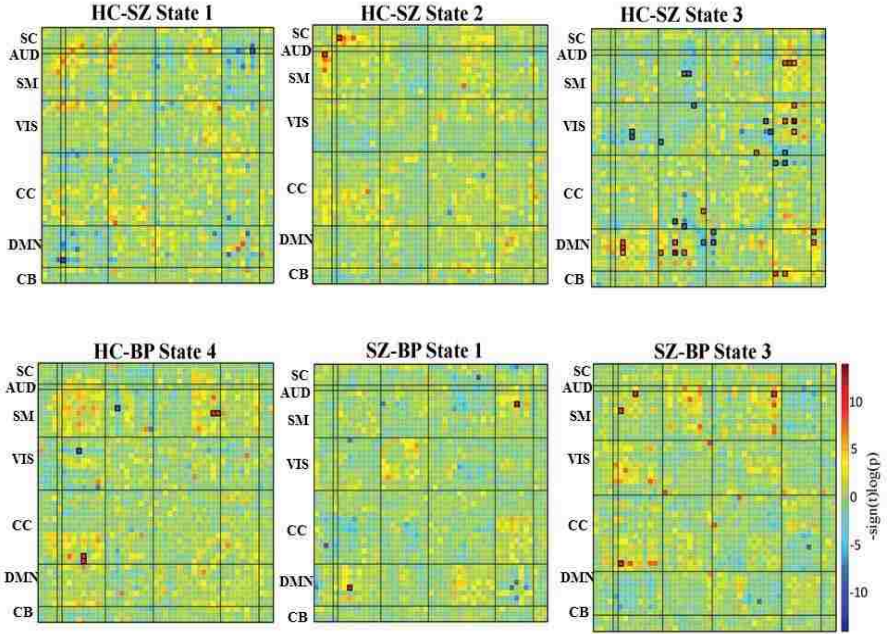

FIGURE 4.4: Group differences in dynamic FC states as obtained using an independent two-sample t-test between groups. The cells that have survived a FDR threshold for multiple comparison correction are enclosed in black patch.Note that, only the comparisons that survived FDR correction are presented here.

Figure 4.4 summarizes the difference between groups measured by the connectivity between ICN component pairs. For better visualization purpose, brain connectome for each of the significant dynamic states is shown in Figure 4.5. Also, Figure 4.6 shows the rendering maps for main effects of dynamic connectivity for all the subjects. To create the rendering maps, we first identified the modularity in the dynamic FC matrix for each state using the Brain Connectivity Toolbox (Rubinov and Sporns, 2010). For each component, the average connectivity within a module was computed and stored as "component weight vector". These positive or negative weights were then used to create weighted SM containing all contributing components for a given dynamic state, and finally the weighted SMs were projected onto a 3-dimensional MNI surface using the AFNI-SUMA (Saad et al., 2004).

In State 1, two component pairs captured the differences between HC subjects and SZ patients as well as between the two patient groups (Figure 4.4 and Figure 4.5). Compared to HC subjects, SZ patients showed greater connectivity between the component pair STG (C36) and left AG (C65), in the temporal-parietal region. Also compared to BP, SZ patients showed greater connectivity between two frontal components: right motor (C15) and dorso-medial prefrontal cortex or dMPFC (C46).

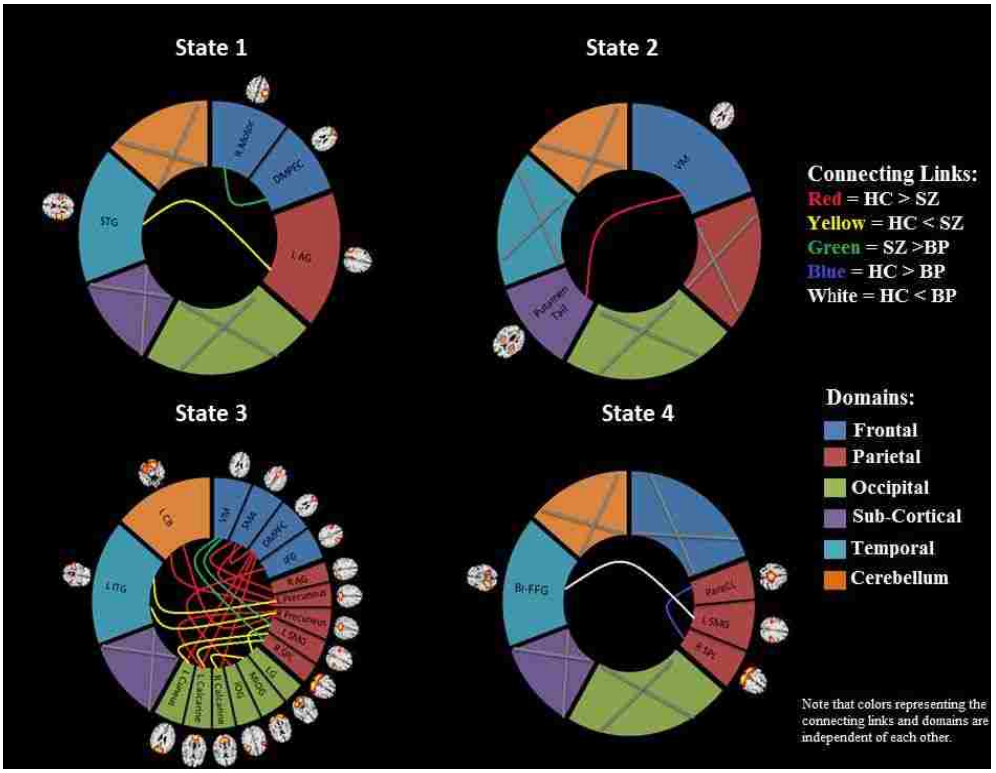

FIGURE 4.5: Connectograms showing a visual summary of significant connectivity differences in dynamic states between different ICN components for control and patient groups.

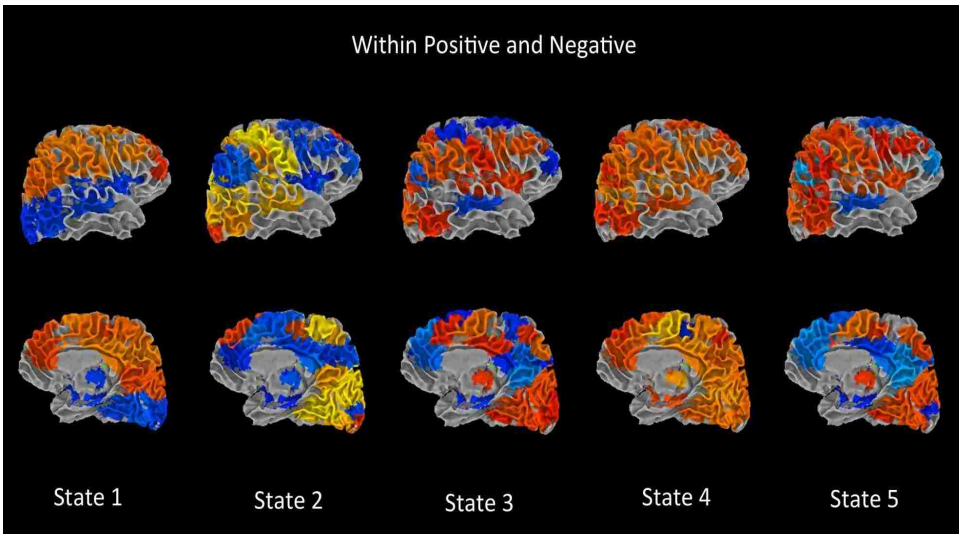

FIGURE 4.6: Main dynamic FNC effects depicted in rendering map using the AFNI-SUMA (Saad et al., 2004).

In dynamic connectivity State 2 (Figure 4.4 and Figure 4.5), HC showed greater connectivity between a sub-cortical component, putamen tail (C78) and a frontal component, ventral motor (C1), compared to the patients with SZ.

In dynamic State 3 (Figure 4.4 and Figure 4.5), most of the differences in connectivity were captured between HC subjects and SZ patients, and between the two patient groups . These connectivity differences were found in frontal, parietal, occipital, temporal and cerebellar regions of the brain. SZ patients showed greater connectivity between several temporal-parietal components, compared to HC. The connectivity between most of the frontal-parietal and frontal-occipital components was greater in HC compared to SZ patients, whereas the connectivity between most of the parietal-occipital components was greater in SZ patients. Also greater connectivity in SZ was found between two frontal-parietal component pairs, ventral motor and left supramarginal gyrus, and ventral motor and right superior parietal lobule, compared to BP. This is the only dynamic state that captured differences between these two patient groups.

Dynamic State 4 revealed differences between HC and BP patients in temporal and parietal regions, where greater connectivity in HC was found between two parietal components, paracentral and superior parietal lobule, and greater connectivity in BP was found between a temporal component bilateral fusiform gyrus and a parietal component left supramarginal gyrus. Dynamic State 5 did not display any significant group differences in functional connectivity. Also, no significant correlation between symptoms and connectivity was found.

4.4 Discussion

We explored dynamic FC patterns with ICA, sliding windows, and clustering. Our analysis of connectivity dynamics in a relatively large sample (n = 159) provides, to our knowledge, the first whole-brain characterization of regional differences in FC variability and distinction of discrete FC states among HC, SZ and BP patients. We identified several ICNs that differentiate SZ and BP from HC subjects.

Dynamic FC captures stable connectivity patterns that are not observed in the stationary FC. FC of the brain is not stationary; rather it's changing over time. Thus observing group-wise differences in connectivity across time as captured by the discrete dynamic states gives us more valuable information that cannot be found within the stationary or mean FC.

In Figure 4.3, each matrix represents the centroid of a cluster and signifies a connectivity state stably present within data. These dynamic connectivity states are fully reproducible and present in numerous subjects. Dynamic State 1 resembles the pattern of stationary FC. FC patterns in States 2-5 represent connectivity show considerable deviation from the mean FC.

One of the notable features that differ between FC states is the connectivity within DMN regions and, between DMN and other functional networks. In States 3 and 5, the DMN regions show strong synchronous activation with themselves, and mostly asynchronous activation with other functional networks. Particularly in State 3, the DMN regions show strong asynchrony with most of the CC components. State 5 shows the similar nature of connectivity between DMN and CC components, but with a reduced number of CC components. Also in States 3 and 5, several SM components show negative correlations with the DMN system, which is not visible in other states. In contrast, States 1, 2 and 4 do not show similar FC patterns between DMN and other ICN networks, where segregation of synchronized activation between DMN and other ICN nodes can be observed.

State 2 captures the FC differences between cortical and subcortical components, where strong asynchronous activation between SC regions (amygdala, putamen head, putamen tail and thalamus) and SM, AUD and VIS were found. CB also shows this asynchrony with these cortical regions. Also substantial reduction in connectivity between DMN regions can be observed in this state. As mentioned in several previous studies, reduced thalamocortical connectivity (Spoormaker et al., 2010), increased subcortical connectivity (Larson-Prior et al., 2011) and a segregation of DMN connectivity (Spoormaker et al., 2010; Larson-Prior et al., 2011) indicated a state of light sleep or drowsiness. Also similar dynamic state related to drowsiness was found among HC subjects in (Allen et al., 2012a).

In (Hutchison et al., 2013b), periods of hypersynchronization were described where extremely high intra-network connectivity between all nodes of oculomotor and motor networks were found in macaques and humans. This relates well to our observed discrete FC states where States 1,2 and 4 show time windows with high correlations throughout the motor system (and some motor components in State

5), while State 3 and 5 represent periods with synchronous activation between VIS areas. From our results, we can predict that periods of hypersynchronization between motor nodes would also include synchronous activation of default mode regions and segregated synchronous activation between the nodes in other ICNs. Also, we can predict that hypersynchronization between VIS areas will be accompanied by synchronization of DMN regions and strong asynchronous activation with other functional networks.

Note that, State 4 is the only dynamic state where we have found significant differences between HC and BP subjects. State 4 shows synchronous activity within most of the network nodes except few VIS and CC components, which show anti-correlation with themselves as well as with other ICN networks. The differences between HC and BP were captured between a pair of SM component (paracentral gyrus) and CC component(R SPL), and between a pair of SM component (left SMA) and VIS component (bi-fusiform gyrus (bi-FFG)).

The differences between groups are not localized in a single dynamic state. Rather the group differences are distributed across four dynamic states (States 1, 2, 3 and 4). This distributive nature of the group differences could be one reason they were not detected in the static FNC, since that metric only shows the average functional network connectivity for the run. Also the dynamic states in Figure 4.4 show higher p-values for several t-tests between ICN components for different groups, which did not pass multiple comparison correction tests. With a larger sample size, more significant group difference could be revealed.

Significant between-group differences in connectivity strength were found in several intrinsic networks including sub-cortical, visual, auditory, sensorimotor, cognitive control, default mode and cerebellum networks. Several components in the DMN

including dMPFC, right and left AG, and right and left preC showed significant connectivity differences with the components in VIS, CC , sensorimotor, AUD and CB networks. Previous studies suggest that DMN may distinguish SZ and BP patients from HC (Calhoun et al., 2011; Zhou et al., 2007; Calhoun et al., 2008b; Zhou et al., 2008). The majority of previous studies report reduced task-related suppression in the DMN in SZ (Zhou et al., 2007, 2008; Jafri et al., 2008; Bluhm et al., 2009; Jann et al., 2009; Kim et al., 2009; Park et al., 2009; Pomarol-Clotet et al., 2010; Wang et al., 2011). Studies showed that failure to deactivate default-mode regions corresponded to gray matter losses in the dorsal ACC and medial prefrontal cortex regions (Zhou et al., 2008; Pomarol-Clotet et al., 2010; Skudlarski et al., 2010; Salgado-Pineda et al., 2011). However, as mentioned earlier, both increased and decreased functional connectivity have been reported in the DMN in SZ. Medial prefrontal cortex is a region known to be associated with information processing when more than one course of action may be required, such as representing the thoughts, actions, and feelings of others across time (Gilbert et al., 2006). Several studies of both SZ and BP (Öngür et al., 2010; Meda et al., 2012; Khadka et al., 2013) have reported subgenual and medial prefrontal abnormalities in BP patients and dorsal medial prefrontal abnormalities in SZ patients. (Huang et al., 2010) reported decreased amplitude of low frequency fluctuation (ALFF) in the medial prefrontal regions in never treated SZ patients, and found to become normalized with antipsychotic therapy (Sambataro et al., 2010; Lui et al., 2010).

Another DMN component found in our analysis is the AG, which is known to be involved in language processing (Hall et al., 2005; Binder et al., 2009; Price, 2010; Clos et al., 2014), as well as memory and social cognition. Therefore, AG dysregulation can help differentiate SZ and BP patients from HC. Our study showed greater connectivity in SZ between the component pair STG and left AG. Notably,

several studies also found functional connectivity abnormalities in STG, which is a major part of the dominant hemisphere language network. Also both structural and functional abnormalities in the STG have been demonstrated in SZ patients in multiple studies as well as in psychotic BP and constitute the best-replicated brain differences correlating with the severity of psychotic symptoms in SZ, most specifically auditory hallucinations and formal thought disorder collectively; abnormalities in these regions likely underpin psychotic phenomena (Aguayo, 1990; Swerdlow, 2010; Fusar-Poli et al., 2011). In our study, group variations in connectivity strength were observed in several temporal lobe components (STG, bi-FFG) and left inferior temporal gyrus (ITG)), known to process auditory information Kim et al. (2009); Sui et al. (2011). This reinforces the fact that aberrant temporal lobe coherence patterns may exhibit significant abnormality in both SZ, and to a lesser extent BP (Calhoun et al., 2008b; Pearlson, 1997). These findings may be useful in explaining the language and thought disruptions in SZ.

Our study showed two other DMN components, left and right preC, which are involved in a wide spectrum of highly integrated tasks, including episodic memory (Cabeza and Nyberg, 2000; Rugg and Henson, 2002), mental imagery recall (Shallice et al., 1994; Gonzalo et al., 2000), and self-processing operations, such as first-person perspective taking (Cavanna and Trimble, 2006). In (Garrity et al., 2007), higher positive symptoms were correlated with increased deactivation in the medial frontal gyrus, preC and the left middle temporal gyrus (MTG). Compared to SZ patients, HC showed greater connectivity between left cerebellum and both left and right preC. The cerebellum may influence motor systems by estimating inconsistencies between intention and action and by adjusting the motor operations appropriately (Kandel et al., 2000), as well playing a role in cognition and

emotion (Schmahmann and Caplan, 2006). Prior studies reveal impaired functional integration of cerebellum in SZ (Honey et al., 2005; Becerril et al., 2011). (Collin et al., 2011) proclaimed the functional connectivity to other brain regions (left thalamus, middle cingulate gyrus and SMA) to be disconnected from the cerebellum in SZ patients.

In our study, several sensorimotor components including SMA, right and left motor, ventral motor (VM), SmG and paracentral showed between-group connectivity differences that were distributed across different dynamic states. (Jeong et al., 2009) reported decreased correlation of the left inferior frontal gyrus (IFG) with left MTG/ left superior temporal sulcus, left SPL/ SmG and other brain regions. Our results showed connectivity differences between SmG and other brain components (with lingual gyrus (LG) in HC<SZ; with VM in SZ>BP; with bi-FFG in HC < BP). Previous studies found impaired functional connectivity between cerebellum and LG in SZ patients (Collin et al., 2011).

Other findings in our analysis include connectivity differences in several cognitive control components (left ITG, left MFG, MTG, left IFG, left superior medial gyrus (SMG), and SPL) with components from other brain networks. Abnormal functional connectivity in left IFG, MFG and IFG was found in SZ patients (Jeong et al., 2009; Müller et al., 2013).

Another key finding in our study is greater connectivity in HC between putamen tail and ventral motor regions, compared to SZ patients. The putamen may be involved in the generation of spontaneous language, and linked to auditory/verbal hallucinations (Hoffman and Hampson, 2012). Several SZ studies showed functional connectivity anomalies in the putamen (Hoffman and Hampson, 2012; Hoffman et al., 2011; Tu et al., 2012).

4.5 Limitations and Future Directions

Several experimental and methodological limitations must be considered while performing the sliding-window analysis method and interpreting results. One limitation is that the non-stationary noise sources in fMRI time series can influence changes in FC over time. Synchronous global modulations of fMRI time series can be caused by variations in respiratory and cardiac rates, as they predominantly occupy the low frequencies (<0.1 Hz) (Wise et al., 2004; Chang and Glover, 2009). Also head motion could generate spatially structured artifacts in FC (Power et al., 2012; Yan et al., 2013). Even though ICA reasonably separates the component sources for sliding-window analysis, it may not have completely separated the effects from other sources of interest. Therefore, to interpret the dynamic results, efficient denoising as well as recording of respiration and cardiac events should be considered. In the current study we performed careful quality control as well as incorporating multiple motion regression steps to mitigate against the impact of motion.

Another important issue for sliding-window analysis is the choice of window size. (Sakoğlu et al., 2010) reported that the ideal window size should be able to estimate FC variability and capture the lowest frequencies of interest in the signal, as well as to detect interesting short-term effects. In this study, dynamics were estimated using an empirically validated fixed sliding-window of 22TRs (33s) similar to that used in (Allen et al., 2012a). Future work should evaluate changes across a variety of windows lengths that could be performed using separate windows (Cribben et al., 2012) or perhaps combined with multi-scale approaches such as wavelet transform (Chang and Glover, 2010).

Several recent studies on microstate-based EEG-fMRI resting-state datasets have showed that EEG microstates and some number of fMRI-based ICNs show correspondence between themselves (Britz et al., 2010; Musso et al., 2010; Yuan et al., 2012). A brain microstate can be defined as a functional/physiological state during which specific neural processes occur (Musso et al., 2010). Using concurrent EEG-fMRI data, the underlying physiological correlates of these dynamic states can be well assessed as demonstrated in (Allen et al., 2013).

We characterized FC as the covariance between ICN TCs. Characterization of FC matrices based on higher-order statistics (e.g. mutual information) or lag-insensitive measures (e.g. cross-correlation) could efficiently recover the underlying biological structure of networks. Another limitation of the study is that smaller acquisition parameters may not lead to optimum results by exploring all possible aspects of dynamic changes in FC. Each subject in this study was scanned for only 5 minutes, which is probably not optimal for considering the rate of change in dynamic states. A longer acquisition time ($\sim$ 10 min) is recommended for a more accurate estimation of connectivity dynamics. To identify centroids of dynamic FC we used k-means clustering, which has several limitations, including difficulty in separating clusters with different sizes and densities, and a high susceptibility to outliers. Future work could include application of alternative clustering models (fuzzy-clustering or density-based clustering techniques) in the connectivity dynamics. Future work focusing on an improved understanding of the association between disease and connectivity dynamics could actually enrich our knowledge of the dynamic properties of the healthy functional brain. In addition, recent work has shown that there are time-varying changes not only in the covariance but also in the associated spatial patterns (Ma et al., 2014). Future studies to characterize both covariance and spatial changes over time are warranted.

4.6 Conclusion

We have performed, to our knowledge, the first whole-brain characterization of intrinsic regional differences in FC variability and a comprehensive analysis of discrete FC states in SZ, BP and HC subjects. One key finding was the aberrant functional connectivity patterns found in several DMN components including dMPFC, bilateral AG, and bilateral preC, in the patient groups. Other significant findings include connectivity anomalies in VIS, SM and CC networks in both patient groups. These findings could be used as distinctive characteristic markers in SZ and BP, and also could help diagnose the patients based on their biological features, rather than exclusively depending on cross-sectional clinical symptoms and information on longitudinal course and outcome.

CHAPTER 5

CLASSIFICATION OF MENTAL DISORDERS USING FUNCTIONAL NETWORK CONNECTIVITY FEATURES

5.1 Brain Connectivity Features for classification

In this work, we conducted a classification study of SZ, BP and HC subjects using static and dynamic FNC features, as well as combined FNC features from both FNC analyses. Several previous studies have shown that SZ and BP patients can be discriminated at group-level by using the information on dysfunctional integration of the brain (Allen et al., 2012a; Arbabshirani et al., 2013a; Rashid et al., 2014; Damaraju et al., 2014b; Friston, 2002). We hypothesized that disrupted functional integration in SZ and BP patients as captured by FNC analysis reveal powerful information for automatic discriminative analysis at subject-level. We expected some connectivity measures to be better captured in a static model and others in a dynamic model (Damaraju et al., 2014b). Static FNC provides information

about the overall mean connectivity and may be more optimal for connectivity that is persistent across the entire experiment than a dynamic FNC approach. On the other hand, information on local connectivity changes at different time windows will be better captured by dynamic FNC. Thus, we hypothesize that both static and time-varying FNC methods capture complementary aspects of connectivity, and combining static and dynamic FNC features will improve classification performance beyond the achievable performance from each type of these features individually. We present machine learning techniques to effectively combine these two types of features for accurate classification of SZ, BP and HC.

5.2 Analysis Methods and Proposed Approaches

Data acquisition, pre-processing, GICA analysis and post-processing, and FNC estimation are described in sections 4.2.1, 4.2.2, 4.2.3, 4.2.4 and 4.2.5.

5.2.1 Classification framework

We evaluated the classification performance for static FNC, dynamic FNC and a combination of both static and dynamic FNC (see Figure 5.1 for illustration of the proposed approaches). Our main focus was to extract reliable features from the FNC matrices and apply proposed classification methods, rather than investigating the performance on different classifiers. For all of the FNC-based classification approaches, we used a linear SVM classifier to evaluate the classification performance.

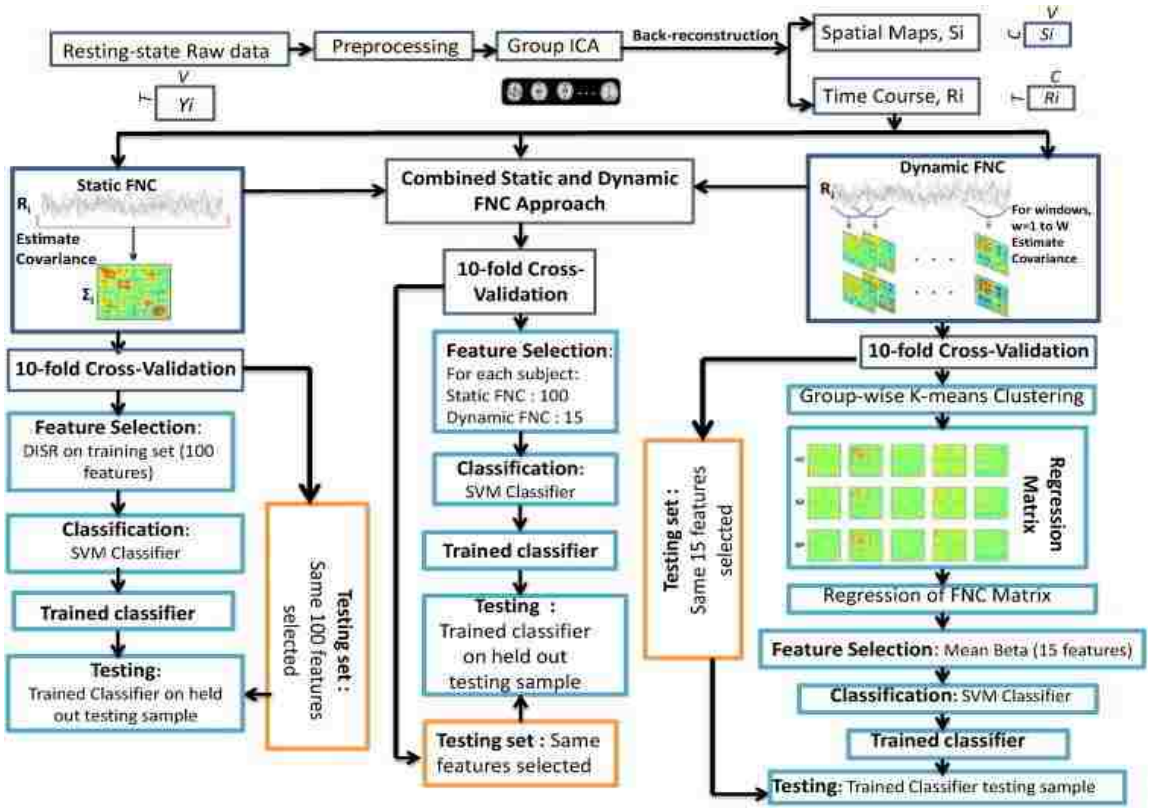

FIGURE 5.1: An overview of proposed classification approach.

5.2.1.1 Static FNC approach

In order to reduce the dimensionality and extract reliable features from this high-dimensional feature vector, we used the double input symmetric relevance (DISR) method (Meyer and Bontempi, 2006) during the cross-validation step. DISR is a mutual information based method which is designed to extract features by finding a combination of variables that can return more information on the output class than the sum of the information returned by each of the variables taken individually. For classification using SFNC features, the DISR method was run once per cross-validation fold. We used a 10-fold cross-validation strategy for estimating the generalization error of the proposed classifier. The details on the feature selection

process using DISR are given in the Figure B.1 and section B.1. In each cross-validation run, 100 features were selected using the DISR method from the training samples. A linear SVM classifier was then trained using the features from training data and then tested on held out testing samples (the same 100 features were selected from the testing data).

Algorithm 1: classification based on static FNC features

1. Estimate static FNC matrices for all the subjects using corresponding ICA time-courses.

2. Define the 10-fold cross validation groups as G_{HC}, G_{SZ} and G_{BP} by first performing a single split of the data into 10 folds, where each fold comprises 6 subjects from the HC group, 6 subjects from the SZ group and 4 subjects from the BP group. These subjects form the testing set (16 testing subjects at each iteration). The remaining subjects comprised the training set for each iteration. We define this step as "test step".

3. For dimensionality reduction and feature selection, apply DISR method and select the top 100 static FNC features (F_{DISR}).

4. Using the selected F_{DISR} features, train a linear SVM classifier.

5. With the left out testing subjects in Step 2, build the testing set and select those identified F_{DISR} features using the DISR method.

6. Classify the subjects in the testing set using the trained classifiers and record the classification performance.

7. Return to Step 2 (test step) and repeat Step 2 through Step 6 in order to iterate over all cross-validation folds.

5.2.1.2 Dynamic FNC approach

For classification using the dynamic FNC matrix, we also used a 10-fold cross-validation for estimating the generalization error. In each cross-validation run, we performed group-wise k-means clustering on dynamic FNC matrix from the training samples. For each of the three groups, we obtained 5 cluster centroids or states. We then grouped these states together and formed a regression matrix with 15 states in total. We call these 15 states the feature states. Note that at each time point the FNC matrix is assumed to be a linear combination of these states. Then for each FNC time point, we regressed out the dynamic FNC matrix against these 15 feature states and obtained the corresponding regression coefficients. We used the mean of these regression coefficients and finalized 15 features for each subject for classification. Details on dynamic feature selection method are provided in the Figure B.2 and section B.2. A linear SVM was then trained using the training features and then tested on held out testing samples.

Algorithm 2: Classification based on dynamic FNC features

1. Estimate dynamic FNC matrices for all the subjects using a windowed FNC approach (Allen et al., 2012a; Rashid et al., 2014; Calhoun et al., 2014).

2. Define the 10-fold cross validation groups as G_{HC}, G_{SZ} and G_{BP} by first performing a single split of the data into 10 folds, where each fold comprises 6 subjects from the HC group, 6 subjects from the SZ group and 4 subjects from the BP group. These subjects form the testing set (16 testing subjects at each iteration). The remaining subjects comprised the training set for each iteration. We define this step as "test step".

3. Apply group-wise k-means clustering to the windowed FNC matrices of the training groups. Based on the elbow criterion, select the optimum number of cluster centroids per group (dynamic connectivity states). In our dynamic FNC analysis the optimum number of cluster centroids was 5 per group.

4. Form a regression matrix, $R_{groups \times entroud}$ centroids with these group-specific cluster centroids.

5. Regress out the windowed FNC matrices at each time points using the regression matrix. Record the beta coefficients, β, at each time window. In our analysis, we estimated and saved 15 β coefficients for each time window.

6. Compute the mean β coefficients for all the time windows for each subject. In our analysis, we have 15 mean β coefficients for each subject. These mean β coefficients are the dynamic FNC features, Feat_{dFNC}, for the classification analysis.

7. Using these Feat_{dFNC} features, train a linear SVM classifier.

8. With the left out subjects in test step (Step 2), build the testing set and select the testing features by computing mean β coefficients using the same approach as training data.

9. Classify the testing subjects using the trained classifiers and record the classification performance.

10. Return to Step 2 (test step) and repeat Step 2 through Step 9 to iterate over all of the cross-validation folds.

5.2.1.3 Combined static and dynamic FNC approach:

For the combined static and dynamic FNC approach, 100 features from static FNC feature vector after dimensionality reduction (as mentioned above in static FNC approach section), and 15 beta coefficient features from the dynamic FNC after regression against the states (obtained similar way as mentioned in dynamic FNC approach section) were used for classification purpose. Also SVM classifiers and a 10-fold cross-validation strategy were applied in a similar way as mentioned above for other two classification approaches.

Algorithm 3: Classification based on both static and dynamic FNC features

1. Estimate both static and dynamic FNC matrices for all the subjects as mentioned in algorithm 1 and algorithm 2.

2. Define the 10-fold cross validation groups as G_{HC}, G_{SZ} and G_{BP} by first performing a single split of the data into 10 folds, where each fold comprises 6 subjects from the HC group, 6 subjects from the SZ group and 4 subjects from the BP group. These subjects form the testing set (16 testing subjects at each iteration). The remaining subjects comprised the training set for each iteration. We define this step as "test step".

3. To select static FNC features for the training set, follow these steps:

   (a) For dimensionality reduction and feature selection, apply DISR method on the static FNC of the training set and select top 100 static FNC features, FeatsFNC.

   To select dynamic FNC features for the training set, follow these steps:

(a) Apply group-wise k-means clustering to the windowed FNC matrices of the training groups. Based on elbow criterion, select the optimum number of cluster centroids per group (dynamic connectivity states). In our dynamic FNC analysis the optimum number of cluster centroids was 5 per group

(b) Form a regression matrix, $R_{groups \times entroud}$ with these group-specific cluster centroids.

(c) Regress out the windowed FNC matrices at each time points using the regression matrix. Record the beta coefficients, β, at each time window. In our analysis, we have recorded 15 β coefficients for each time window.

(d) Compute the mean β coefficients for all the time windows for each subject. In our analysis, we have 15 mean β coefficients for each subject. These mean β coefficients are the dynamic FNC features, Feat_{dFNC}, for the classification analysis.

4. Combine both Feat_{sFNC} and Feat_{dFNC} features for the training set, $\text{Feat}_{sFNC+dFNC}$

5. Using these $\text{Feat}_{sFNC+dFNC}$ features, train a linear SVM classifier.

6. With the left out subjects in step 1, build the testing set and select the testing features as follows:

(a) select same F_{sFNC} features using DISR method as mentioned for the training data.

(b) select F_{dFNC} features by computing mean β coefficients using the same approach as training data.

(c) Combine these F_{sFNC} and F_{dFNC} features for the testing set.

7. Classify the testing subjects using the trained classifiers and record the classification performance.

8. Return to Step 2 (test step) and repeat Step 2 through step 7 to iterate over all of the cross-validation folds.

5.3 Results

5.3.1 Intrinsic Connectivity Networks

ICA was successfully used to decompose the functionally homogeneous cortical and subcortical regions with temporally coherent activity. Out of the 100 components obtained, we characterized 49 components as ICNs that depicted peak cluster locations in gray matter with minimal overlap with white matter, ventricles and edges of the brain and also exhibit higher low frequency temporal activity . We used the time-courses of these 49 ICNs to compute static and dynamic FNC matrices. The spatial maps of 49 ICNs identified with group ICA are shown in Figure 5.2. ICNs are grouped by their anatomical and functional properties, which include the following: sub-cortical (SC), auditory (AUD), visual (VIS), sensorimotor (SM), cognitive control (CC), default mode (DM) and cerebellar (CB) components. The observed ICN networks are very similar to those found in previous studies with low model order ICA (Calhoun et al., 2008a) as well as high model order ICA (Kiviniemi et al., 2009; Smith et al., 2009; Allen et al., 2011).

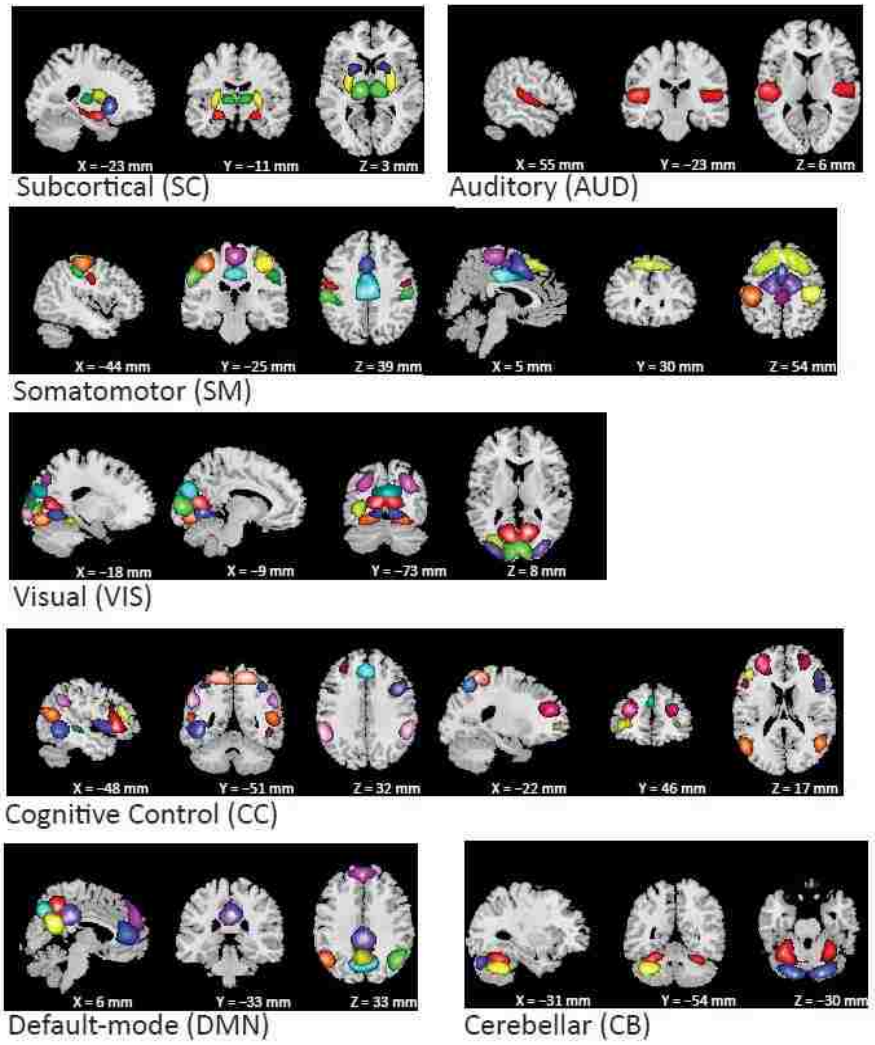

FIGURE 5.2: Thresholded group mean spatial maps of 49 ICNs.

5.3.2 Static FNC Features

For the static FNC classification algorithm, first we computed the pair-wise correlation (covariance) between the time-courses of 49 ICNs for each subject. Thus, for static FNC, each subject has a feature vector containing $\binom{49}{C_2}$=1176 elements, resulting in a high-dimensional FNC matrix for all the subjects (subject$\times$ FNC =159 $\times$ 1176). Out of these 1176 static FNC features, we then extracted top 100 contributing pair-wise correlations or static FNC features between ICNs using DISR. Figure 5.3 highlights the top 15 contributing features used from HC, SZ

and BP groups for classification analysis using static FNC (for simplicity we are only showing top 15 static FNC features). Both positive and negative connectivity between these top components were found. This figure summarizes the connectivity strengths between the top component pairs, by dividing them into brain networks. Here, static FNC component pairs that showed connectivity differences across groups include connectivity between putamen and inferior occipital gyrus (IOG), ITG and SmG, inferior frontal gyrus (IFG) and SPL, interior parietal lobule (IPL) and middle cingulate cortex (MCC), lingual gyrus (LG) and SMA, insula and calcarine, and IOG and postcentral gyrus. Also, detailed information for each spatial map such as regions of activation, Brodmann area, volume and peak activation t-value and coordinates for top 15 components are provided in Tables 5.3 and 5.4.

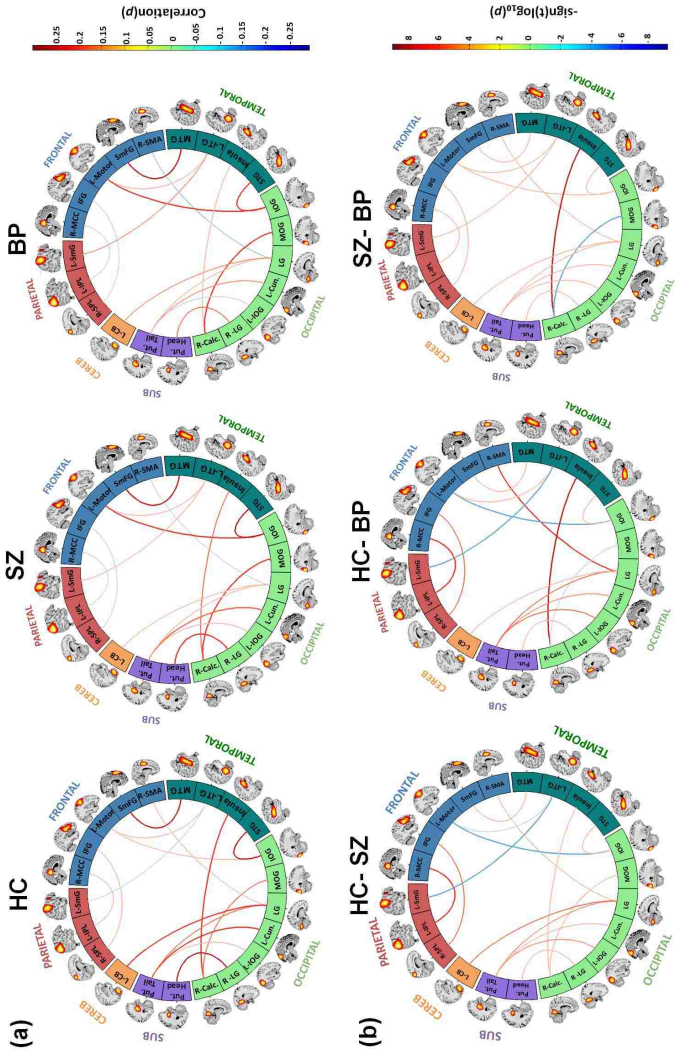

FIGURE 5.3: Connectograms showing top 15 static FNC features (a) across groups, and (b) their group differences.

5.3.3 Dynamic FNC features FNC estimation

For dynamic FNC analysis, we first applied the sliding-window approach (Allen et al., 2012a; Rashid et al., 2014) and computed the pair-wise correlation between the time-courses of 49 ICNs at each dynamic window (see section 2.5), resulting into a dynamic FNC matrix, (subject×time×FNC =159×180×1176). We then obtained the dynamic FNC features by regressing out the dynamic FNC matrix against the feature states (formed by the regression matrix) at each FNC time point, and computing the mean beta coefficients for each subject. For more details on dynamic FNC feature selection method, see section B.2.

The k-means clustering was applied and 5 centroids were obtained for each of the HC, SZ and BP groups at each CV run. For each of the groups and for each of the 5 dynamic states, we computed the correlation between dynamic states. These group-wise centroids almost always showed very high correlations across all the CV runs. Table B.1 provides the mean correlation for each of the dynamic states computed across 10 CV runs.

Figure 5.4 displays the training and testing dynamic FNC features. In figure 5.4A (top), the group-wise mean training beta coefficients and figure 5.4A (bottom) the bar plot showing group-wise mean training features (represents the summary of the information provided in figure 5.4A (top)) for 15 feature states have been presented. While the plot on the top of figure 5.4A is showing the actual values, the bar plots are showing these information in an average sense. Recall that, we combined the 5 dynamic states for each group and formed a regression matrix with a total of 15 states (feature states) for all three groups. Based on the formation of our regression matrix, HC group is expected to dominate between state 1 and state 5 in terms of dFNC feature values. Similarly we expect the SZ and BP groups to

show dominating dFNC feature values between state 6 and state 10, and between state 11 and state 15, respectively. We will also refer to the states ranging from 1 to 5 as HC feature states, 6 to 10 as SZ feature states, and 11 to 15 as BP feature states.

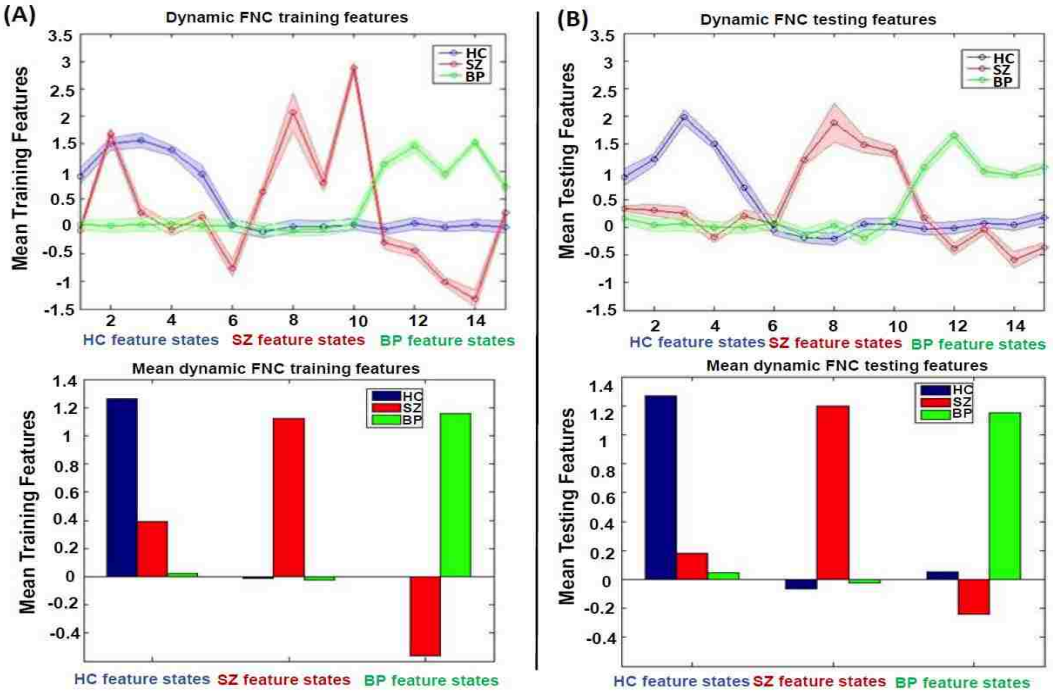

FIGURE 5.4: Mean training and testing features for dynamic FNC classification approach.

From figure 5.4A (top), we can see that the HC group shows greater mean beta values (i.e. more dynamic FNC feature values) for the HC feature states, and nearly zero for all other feature states. The bar plot in figure 5.4A (bottom) also confirms this trend where the mean beta value of the HC group for the HC feature states is 1.26 and nearly zero for the SZ and BP feature states. It was expected that the SZ group would show dominating feature values in SZ feature states, and nearly zero values for other feature states. However, the SZ group shows a mean of 0.39 in HC feature states, 1.12 in SZ feature states, and negative -0.56 in BP feature states. Also in the bar plot, BP group shows a mean beta value of 1.16 in BP feature states.

Similar trends for mean dFNC features in the testing set were found, and shown in figure 5.4(B). Here, HC group shows a mean beta value of 1.26 in HC feature states and nearly zero value otherwise. Similarly, the SZ group showed a mean feature value of 0.18 for the HC feature states, 1.2 for the SZ feature states, and -0.24 for the BP feature states. Also, the BP group shows a mean beta value of 0.05 for the HC feature states, -0.02 for the SZ feature states, and 1.15 for the BP feature states.

5.3.4 Classification Framework

Table.5.1 shows the confusion matrices for proposed classification approaches using static, dynamic and combined FNC features as obtained from the 10-fold cross-validation framework. Also, using the confusion matrices we computed: overall classification accuracy, group-wise sensitivity, specificity, positive predictive value (PPV) and negative predictive value (NPV) with Wilson's binomial 95% confidence interval (CI) (Wilson, 1927) (Table 5.2 and figure 5.5.)

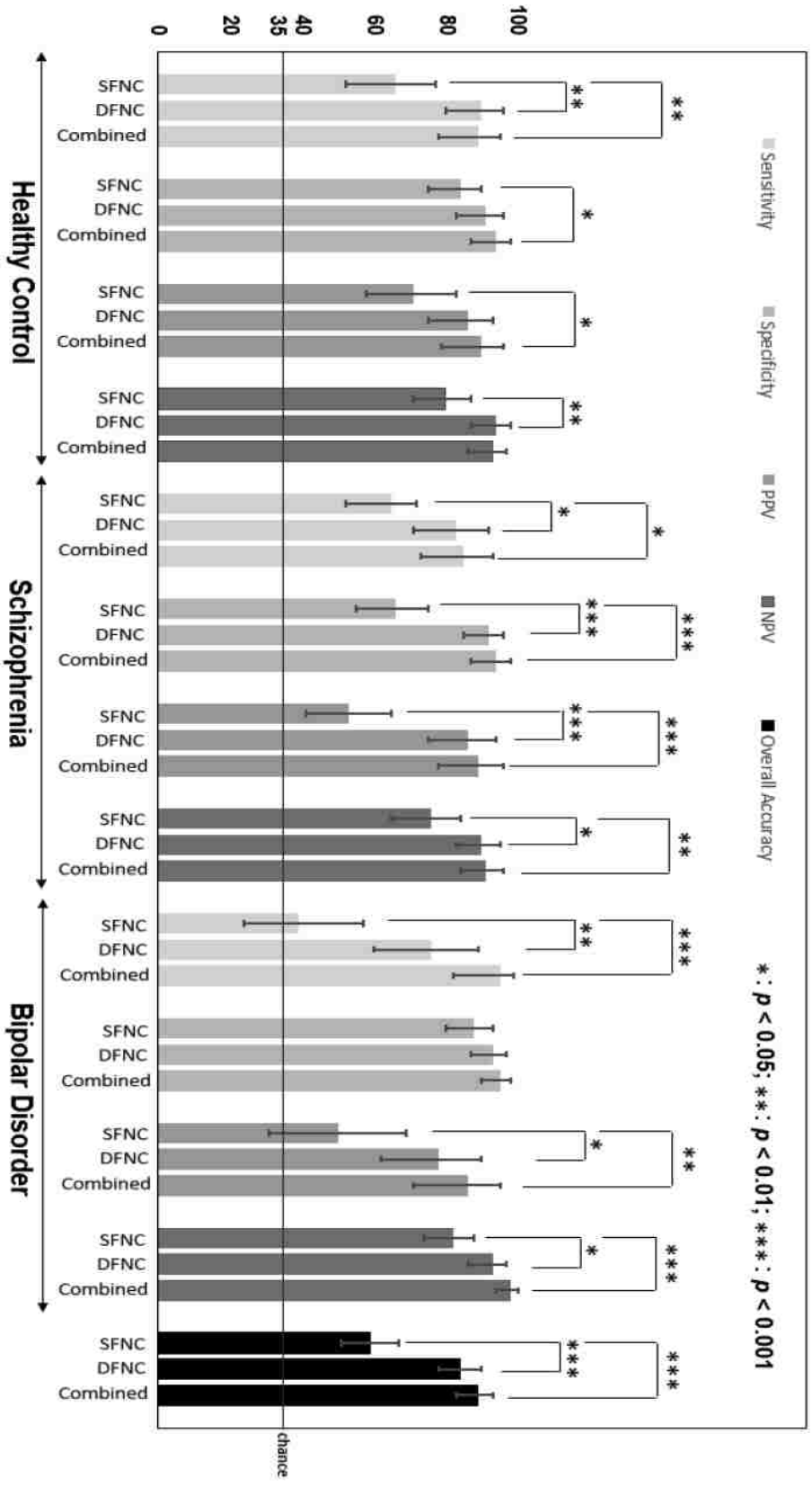

FIGURE 5.5: Performance evaluation of proposed classification approaches.Here, PPV=positive predictive value and NPV=negative predictive value.

TABLE 5.1: Confusion matrices using different FNC classification approaches

		Static FNC Approach (Predicted Class)			Dynamic FNC Approach (Predicted Class)			Combined Static and Dynamic FNC Approach (Predicted Class)		
		HC	SZ	BP	HC	SZ	BP	HC	SZ	BP
True Class	HC	40	18	3	55	3	3	54	5	2
	SZ	9	39	12	5	50	5	5	51	4
	BP	7	16	15	4	5	29	1	1	36

The static FNC approach shows an overall classification accuracy of 59.12% and CI of [51.05, 66.84]. The dynamic FNC approach showed an overall classification accuracy of 84.28% and CI of [77.67, 89.56]. The combined static and dynamic FNC approach showed an overall accuracy of 88.68% and CI of [82.7, 93.15]. The results from statistical significance levels among three classifiers for these statistical measures are provided in figure 5.5.

To determine the chance levels (see section B.3 and Figure B.3 for details) for individual classifier accuracy, we performed 300-run permutation tests in a 10-fold cross-validation framework . Our results show that, for classifiers using sFNC, dFNC and combined FNC features, the average accuracy is around 35% (sFNC=34.88%, dFNC=34.56% and Combined=34.82%), which is very close to the random chance level (33.33%).

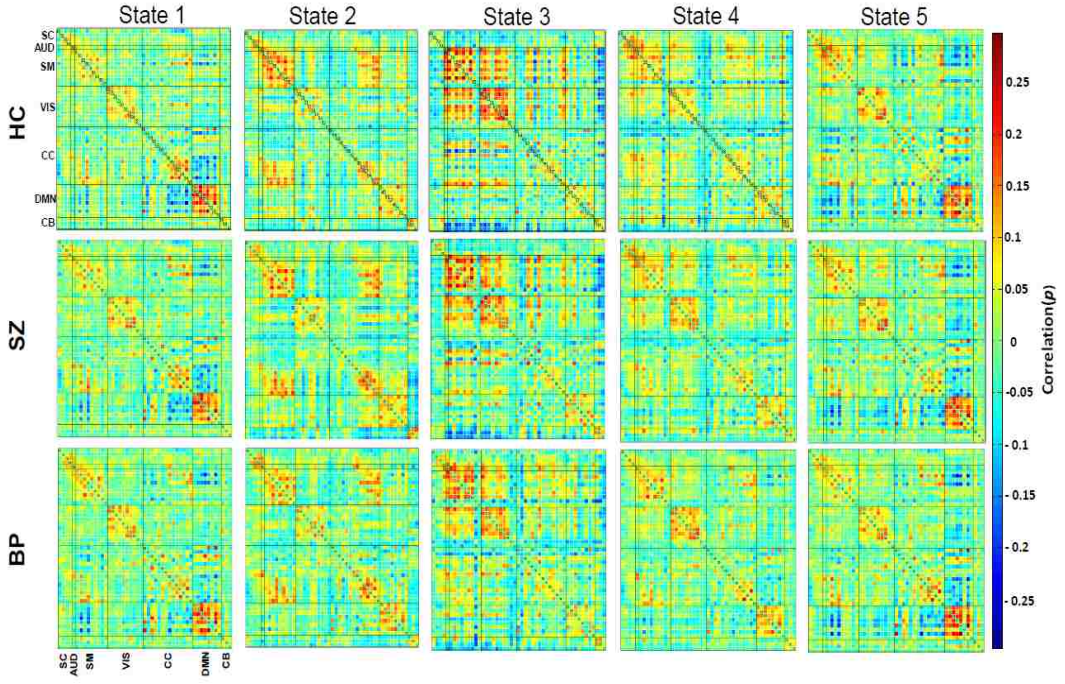

FIGURE 5.6: Dynamic states for three groups averaged across all 10 cross-validation folds.

5.4 Discussion

We investigated whether resting-state FNC features are able to discriminate between SZ patients, BP patients and HC subjects. Using ICA, the dataset was decomposed into independent subject-specific SMs and corresponding TCs. Both static and dynamic FNCs were computed between each pair of functional networks. For dynamic FNC, the time-course of each subject was windowed and then clustered into discrete dynamic states. For all classification approaches, SVM classifiers were trained and then evaluated using a 10-fold cross-validation framework.

In our classification approach using static FNC, top static FNC features show group differences in both connectivity strength (greater or weaker connectivity) and directionality of connectivity (positively or negatively connected). Note that, in this study we did not perform any univariate test between component pairs to investigate significant group differences. Our static classifier differentiates the subjects at a multivariate level by considering the whole pattern from static features.

Component pairs that show differences in the directionality of connectivity between control and patient groups include IFG (frontal component) and SPL (parietal component) (controls showing positive connectivity and both patient groups showing negative connectivity), IPL (parietal component) and MCC (default-mode component) (controls showing positive connectivity and both patient groups showing negative connectivity), LG (occipital component) and SMA (frontal component) (controls showing positive connectivity and both patient groups showing negative connectivity), and ITG (temporal component) and SmG (parietal component) (controls showing negative connectivity and both patient groups showing positive connectivity).

Another top component that differentiated BP from HC and SZ groups is putamen head and IOG (occipital component) (HC and SZ showing positive connectivity and BP showing negative connectivity). Other component pairs that showed differences in connectivity strength across groups include insula (temporal component) and calcarine gyrus (HC showing greater connectivity, SZ showing weaker connectivity, and BP showing the weakest connectivity), and IOG and postcentral gyrus (both patient groups showing greater connectivity than control group).

Note that, the temporal lobe has consistently been shown to play an important role in discriminating between HC subjects and patients with SZ and BP (Altshuler et al., 2000; Calhoun et al., 2008b; Johnstone et al., 1989). Previous functional connectivity studies also showed abnormal fronto-temporal functional connectivity in SZ (Wolf et al., 2007; Spoletini et al., 2009; Ford et al., 2002b). However, to further link the findings to prior literature and speculate about how connectivity in these top features relates to SZ symptoms, information such symptom profiles for SZ patients are required

Interestingly, in the dynamic FNC classification approach, SZ shows dominating feature values for the non-SZ feature states (Figure 5.4). This supports the overlapping findings of the SZ group with both HC and BP groups. Our dynamic FNC approach was able to utilize this characteristic of the SZ group to reliably differentiate them from the HC and BP groups.

Figure 5.6 shows the 15 dynamic states averaged across 10-fold runs. These dynamic states show distinct patterns such as DMN showing strong positive within-network correlation and negative between-network correlation with AUD, SM and CC (state 1 and 5), negative correlation between SC and AUD, VIS and SM networks (state 3). Among these dynamic states, several similar states were found

in the previous studies. For example, similar dynamic states as states 1, 3 and 5 were found in (Damaraju et al., 2014b; Allen et al., 2012a).

Note that, the 15 dynamic states, which had played a significant role while obtaining dynamic features, were not the features that were used by the classifier (that is, the differences in pairwise correlation across different states and different groups were not used as dynamic features, rather the states were used as regression matrix while obtaining dynamic features or beta coefficients). In the higher dimensional space, our classifier separated the patterns from these 15 states, and computed the fitness score or beta coefficients.

This study shows that using static and dynamic connectivity features we can reliably discriminate HC, SZ and BP at the individual subject-level. Previous studies showed group-level discrimination of SZ and BP from HC subjects by using disconnected FNC properties in these patient groups. Using FNC approaches, these studies have identified disrupted connectivity patterns in SZ and BP patients during rest and task in several brain regions (Arbabshirani et al., 2013a; Rashid et al., 2014; Calhoun et al., 2014; Hutchison et al., 2013b). Also our previous work reported disrupted connectivity in several dynamic states for SZ and BP patients (Rashid et al., 2014). The improved classification accuracies in this current study for the dynamic FNC approach and the combined static and dynamic approach also support a dysconnection hypothesis in SZ and BP (Friston and Frith, 1995; Bokde et al., 2006; Jafri et al., 2008).

Dynamic FNC provides the information about how the connectivity changes over time, rather than representing the mean FC (Calhoun et al., 2014). It provides the local functional connectivity at each time window. This is likely capturing important information that is missed in static FNC approach and indeed, the

dynamic FNC approach provides the higher overall accuracy rate compared to the static FNC approach. Moreover, when both static and dynamic FNC features were combined, the classification approach achieved the highest overall accuracy rate (thought not significant in the statistical sense); as this approach utilizes the information from overall mean FNC that may not be captured by the dynamic FNC approach.

5.5 Limitations and Future Directions

There are several methodological and experimental limitations associated with sliding-window analysis method and result interpretations. One issue for sliding-window analysis is the choice of appropriate window size. Is has been reported in (Sakoğlu et al., 2010) that the ideal window size should be able to estimate FC variability, capture lowest frequencies of interest in the signal, and detect interesting short-term effects. Our dynamic FNC approach was based on an empirically validated fixed sliding-window of 22TRs (33sec) similar to that used in (Allen et al., 2012a).Evaluation of changes across variety of window lengths performed using separate windows (Cribben et al., 2012) and comparisons with time-frequency approaches which do not require windowing at all (Yaesoubi et al., 2015) will be interesting to examine in future work.

It is very difficult to make comparisons between different automatic classification approaches of mental disorders, as there are several limitations and considerations associated with these studies. Factors such as study size, MRI scanner parameters, nature of extracted features, type of classifier, medication and disease severity in the patient group effects the classification frameworks. Also, without standard training and testing datasets, comparison of different approaches based only on

the classification accuracy rate becomes highly ambiguous. It would be interesting to compare classification performance for diagnosis using the DSM criteria versus a Biotype-style approach as promoted in the BSNIP study (Keshavan et al., 2013), where biological features are used as the initial classifier to derive new diagnostic entities not based on traditional clinical classifications of mental illness.

Also, potential factors such as awareness or subject's anxiety level at the scanner were not available for our subjects. These factors could potentially contribute to effectively differential groups given that both awareness and anxiety are known to affect patterns of brain. Thus, the factors may be important and should be investigated in future studies, in order to fully interpret the results.

In this study we showed that both resting state static and dynamic FNC features could be successfully used for automatic discrimination between three groups including HC, SZ and BP patients. To the best of our knowledge this the first study using resting-state dynamic FNC features as well as combined static and dynamic FNC features to classify SZ and BP patients. Here we separated the data into training and testing dataset during the cross-validation folds. Our approach has some bias as the whole dataset was first processed together, group ICA was performed together, and the FNCs were computed together. To resolve this issue, separate training and testing preprocessing, group ICA analysis and FNC computation is recommended. However, given that we were interested primarily in a comparison of static, dynamic, and combined connectivity features, and all used the same input, this should have little to no impact on our results.

TABLE 5.2: Performance evaluation of classifier using different FNC classification approaches

	sFNC			**dFNC**			**sFNC + dFNC**		
Overall Accuracy (%)	59			84			89		
Confidence Interval, CI (%)	[52,67]			[78,90]			[83,93]		
Statistics by Class (%)	HC	SZ	BP	HC	SZ	BP	HC	SZ	BP
Sensitivity [CI]	66 [52,77]	65 [52,77]	39 [24,57]	90 [80,96]	83 [71,92]	76 [60,89]	89 [78,95]	85 [73,93]	95 [82,99]
Specificity [CI]	84 [75,90]	66 [55,75]	88 [80,93]	91 [83,96]	92 [85,96]	93 [87,97]	94 [87,98]	94 [87,98]	95 [90,98]
PPV [CI]	71 [58,83]	53 [41,65]	50 [31,69]	86 [75,93]	86 [75,94]	78 [62,90]	90 [79,96]	89 [78,96]	86 [71,95]
NPV [CI]	80 [71,87]	76 [65,84]	82 [74,88]	94 [87,98]	90 [83,95]	93 [86,97]	93 [86,97]	91 [84,96]	98 [94,100]

ICN regions	BA	tmax	Peak (mm) (X Y Z)
Subcortical Networks			
Putamen (78)			
R Putamen		63.69	30 0 3
L Putamen		58.3	-27 -6 9
Putamen (91)			
L Putamen	34	73.94	-24 9 -6
Auditory Networks			
STG (36)			
L Superior Temporal Gyrus	41	50.57	-48 -30 12
R Superior Temporal Gyrus	13	39.86	45 -15 3
Visual networks			
Lingual Gyrus (10)			
L Lingual Gyrus	18	58.58	-108
Inferior Occipital Gyrus (11)			
R Inferior Occipital Gyrus	18	54.54	-129
L Middle Occipital Gyrus	18	54.21	27 -99 -6
Cuneus (16)			
L Cuneus	18	64.24	0 -81 24
Calcarine (29)			
R Calcarine	30	62.36	12 -69 9
Inferior Occipital Gyrus (32)			
L Inferior Occipital Gyrus	19	44.72	-114
R Fusiform Gyrus	18	17.32	30 -78 0
Lingual Gyrus (33)			
R Lingual Gyrus	19	51.03	21 -54 -9
Middle Occipital Gyrus (54)			
L Middle Occipital Gyrus	19	47.16	-33 -90 12
R Middle Occipital Gyrus	19	47.35	30 -93 12
Sensorimotor Networks			
Postcentral (14)			
L Postcentral Gyrus	4	51.81	-36 -24 51
Superior Medial Gyrus (27)			
L Superior Medial Gyrus	8	43.82	3 30 54
SMA (35)			
R supplementary motor area	24	43.01	12 -6 51
SupraMarginal (38)			
L SupraMarginal Gyrus	3	45.53	-60 -21 36
R Postcentral Gyrus	3	40.27	57 -18 33
L Inferior Frontal Gyrus	44	21.43	-54 9 24
R Inferior Frontal Gyrus	9	15.86	60 12 27

TABLE 5.3: Regions of activation, Brodmann area (BA), peak activation t-value and coordinates for top 15 static FNC feature components

ICN regions	BA	tmax	Peak (mm) (X Y Z)
Cognitive Control			
Inferior Temporal Gyrus (64)			
L Inferior Temporal Gyrus	37	47.57	-108
R Inferior Temporal Gyrus	37	20.76	54 -48 -9
Middle Temporal Gyrus (92)			
R Middle Temporal Gyrus	21	51.2	57 -21 -9
L Middle Temporal Gyrus	21	41.31	-93
Superior Parietal Lobule (60)			
R Superior Parietal Lobule	7	48.93	15 -51 63
Inferior Parietal Lobule (63)			
L Inferior Parietal Lobule	40	47	-57 -42 36
R SupraMarginal Gyrus	40	47.42	57 -45 33
R Inferior Frontal Gyrus	47	16.04	51 18 -6
Inferior Frontal Gyrus (57)			
R Inferior Frontal Gyrus	9	50.3	45 12 30
L Inferior Frontal Gyrus	46	30.38	-45 18 27
Right Inferior Parietal Lobule	40	16.96	36 -51 51
Insula Lobe (98)			
R Insula Lobe	47	58.98	42 12 -3
L Insula Lobe	47	48.66	-39 18 -3
Default Mode Networks			
Middle Cingulate Cortex (75)			
R Middle Cingulate Cortex	31	59.83	6 -33 33
Cerebellar Networks			
Cerebellum (3)			
L Cerebellum (VIII)		56.24	-135
R Cerebellum (Crus 2)		21.93	42 -54 -39

TABLE 5.4: Regions of activation, Brodmann area (BA), peak activation t-value and coordinates for top 15 static FNC feature components

CHAPTER 6

INFLUENCE OF GENETICS ON TIME-VARYING FUNCTIONAL NETWORK CONNECTIVITY IN SCHIZOPHRENIA

6.1 Genetics of the Brain Dynamics

It has been evident from several studies that a majority of complex behaviors and psychiatric disorders have a highly heritable component (Sullivan et al., 2000). However, identifying these particular genes and understanding the neural mechanisms that relate them to specific behavioral problem remain very difficult (Meyer-Lindenberg and Weinberger, 2006). Studies suggest that the genetic effects on behavior should be naturally mediated. Thus, the most efficient approach to understand the functional impact of genetic variation would be to study the influence of genes on the human brain.

SZ is a psychotic disorder characterized by disintegration in perception of reality, thought processes, and behaviors problems cognitive functionality and chronic course with lasting problem (Heinrichs and Zakzanis, 1998). SZ can be distinguished by gray and white matter abnormalities and disrupted connectivity across large-scale brain networks (Mohamed et al., 1999). Recent studies show that connectivity dynamics can capture uncontrolled but reoccurring patterns of interactions among intrinsic networks during a task or at rest that cannot be detected with static functional connectivity analyses. Some of these studies proposed novel approaches to study dynamic connectivity and investigated group difference in connectivity between patients and controls (Calhoun et al., 2014; Rashid et al., 2014). However, the underlying genetic basis of SZ remains elusive.

An efficient strategy to unravel the genetic risk factors of SZ is through investigating the effects of genetic variations on intermediate phenotypes such as aberrant brain structure and function, as they are more related to biological mechanisms compared to behavioral measures. A recent study showed that compared to behavioral measures, SZ risk variant were found to show more effects at brain anatomy and function (Rose and Donohoe, 2013). Imaging genetics offers opportunity to establish neurogenetic risk mechanism associated with brain structure and function. Thus, this approach makes it possible to identify neural systems in mediating genetic risk for mental disorders by associating the genetic variants with neuropsychiatric, behavioral or cognitive phenotypes.

Previous FC studies strongly implicate disrupted dFNC as a potential biomarker for SZ. However, to our knowledge, there has not been any work to characterize both genetic and imaging aspects together, using dFNC. We studied 61 SZ patients and 87 HC with good-quality genome-wide SNP data and fMRI data. A pre-filtering step was applied to locate potentially susceptibility based on a large

cohort. These potential causal loci were then analyzed for multivariate associations with dFNC states using parallel-ICA (Liu and Calhoun, 2000). As a multivariate approach, parallel-ICA extracts genetic and imaging components, respectively from the SNP data and dFNC states to capture clusters of SNPs or connectivity between functional networks exhibiting co-variations across subjects which simultaneously emphasizing imaging-genetic associations in order to identify genetic factors explaining variation in dFNC states. This approach also enables us to study genetic variants clustered into components at a pathway level, potentially providing more insight into the underpinnings of SZ. To guard against overfitting issue, the identified dFNC-SNP associations were evaluated with a permutation test.

6.2 Analysis Methods and Proposed Approaches

6.2.1 Participants

We used rsfMRI data and SNP data obtained from 163 HC (117 males, 46 females; mean age 36.9) and 151 age- and gender matched patients with SZ (114 males, 37 females; mean age 37.8) during eyes closed condition at 7 different sites across United States and pass data quality control. Informed consent was obtained from each participant prior to scanning in accordance with the Internal Review Boards of corresponding institutions. A total of 162 volumes of echo planar imaging BOLD fMRI data were collected with a TR of 2 s on 3T scanners. After preprocessing, we obtained data from a total of 148 participants (87 HC and 61 SZ patients matched for age) for which both fMRI and SNP data were collected.

6.2.2 Imaging Data Acquisition and Pre-processing

Imaging data was collected on a 3T Siemens Tim Trio System and on a 3T General Electric Discovery MR750 scanner at one site. rsfMRI scans were acquired using a standard gradient-echo echo planar imaging paradigm: FOV of 220 $\times$ 220 mm (64 $\times$ 64 matrix), TR = 2 s, TE = 30 ms, FA = 770, 162 volumes, 32 sequential ascending axial slices of 4 mm thickness and 1 mm skip. Subjects had their eyes closed during the resting state scan.

Data processing was performed using a combination of toolboxes (AFNI, SPM, GIFT) and custom code written in Matlab. We performed rigid body motion correction using the INRIAlign (Freire and Mangin, 2001) toolbox in SPM to correct for subject head motion followed by slice-timing correction to account for timing differences in slice acquisition. Then the fMRI data were despiked using 3dDespike algorithm from AFNI to mitigate the impact of outliers. The fMRI data were subsequently warped to a MN) template and resampled to 3 mm^3 isotropic voxels. Instead of Gaussian smoothing, we smoothed the data to 6 mm FWHM using AFNI3s BlurToFWHM algorithm, which performs smoothing by a conservative finite difference approximation to the diffusion equation. This approach has been shown to reduce scanner specific variability in smoothness providing "smoothness equivalence" to data across sites (Friedman et al., 2008). Each voxel time course was variance normalized prior to performing group independent component analysis as this has shown to better decompose subcortical sources in addition to cortical networks.

After preprocessing the data, functional data from both control and patient groups were analyzed using spatial GICA1 framework as implemented in the GIFT software (Calhoun et al., 2001c; Erhardt et al., 2011b). Spatial ICA decomposes the

subject data into linear mixtures of spatially independent components that exhibit a unique TC profile. A subject-specific data reduction step was first used to reduce 162 time point data into 100 directions of maximal variability using principal component analysis. Then subject reduced data were concatenated across time and a group data PCA step reduced this matrix further into 100 components along directions of maximal group variability. One hundred independent components were obtained from the group PCA reduced matrix using the infomax algorithm (Bell and Sejnowski, 1995). To ensure stability of estimation, we repeated the ICA algorithm 20 times in ICASSO, and aggregate SMs were estimated as the modes of component clusters. Subject specific SMs and TCs were obtained using the spatiotemporal regression back reconstruction approach (Calhoun et al., 2001c; Erhardt et al., 2011b) implemented in GIFT software.

For dynamic FNC analysis, we computed correlations between ICN TCs using a tapered sliding temporal window (Tukey window having a width of 22 TRs=44 sec; sliding in steps of 1 TR) to capture the variability in connectivity. Final dynamic FNC estimates for each window were concatenated to form a C$\times$C$\times$W array representing the changes in correlation between components as a function of time. We performed k-means clustering on dynamic FNC matrix and obtained 5 cluster centroids or dynamic states based on the elbow criteria.

6.2.3 SNP Data Collection and Pre-processing

The genotyping and genetic quality control procedures were same as described in our previous work (Chen et al., 2012), which is briefly summarized here. DNA was extracted from saliva sample collected from the participants. Genotyping for all subjects was performed at the University of California at Irvine using a custom

made assay by selecting Infinium MEGAEx chip as well all SNP loci on the Psych chip. BeadStudio was used to make the final genotype calls and PLINK (Purcell et al., 2007) was employed for a series of quality controls including: (a) gender consistency check, (b) sample relatedness (not closer than second degree relatives), (c) genotyping call rate (>90% at both the individual and SNP level), (d) Hardy – Weinberg equilibrium in the control population ($p < 1 \times 10^6$), (e) minor allele frequency (MAF > 0.05), and (f) missing calls were replaced using high linkage disequilibrium (LD) loci if available or otherwise removed. A total of 977,242 SNP loci were retained after quality control and discrete numbers were then assigned to the categorical genotypes: 0 (no minor allele), 1 (one minor allele), and 2 (two minor alleles). With PCA, three principal components were identified as ethnicity-related and eliminated from the data. A pre-filtering step was conducted leveraging the Psychiatric Genomic Consortium SZ study (Sullivan, 2010), and we located 1546 SNPs, discriminating patients from controls via a univariate SNP-wise test with p-values less than 5×10^{-7} uncorrected.

6.2.4 Imaging Genetics Framework

Figure 6.1 provides an illustration of the proposed imaging genetics approach. parallel-ICA was performed through the Fusion ICA Toolbox (FIT, http://mialab.mrn.org/software/fit/index.html) using the imaging (dynamic states) and genetic (SNPs) features. The algorithm was configured with a threshold of 0.25 for constrained correlations to avoid false positive associations and to only constrain one pair of components. An endurance parameter was set to -5×10^{-4} to control the decreasing slope of the entropy term and avoid over fitting. We also

performed a permutation test to assess the validity of identified dFNC-SNP association by investigating the occurrences of inter-modality correlations by chance in permuted dFNC and SNP datasets. The null distribution was constructed with the top correlation obtained from each test run. We then counted the instances with correlations greater than that observed from the original data and calculated the two-tail probability as the significance level.

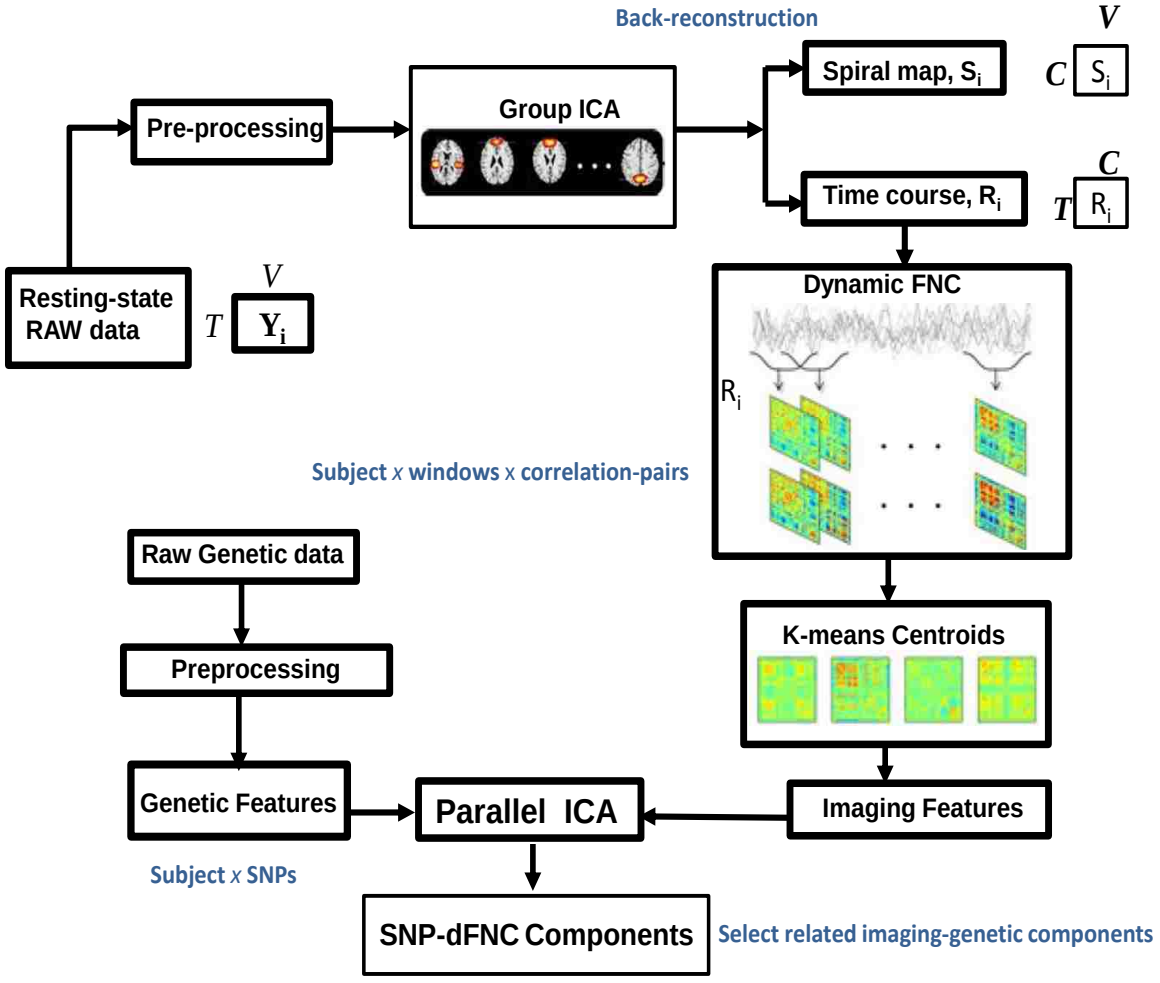

FIGURE 6.1: An overview of proposed imaging genetics approach.

6.3 Results

Figure 6.2 illustrates the five dynamic FNC states for HC and SZ patients obtained using k-means clustering, and their state-wise group differences as computed using two-sample t-tests.

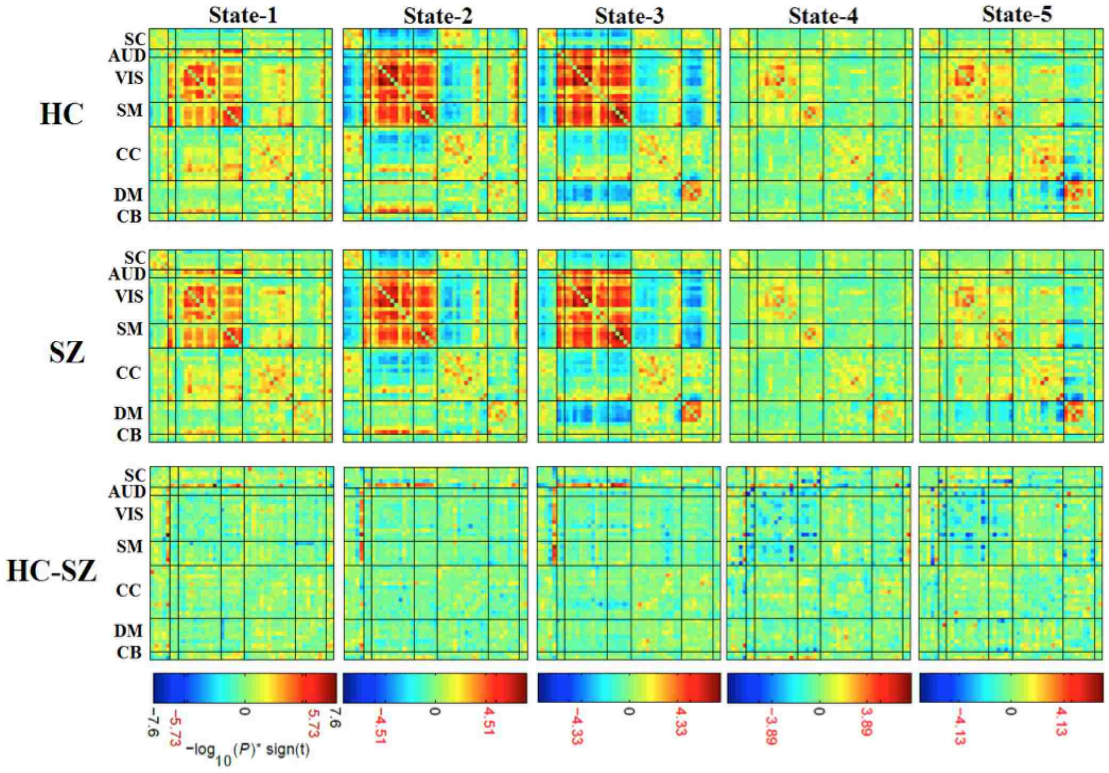

FIGURE 6.2: Dynamic FNC states for healthy (HC), schizophrenia (SZ) and group difference between HC and SZ. Note that, this figure corresponds to the Figure 6.1 "Imaging Features" box.

parallel-ICA identified one dFNC-SNP pair components with a significant correlation ($r = 0.52$, p-value $< 6.95 \times 10^{9}$). The final set of associated SNPs was selected from the results of entire dataset. In a 1000-run permutation test, the absolute values of the dFNC-SNP top correlations ranged from 0.15 to 0.67 with a median of 0.26, yielding a p-value of 0.011. In Figure 6.3, both z-scored dFNC and SNP significant component values resulting from the parallel ICA algorithm is shown.

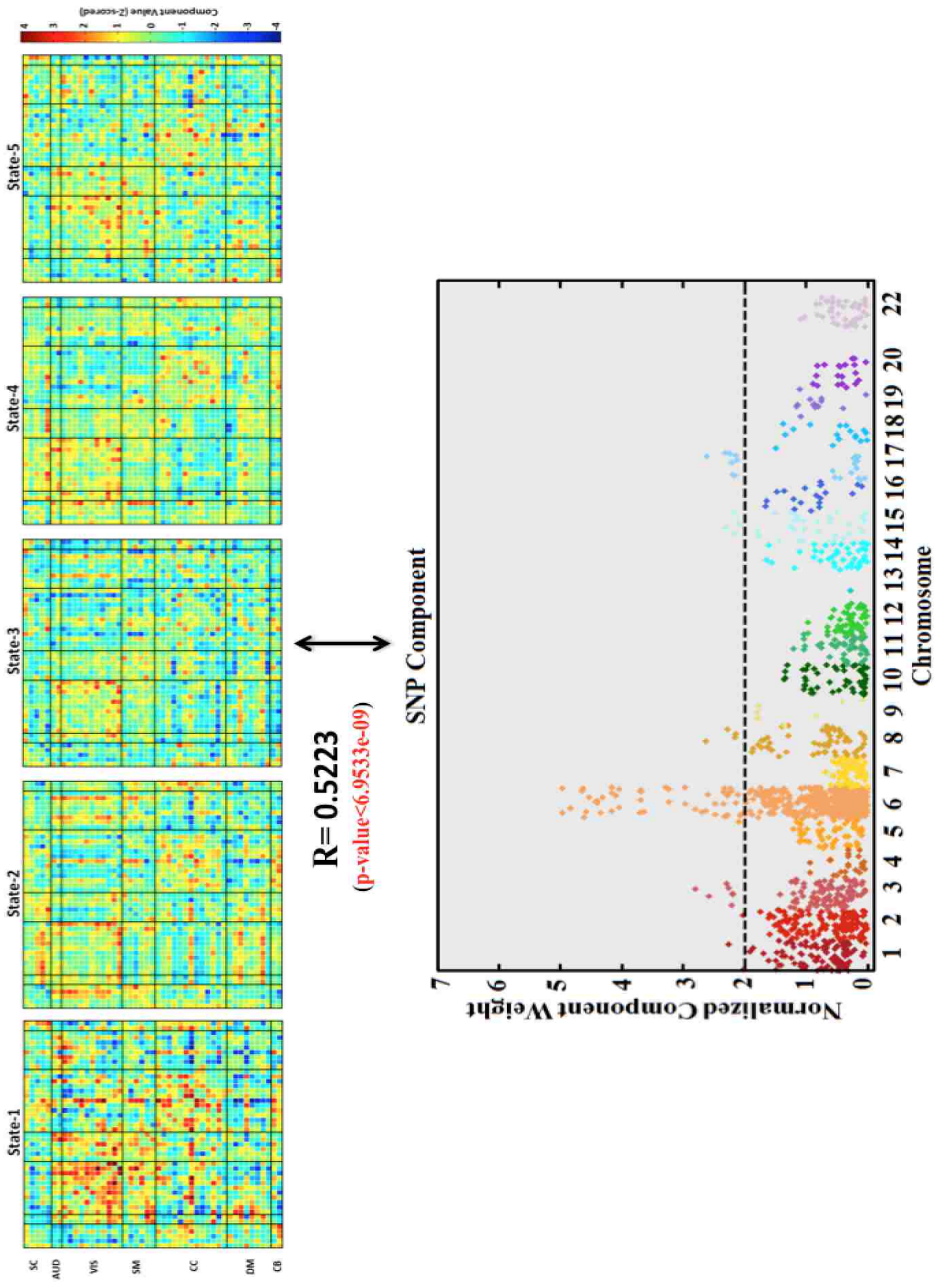

FIGURE 6.3: Results from parallel-ICA showing significantly correlated dFNC component (top), and SNP component (bottom).

The significant dFNC component values were then thresholded at $|z|>3$, extracting top 5% connectivity between ICN pairs from the five dynamic states (Figure 6.4), where the significant SNP component values were thresholded at $|z|>2$, as seen in the Manhattan plot in Figure 6.3. Most of the high positive and negative component values were observed in the dynamic state 1, a state that was found

to be dominated by the HC subjects in terms of occupancy. On the other hand, the SNP component showed higher component values at chromosome 6.

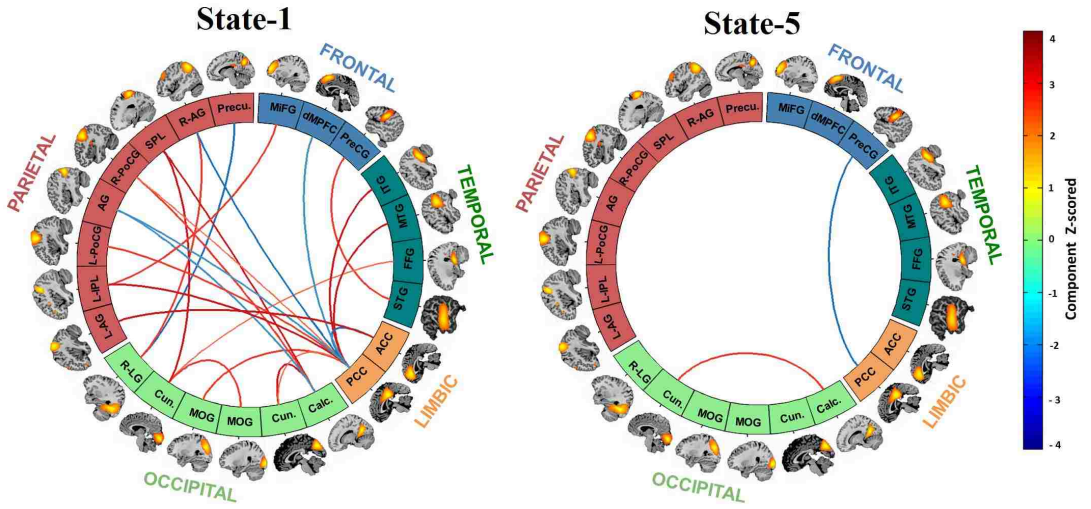

FIGURE 6.4: Connectograms showing the top component pairs observed in State-1 and State-5 after thresholding the significant dFNC component at |z|>3 as obtained from the imaging features.

The top significant dFNC observed in the significant dFNC component is shown as connectograms in Figure 6.4, where the contributions were limited to state 1 and state 5.

Figure 6.5 presents the scatterplot for loading parameter of the significantly associated components, and group-wise violin plots and summary statistics for both dFNC and SNP loadings. From ANOVA test, the group mean of dFNC loading was significantly lower in the patients with SZ (mean=0.0066, standard deviation=0.0159) compared to controls (mean=0.0152, standard deviation=0.0212). Also, the ANOVA results showed that the group mean of SNP loading was lower in SZ group (mean=-0.0265, standard deviation=0.0977) compared to HC (mean=-0.0069, standard deviation=0.1012), although not statistically significant.

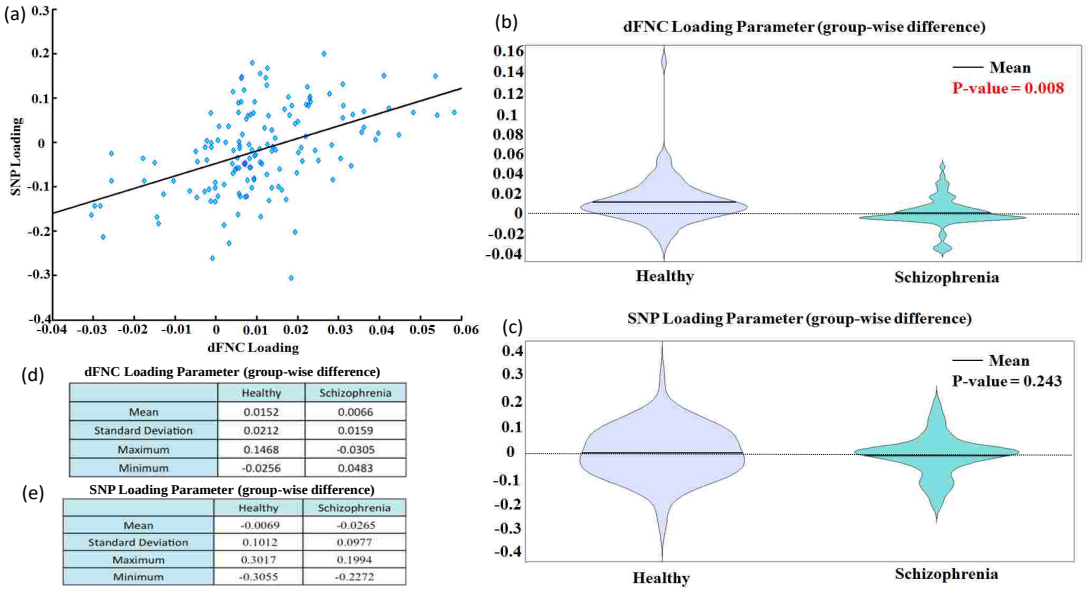

	Healthy	Schizophrenia
Mean	0.0152	0.0066
Standard Deviation	0.0212	0.0159
Maximum	0.1468	-0.0305
Minimum	-0.0256	0.0483

	Healthy	Schizophrenia
Mean	-0.0069	-0.0265
Standard Deviation	0.1012	0.0977
Maximum	0.3017	0.1994
Minimum	-0.3055	-0.2272

FIGURE 6.5: (a) Scatterplot showing dFNC loading parameters versus SNP loading parameters from the significant parallel-ICA component.(b) Group-wise violin plots of dFNC loading parameters. (c)Group-wise violin plots of SNP loading parameters.(d)Table showing group-wise statistics for dFNC loading parameter. (e) Table showing group-wise statistics for SNP loading parameter

We also computed the correlations between the polygenic risk scores and both dFNC and SNP components' loadings. The scatterplots of polygenic risk scores versus component loadings are shown in Figure 6.6. The correlation between the risk scores and dFNC loadings was -0.2561(p-value=0.0017), whereas the correlation between the risk scores and SNP loadings was -0.5401 (p-value= 1.4024×10^{-12}).

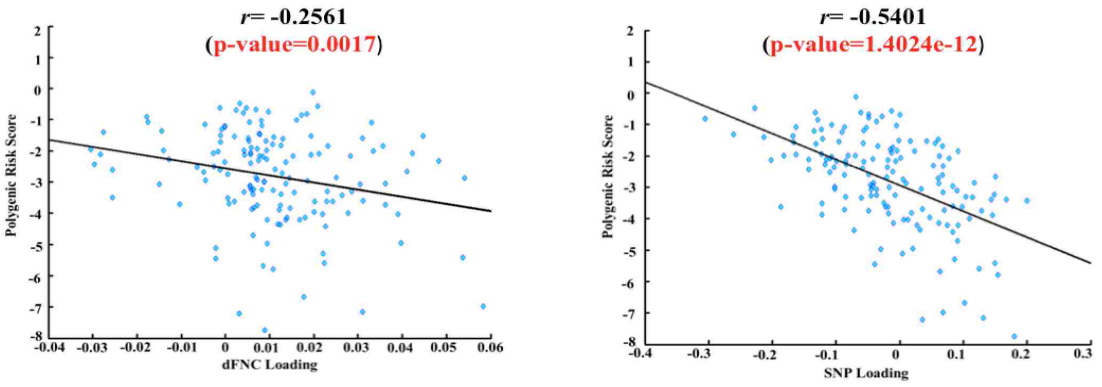

FIGURE 6.6: Scatterplots showing polygenic risk scores versus dFNC loading parameters (left), and SNP loading parameter (right) for the significant parallel-ICA component.

The significant SNP component was predominantly contributed to by 83 SNPs (top 5% based on absolute values of the component weights). 24 SNPs were mapped to 13 unique genes using UCSC hg19 assembly (http://hgdownload.cse.ucsc.edu/), while the rest were from inter-genic regions. We examined the genetic architecture of our findings using Reactome Pathway Analysis (RPA: https://www.reactome.org), where the 13 genes were compared with the whole genome as background. The results obtained from RPA are provided in Table 6.2. We also analyzed our query genes to find the biological functions of these top genes, which are provided in Table 6.3.

6.4 Discussion

In this study we investigated the genetic underpinnings of dysfunctional dynamic FNC in SZ. A multivariate approach, parallel-ICA, was used to extract SNP and dFNC components, and retrieve intermodality associations. Due to the limited sample size compared to genome-wide SNPs, we preselected 1546 risk loci based

upon group difference to focus the dFNC-SNP association analysis on polymorphisms likely relevant to SZ. Finally one significant dFNC-SNP pair was identified and the permutation test indicated a low possibility that the observed correlation was due to overfitting, though the current result still awaits further validation in a larger cohort.

Most of the significant component pairs with both positive and negative component scores were captured by dynamic state 1 (Figure 6.4). Dynamic state 1 represents a state that is dominated by the HC in terms of occupancy rate (Table 6.1; HC=22% and SZ=14%). The results from Figure 6 also confirm that, the higher the polygenic risk score is for a given subject, the less likely it is to be in state 1.

Our findings on top dynamic FNC component pairs (Figure 6.4) included both positive and negative connectivity among a limbic component, posterior cingulate cortex (PCC) and several frontal, temporal, parietal and occipital components. Previous studies also reported aberrant FNC in SZ subjects associated with many of these components, for example, dMPFC (Huang et al., 2010).

The result obtained from GeneMANIA report that 40.49 % of the 13 listed genes show co-expression. There is 59.51% genetic interaction among the query genes. Reactome Pathway Analysis (RPA) further shows that these selected genes are involved in different cellular processes including the immune system, metabolism and neuronal systems (Table 6.2).

Among the top 13 genes, CHRNA3, ATXN7 and SMG6 are previously found to be involved in neurological, psychological and developmental disorders, while RERE

State#	#dFNC Cells	Occupancy (HC/SZ)
1	23	22%/14%
2	0	32%/11%
3	0	20%/18%
4	0	9%/32%
5	2	16%/27%

TABLE 6.1: Significant dynamic FNC cells and group-wise occupancy rate across each state

and HLA-C are involved in immunological disease (Table 6.3). It would be interesting to further explore these genes and the corresponding SNPs in correlation to neuroimaging studies and SZ.

The proposed parallel-ICA framework, to our best knowledge, is the first study to identify interactions between dynamic functional connectivity and genetic information. Our findings showed that genetic SNP factors could be investigated by using endophenotypic neuroimaging findings in a multivariate format.

TABLE 6.2: Reactome Pathway Analysis using the top genes

Canonical Pathway	**P-value**	**Gene Name**
Neuronal System	0.604202	CHRNA3
Neurotransmitter Receptor Binding And Downstream Transmission In The Postsynaptic Cell	0.313669	CHRNA3
Transmission across Chemical Synapses	0.431053	CHRNA3
Immune System	9.28E-05	HLA-C
Metabolism	0.064322	SLC44A4, ATXN7
Gene Expression	0.866556	EHMT2, THOC7, SMG6

TABLE 6.3: Biological functions of the top genes

Functions	P-value	Gene Name
Neurological Disease, Psychological Disorders	4.64E-02	CHRNA3
Hereditary Disorder, Neurological Disease	6.78E-04	ATXN7
Molecular Transport, RNA Trafficking	3.10E-04	SMG6, THOC7
Visual System Development and Function	4.45E-02	ATXN7
Cell Morphology, Embryonic Development	6.76E-03	CCHCR1
Nervous System Development and Function, Tissue Morphology	1.55E-02	ATXN7
Developmental Disorder, Neurological Disease	3.34E-02	SMG6
Immunological Disease	1.08E-02	RERE
Immunological Disease, Inflammatory Disease, Inflammatory Response	6.78E-04	HLA-C

CHAPTER 7

SUMMARY AND CONCLUSIONS

7.1 Summary

In this doctoral dissertation, we developed and presented time-varying FNC-based methods for functional neuroimaging by applying two main concepts- Independent Component Analysis (ICA) and automatic classification approach using support vector machine (SVM). While ICA has been used to decompose the fMRI data into functionally specialized brain components and then group them into functional networks to assess the FNC among different networks, SVM has been used for training these connectivity features for automatic classification purpose. We have extended these concepts to formulate new methods for time-varying FNC, multi-modal data analysis and classification algorithms.

In this thesis, we employed a 'chronnectomic' approach (i.e., identifying time-varying and reoccurring patterns of connectivity among brain regions) to evaluate transient states of connectivity among brain networks in a large, population-based

cohort study with typically developing children. We investigated age-related aspects of functional maturation during childhood with both modularized and disconnected dynamic states. In addition, we characterized the "chronnectopathy" (i.e. dysfunctional chronnectivity) associated with autistic traits. Dynamic FNC was evaluated using a sliding-window approach, and revealed four transient states. Inter-network connectivity increased with age in modularized dynamic states, illustrating an important pattern of connectivity in the developing brain. Furthermore, we demonstrated that higher levels of autistic traits were associated with longer dwell times in a globally disconnected state. These results provide a roadmap to the chronnectomic organization of the developing brain and suggest that characteristics of functional brain maturation are related to autistic traits.

To extend our understanding on time-varying FNC in adult subjects, including both HC subjects and patients with severe mental disorders, we utilized ICA on rsfMRI data to obtain ICNs in cohorts of HC and age matched SZ and BP patients. Subsequently, we investigated difference in FNC between HC and patients. We quantified differences in both static (average) and dynamic (windowed) connectivity during the entire scan duration. Disease-specific differences were identified in connectivity within different dynamic states. Notably, results suggest that patients make fewer transitions to some states (states 1, 2 and 4) compared to HC, with most such differences confined to a single state. SZ patients showed more differences from HC subjects than did BP, including both hyper and hypo connectivity in one common connectivity state (state 3). Also group differences between SZ and BP patients were identified in patterns (states) of connectivity involving the frontal (dynamic state 1) and frontal-parietal regions (dynamic state 3). These results provide new information about these illnesses and strongly suggest that state-based analyses are critical to avoid averaging together important factors

that can help distinguish these clinical groups.

We developed new classification algorithms for automatic classification of SZ, BP and HC subjects based on their static and dynamic FNC features. We also presented comparison based on classification performance between static and dynamic FNC. Results show that dynamic FNC has significantly higher predictive accuracy than static FNC. However, static and dynamic FNC have distinct advantages and appear to capture complementary aspects of connectivity. Combining static and time-varying FNC features improved (but not statistically significant) the classification performance beyond each type of feature alone. A three-way classification methodology based on static and dynamic FNC features discriminates individual subjects into appropriate diagnostic groups with high accuracy. Results from this study further justify the necessity of studying time-varying FNC more extensively. Our proposed classification framework is potentially applicable to additional mental disorders.

We also introduced a novel imaging-genetics framework using parallel-ICA algorithm, to explore the association between time-varying FNC and genetic features (SNP). Our preliminary results suggest that genetics features as captured by SNP data can influence brain's time-varying FNC, which may potentially explain the dysfunctional connectivity in patients with SZ. By jointly analyzing the features from both modalities, we may therefore be able to develop relevant biomarkers to diagnosis severe mental disorders such as SZ.

The published frameworks and results (Rashid et al., 2014, 2015, 2016a,c,b), also presented in this dissertation, show considerable improvement over existing methods and have proved to be viable for uncovering new and improved FNC-related biomarkers in typical development, as well as patients with mental disorders. We

sincerely hope that this work contributes to signify the important role played by time-varying FNC as measured from fMRI data for diagnosis of severe mental disorders.

7.2 Future Work

There are still many aspects to be explored in the future regarding the methodological development and application of FNC analysis. As mentioned in Chapter 3, our developmental FNC study was cross-sectional and all participants were of school-age, so the interpretation of our results can not be extended to other stages of development. A future work should include longitudinal studies to reveal trajectories of dynamic FNC in typical and atypical development.

Another future work can include evaluation of different window sizes in sliding-window analysis. Throughout our FNC analyses, we employed a fixed window size of 22 TR to perform sliding-window approach. FNC changes across a variety of windows sizes should be compared in order to optimally estimate connectivity variability and capture the lowest frequencies of interest in the signal, as well as to detect interesting short-term effects..

Our proposed classification algorithms in Chapter 5 only included fMRI data and incorporated FNC-related featured. There are several biomarkers based on different modalities for mental disorders such as SZ (see Chapter 6). Future work may include comparing and combining features from multiple modalities, such as FNC measures from fMRI data and genetic variations from SNP data for more robust and accurate classification framework. Recently, only a few studies have combined two or three modalities for classification purposes. Yang et al., combined fMRI

and genetics data for automatic classification of SZ patients from HC (Yang et al., 2010). Another recent study proposed a classification framework by combining fMRI, diffusion tensor imaging (DTI) and sMRI to classify SZ patients (Sui et al., 2011).

APPENDIX A

APPENDIX A

A.1 Static connectivity results

Figure A.1 shows the mean static FNC for all 774 subjects. To assess how the static FNC develops and forms the adult-like connectivity patterns, we searched for age- and sex-specific static FNC profiles. Both positive and negative associations between connection strength and age were found in the static FNC. In particular, for CC components, the within-network connectivity showed decreasing patterns with age, and between-network connectivity mostly showed increasing patterns with age. We specifically focused on the default-mode connectivity as functions of age and sex. In the DMN, the average between-network connectivity were increasing with age for DMN components left MCC, right AG and left preC, and decreasing with age for DMN components right preC and left AG (Figure A.2). Also, both male and female dominated connectivity patterns were found in static FNC. The average between-network connectivity were greater for girls for DMN

components left MCC and left preC, and greater for boys for DMN components right AG, right preC and left AG (Figure A.2).

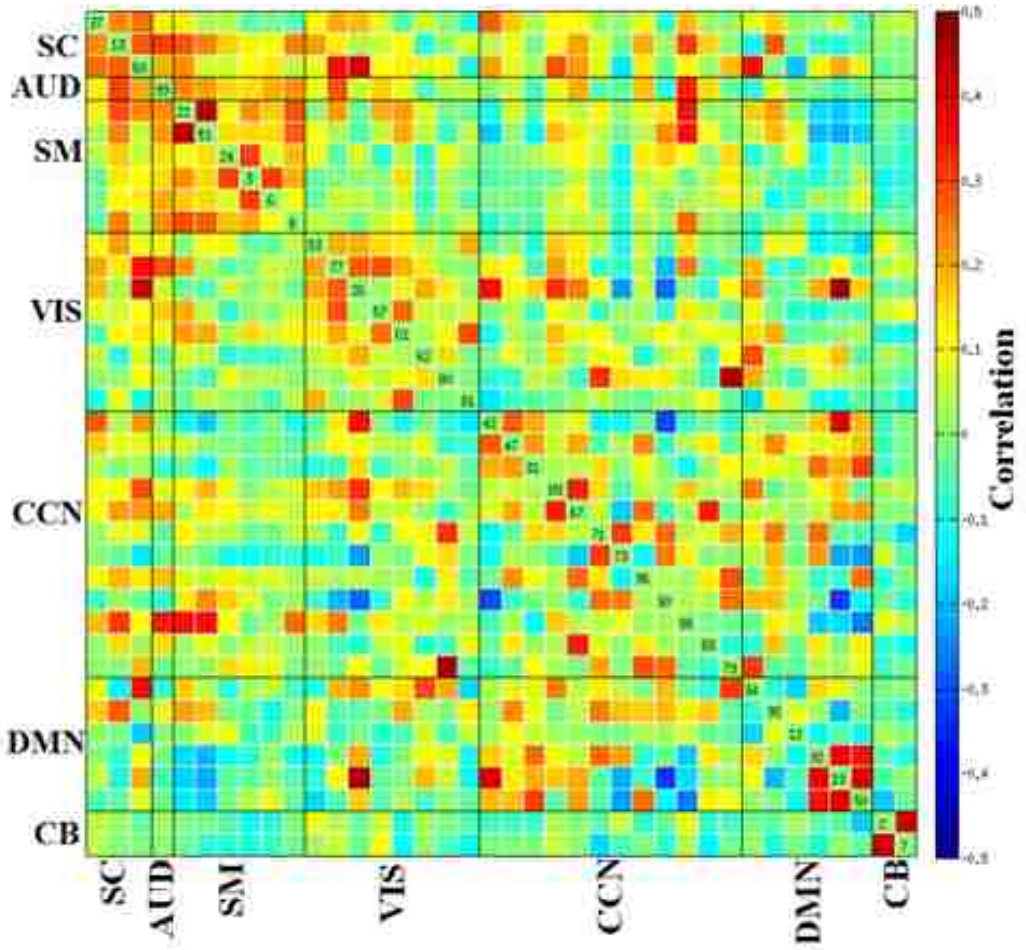

FIGURE A.1: Mean static functional network connectivity (sFNC) map for 774 subjects.

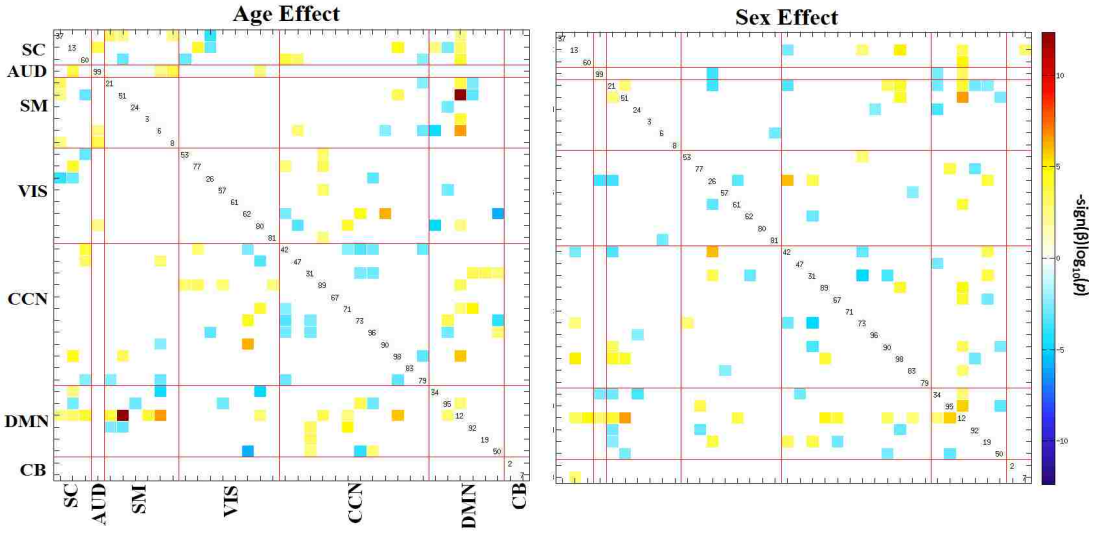

FIGURE A.2: Age- and sex-related associations in static FNC. For age analyses, red indicates positive association between that particular pairwise connection and age, whereas blue indicates a negative age association. For analyses of sex, red indicates where female subjects showed stronger connectivity than male subjects, and blue indicate where male subjects showed stronger connectivity compared to female subjects. All the results presented here survived the false discovery rate (FDR) multiple comparison correction threshold of $p_{FDR} = 0.05$.

A.2 Validation framework for connectivity measures

A.2.1 Reproducibility of clusters

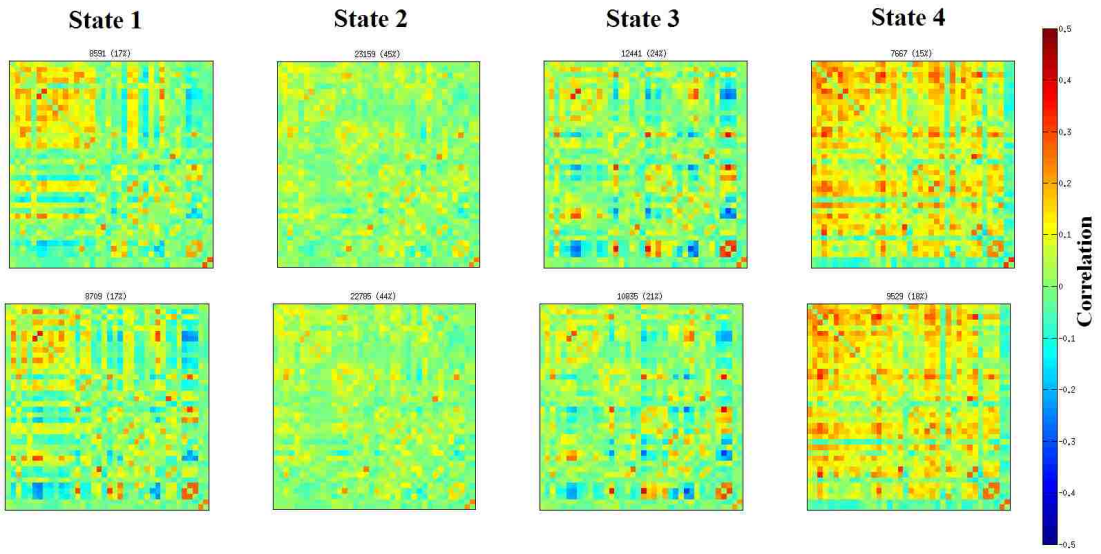

FIGURE A.3: Reproducibility of clusters was established via non-overlapping split-half samples of subjects. For half-split cross-validation, the subjects were split into two groups with equal number of subjects, and the k-means algorithm was applied with 500 repetitions to the subject exemplars in that group (∼1500 instances). The total number and percentage of occurrences is listed above each centroid.

A.3 Sensitivity analyses of dynamic connectivity findings

A.3.1 Sensitivity analysis based on behavioral problems

In order to ensure that the results were not driven by subjects with higher levels of behavioral problems as measured by CBCL scores, sensitivity analyses were run. To perform the sensitivity analysis, we excluded all the subjects showing any child

behavioral problem using CBCL scores from the original dataset (after exclusion, number of subjects=531). We then computed the age- and sex-specific effects on dynamic FNC (Figure A.4) and summary measures of the dynamic FNC such as MDT and FT (Figure A.5). These results also produced the same direction of effects for each of these connectivity measures, as found with the whole dataset.

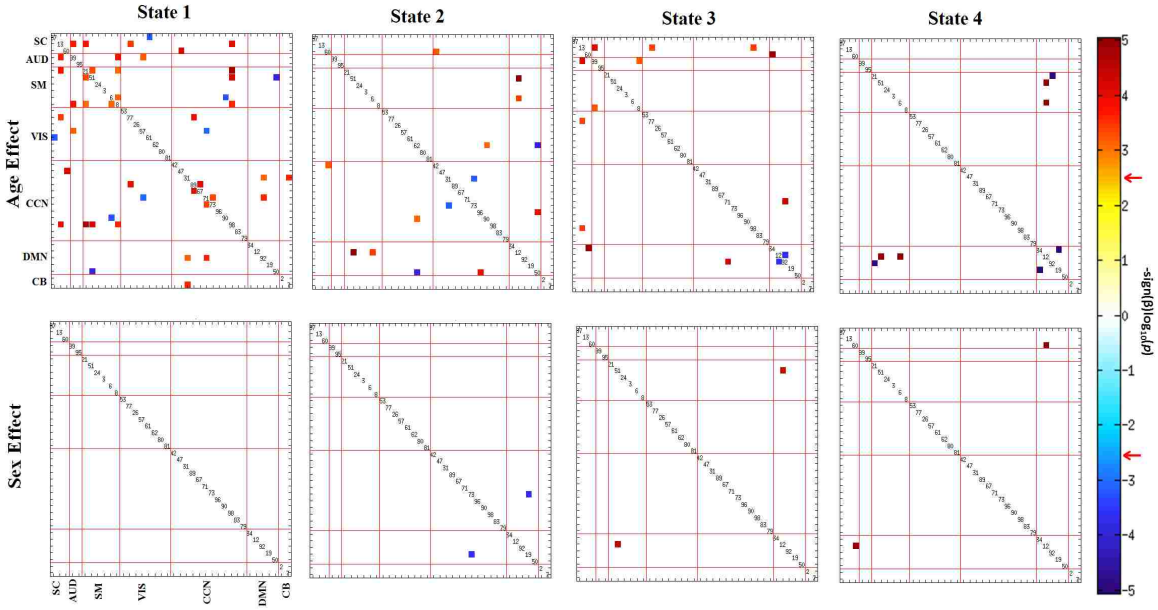

FIGURE A.4: Results from age- and sex-related associations across dynamic connectivity states after excluding subjects with higher levels of behavioral problems. For age analyses, red indicates positive association between that particular pairwise connection and age, whereas blue indicates a negative age association. For analyses of sex, red indicates where female subjects showed stronger connectivity than male subjects, and blue indicate where male subjects showed stronger connectivity compared to female subjects. All the results presented here survived the false discovery rate (FDR) multiple comparison correction threshold of $p_{FDR} = 0.05$, and the FDR threshold is depicted on the color bar with red arrows.

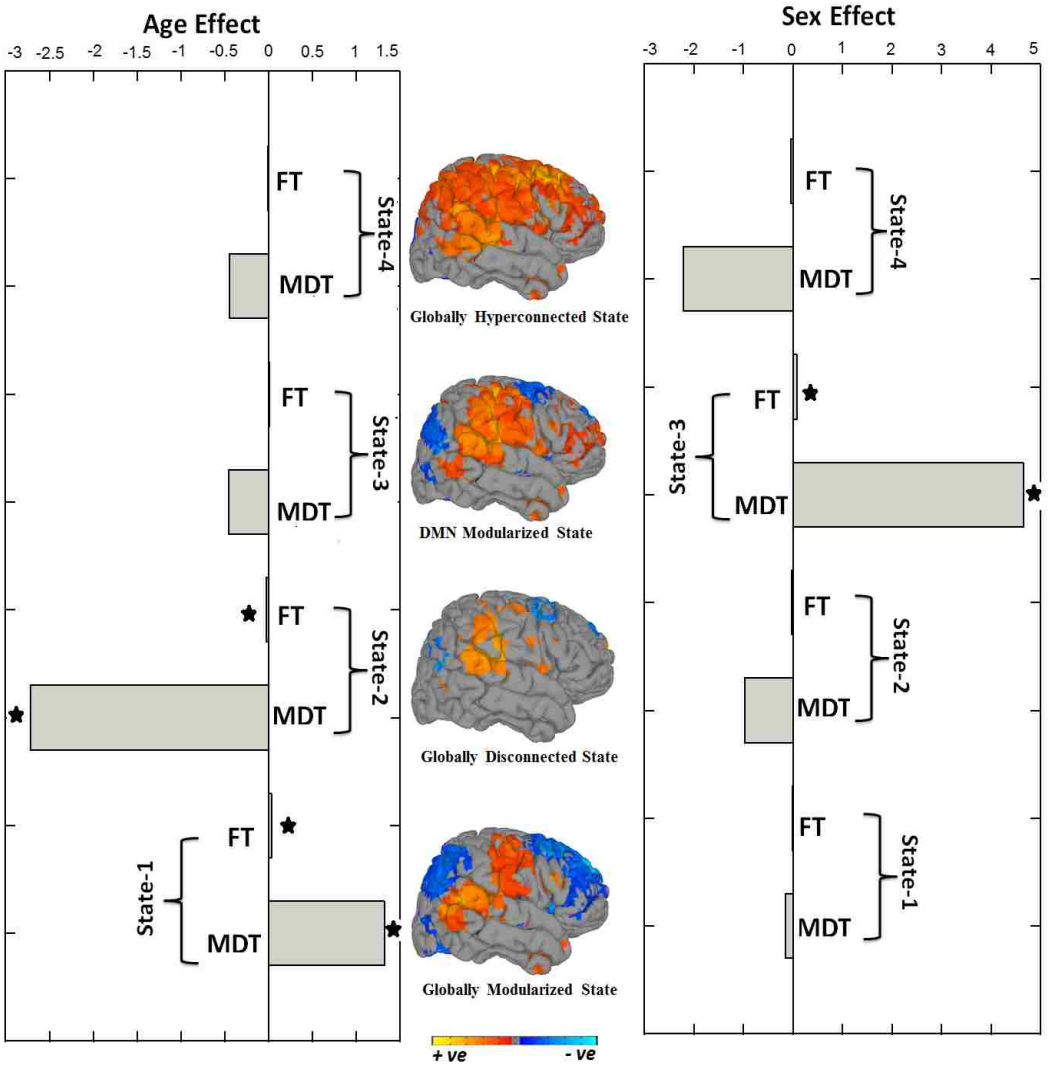

FIGURE A.5: Bar plots showing the summary metrics from the four dynamic connectivity states in relation to age and sex after excluding subjects with higher levels of behavioral problems. Asterisks (*) indicate the results survived the false discovery rate (FDR) multiple comparison correction threshold of $p_{FDR} = 0.05$. The rendering brain maps are showing modularized positive (red) and negative (blue) connectivity for the corresponding dynamic states.

A.3.2 Case-control study for autism

We also designed a case-control study for subjects with ASD and autistic traits, where we had age, sex and IQ matched 88 healthy subjects and 22 subjects with autistic traits and ASD. We assessed the difference in dynamic FNC states between HC and autistic traits and ASD groups (Figure A.6). Note that, these results are

showing group differences between HC and ASD in state-1 and state-4, two of the dynamic states that did not capture any SRS effects (effects of autistic trait) in terms of MDT and FT for the original analyses with 774 subjects

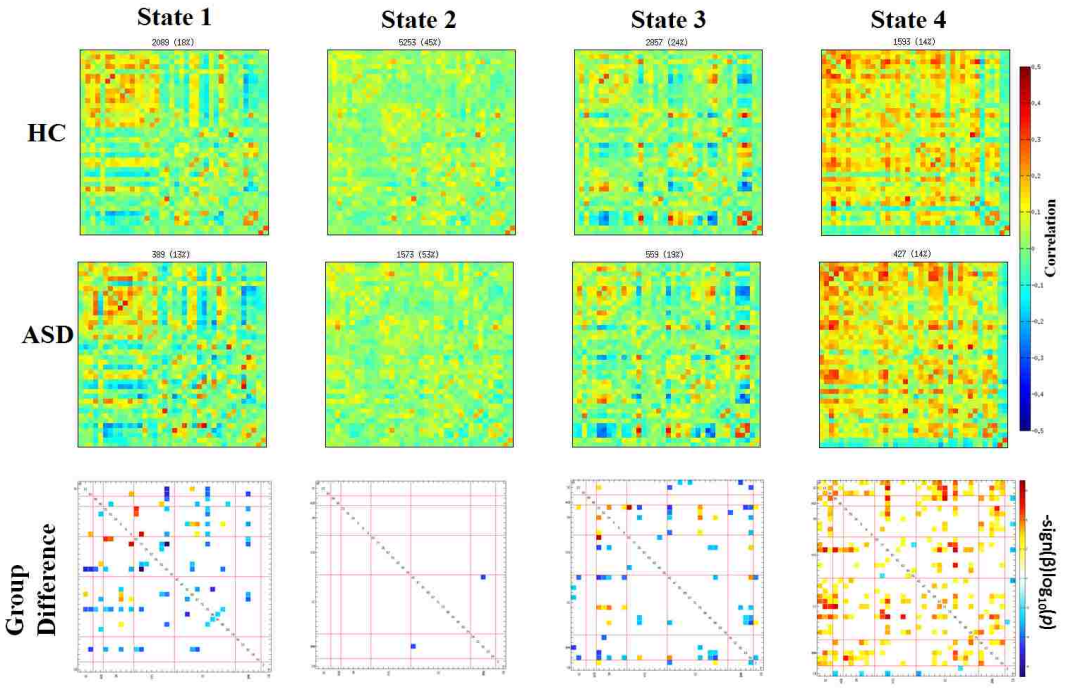

FIGURE A.6: The medians of cluster centroids by state for HC (top) and ASD (middle) along with the count of subjects that had at least one window in each state are shown. The bottom row shows the FDR-corrected (indicate $p < 0.05$) results of two-sample t-test performed across subject median dFNC maps by state.

A.3.3 Sensitivity analysis based on autistic trait and autism

We also performed a sensitivity analysis to evaluate the effects of SRS scores on summary measures of the dynamic states (MDT and FT). We removed the subjects who are diagnosed with ASD, as well as the subjects with SRS scores above the screening cutoff. Using this subset of the subjects (after exclusion, number of subjects=528), we performed the analyses for SRS score effects on MDT and FT (Figure A.7). The SRS sensitivity analysis did not reveal any FDR-corrected effect

of autistic traits. However, the direction of the effects remained the same as the original analysis (with 774 subjects).

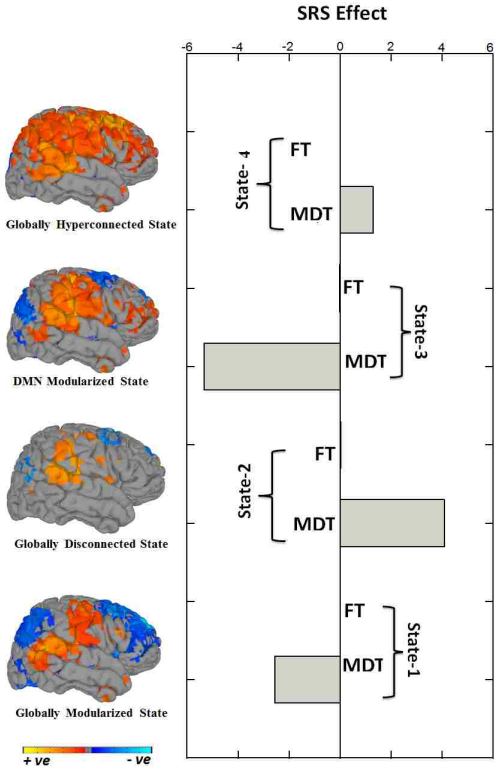

FIGURE A.7: Bar plots showing summary metrics from the 4 dynamic connectivity states in relation to autistic traits after removing subjects with autistic traits and ASD. The rendering brain maps are showing modularized positive (red) and negative (blue) connectivity for the corresponding dynamic states.

A.3.4 IQ-adjusted analyses

As ASD is often accompanied by deficits in cognition, it was important to also rule-out that any observed associations between autistic traits and dynamic connectivity were not simply a reflection of general intellectual ability. Analyses associating autistic traits with dynamic connectivity remained largely unchanged after adjusting for non-verbal IQ. Specifically, for whole-matrix associations in the four dynamic states, the general pattern of association remained. For the summary

measure MDT, regression coefficients did not change more than 5%, suggesting the association is not confounded by IQ.

A.3.5 Analyses of motion parameters

A.3.5.1 Analyses using original 5mm cut-off for maximum translation:

We investigated the effect of mean framewise-displacement (FD; calculated as the total absolute displacement in all dimensions (Power et al., 2012)) in the current sample (774 subjects, maximum translation <5mm), using the following regression models:

$$\text{Model}_{\text{max\_trans}<5mm} : MDT_i \sim \beta_0 + \beta_1 age_i + \beta_2 sex_i + \beta_3 FD_i^{\text{mean}} + \varepsilon_i \quad \text{(A.1)}$$

$$\text{Model}_{\text{max\_trans}<5mm} : MDT_i \sim \beta_0 + \beta_1 SRS_i + \beta_2 \text{age}_i + \beta_3 \text{sex}_i + \beta_3 FD_i^{\text{mean}} + \varepsilon_i \quad \text{(A.2)}$$

The following Table A.1 highlight the results from this analyses, where no association between mean FD and MDT was observed, and the original age, sex and SRS score associations with MDT remained highly consistent in terms of both directionality and significance of the effect.

Also, note that, no significant correlation between mean FD, and age, sex and SRS score was found in this follow-up analysis.

A.3.5.2 Analyses using 3mm cut-off for maximum translation:

(i)Age and Sex associations

		State 1	State 2	State 3	State-4
Age	β	0.0113	0.0048	-0.1136	-0.0443
	ρ	0.9249	-2.0628	0.7902	0.9287
Sex	β	-0.2260	-2.4168	4.2423	-1.0998
	ρ	0.7581	0.1009	<2E-10	0.2707
SRS	β	0.9516	10.4629	-4.6043	-0.4676
	ρ	0.4753	0.0003	0.0079	0.8082

TABLE A.1: Association of age, sex and SRS with mean dwell time with maximum translation <5mm

Sample size	**<3mm**	**<5mm**
Age and sex	689	774
SRS	500	560

TABLE A.2: sample sizes with maximum translation cut-offs 3mm and 5mm

First, we exclude subjects with maximum translation greater than 3mm. This new and conservative exclusion criterion resulted in 689 subjects with both age and sex information, and 500 subjects with age, sex and SRS score information. Table A.2 summarizes the sample sizes for original exclusion criterion (maximum translation $>$ 5mm) and the conservative exclusion criterion (maximum translation >3mm).

Next, we performed linear regression analysis to find the association between MDT and age and sex using the subjects from conservative (3mm) inclusion criterion. The following tables show the effect of age and sex on MDT. These results in Table A.3 confirm that the directionality and significance of age and sex associations even with this conservative cut-off have remained highly consistent and do not change the conclusions (where age is showing negative association with the MDT in state-2, and sex is showing positive association with MDT in state-3).

$$\text{Model}_{\text{max\_trans}<5mm} : MDT_i \sim \beta_0 + \beta_1 age_i + \beta_2 \text{sex}_i + \varepsilon_i \tag{A.3}$$

We wanted to see if the mean FD correlates with MDT of the subjects after applying the new 3mm inclusion criterion. To do this, we used the following

		State 1	State 2	State 3	State 4
Age	β	0.7633	-1.8050	-0.5327	-0.0310
	ρ	0.0515	0.0054	0.2426	0.9499
Sex	β	-0.5505	-1.9088	4.2280	-1.1953
	ρ	0.4842	0.1428	$< 2E-10$	0.2280

TABLE A.3: Association of age and sex with mean dwell time with maximum translation <3mm

regression model:

$$\text{Model}_{\text{max\_trans}<3mm} : MDT_i \sim \beta_0 + \beta_1 SRS_i + \beta_2 \text{age}_i + \beta_3 \text{sex}_i + \beta_3 FD_i^{\text{mean}} + \varepsilon_i \quad \text{(A.4)}$$

The results from the above linear regression analysis model also showed no association between mean FD and MDT, while the associations between age and sex with MDT remained highly consistent and not changing the conclusions

(ii) SRS score association

We also performed linear regression analyses on MDT and SRS scores with and without providing mean FD as a covariate in the model (for subjects with 3mm cut-off). The following Table A.4 shows that the results remained highly consistent and do not change any conclusions in terms of significance and directionality, with no association between MDT and mean FD.

$$\text{Model}_{\text{max\_trans}<5mm} : MDT_i \sim \beta_0 + \beta_1 age_i + \beta_2 \text{sex}_i + \varepsilon_i \quad \text{(A.5)}$$

$$\text{Model}_{\text{max\_trans}<3mm} : MDT_i \sim \beta_0 + \beta_1 SRS_i + \beta_2 \text{age}_i + \beta_3 \text{sex}_i + \beta_3 FD_i^{\text{mean}} + \varepsilon_i \quad \text{(A.6)}$$

Again, note that, no significant correlation between mean FD, and age, sex and SRS score was found in this follow-up analysis.

	SRS effect	State 1	State 2	State 3	State 4
Standard Model	β	0.6470	6.2354	-2.0674	-0.6791
	ρ	0.6381	0.0060	0.1964	0.6950
FD-Adjusted	β	0.6441	6.2237	-2.100	-0.6640
	ρ	0.6399	0.0061	0.1894	0.7017

TABLE A.4: Association of SRS with mean dwell time with maximum translation <3mm, with and without additionally adjusting for framewise-displacement

A.4 Elbow criterion for k-means clustering

In k-means clustering approach, a dataset is grouped into a user-defined number (k) of clusters. This algorithm clusters the data into k clusters, even if the number of clusters defined by the user for the given dataset is not correct. Thus, while using this algorithm, it is required to determine the optimum number of clusters. One of the commonly used methods to validate the optimum number of clusters is the elbow criterion (Kodinariya and Makwana, 2013).

For elbow criterion, k-means clustering algorithm is repeatedly run on the same dataset for a range of values of k (for example, choose k from 2 to 20 in Figure A.8), and for each value of k, calculate the sum of squared errors (SSE). Finally, a line chart of the SSE for each value of k is plotted and investigated. If the line chart resembles an arm, then the 'elbow' on the arm is the best or optimum value of cluster number k. The main idea is to obtain a small SSE, while considering the fact that SSE tends to decrease to 0 as the value of k is increased. In fact, the SSE is exactly 0 when k is equal to the number of data point. Thus, in order to choose a small value of k that still has a low SSE, the elbow from the line chart guides the user where the decreasing values with increasing k will start.

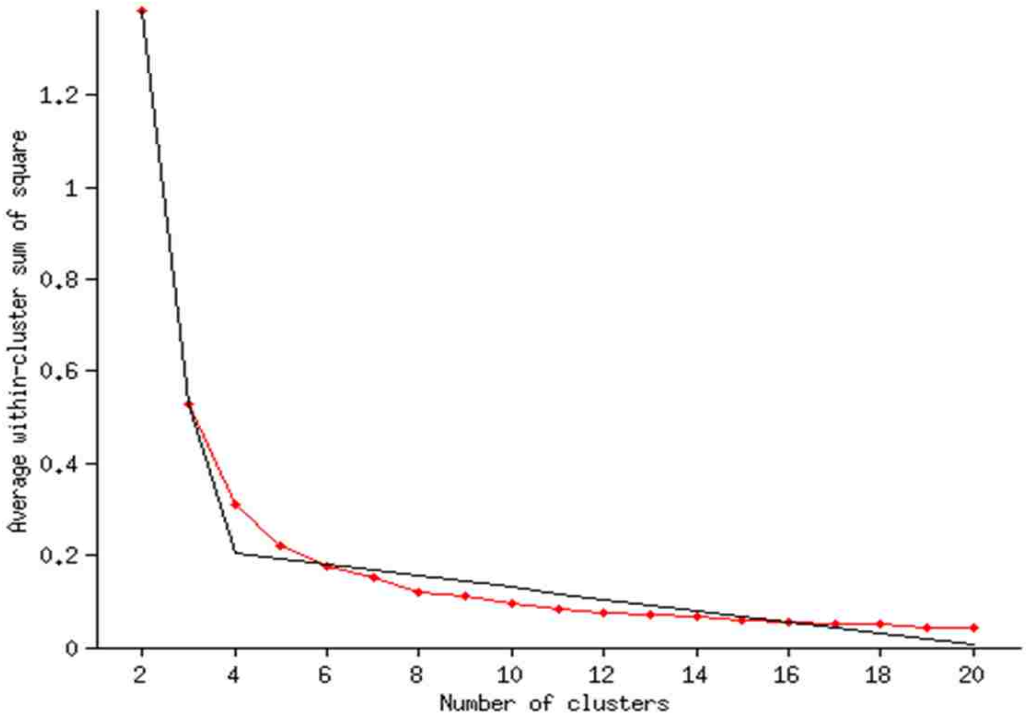

FIGURE A.8: Elbow criterion for k-means clustering algorithm. The red curve is showing the observed values of the average within-cluster sum of square for cluster size, k=2 to 20. The black curve is the best fit of the elbow-shaped curve to the observed data (red curve), by minimizing the distance between the observed data and the elbow-shaped curve. Here, optimum number of clusters is 4 as shown by the elbow-shaped curve.

A.5 Intrinsic connectivity network selection

For all independent components or ICs, we computed what percentage of the thresholded component spatial maps overlap with gray matter. If the overlap with gray matter was above 60% (showing high overlap with gray matter, and low spatial overlap with known vascular, ventricular, motion, and susceptibility artifacts, and time courses dominated by low frequency fluctuations), we considered that component as ICN. Otherwise we excluded it. Also, we investigated the spectral characteristics of the component time courses using two previously used metrics to classify components (Robinson et al., 2009):

1. Dynamic range: it is defined by the difference between peak power and minimum power at frequencies to the right of the peak. The following Figure A.9 shows depiction of dynamic range.

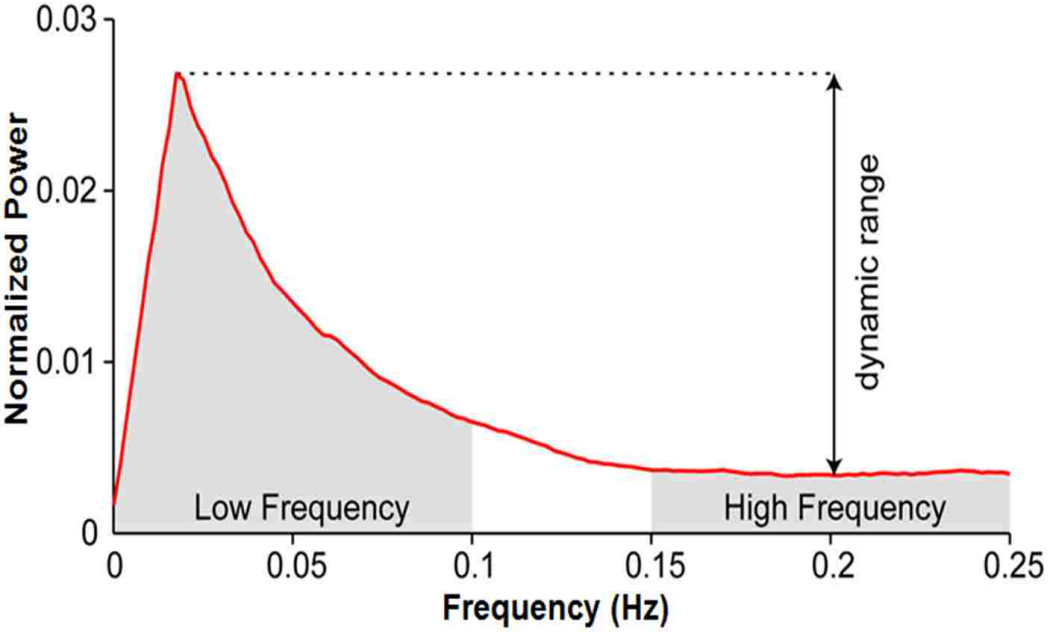

FIGURE A.9: Example of the average power spectrum of an independent component illustrating the features used to compute dynamic range and low frequency to high frequency power ratio (Allen et al., 2012a).

2. (ii) Low frequency to high frequency power ration: it is defined by the ratio of the integral of spectral power below 0.10 Hz to the integral of power between 0.15 and 0.25 Hz. A component is highly likely to be an ICN if it has a higher low frequency spectral power (that is, the ratio of low frequency to high frequency power would be higher). Figure A.10 shows an example of scatterplot of low frequency to high frequency ratio, versus dynamic range for components characterized as ICN, artifacts or mixture of both types.

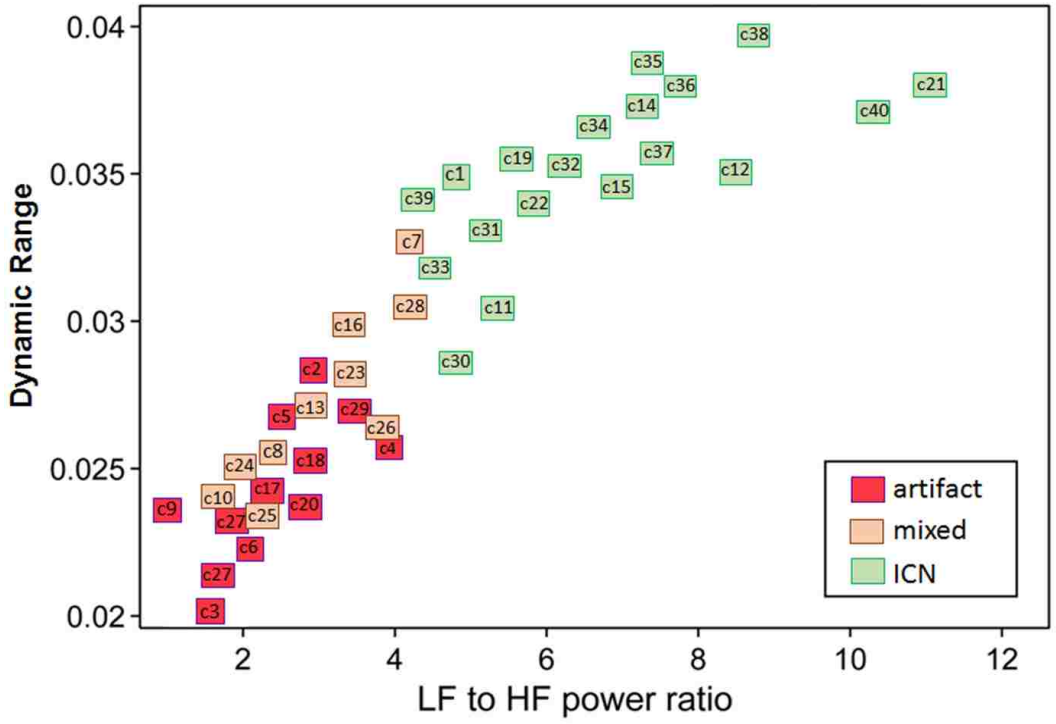

FIGURE A.10: Example of scatter plot of low frequency to high frequency power ratio versus dynamic range for independent components. Component spatial maps were used to characterize components as ICNs, artifacts or mixture of the two (Allen et al., 2012a).

A.6 Subject exemplars selection and k-means clustering algorithm

As mentioned in chapter 3, we initialized the cluster centroid by using the subject exemplars (most variable FC windows) to find a starting point. Previous studies on dynamic connectivity using fMRI, EEG and MEG modalities have suggested that, k-means clustering is very sensitive to the starting point, and by using a better staring point, k-means can perform optimally. This choice of starting points for clustering may affect the findings of dynamic states, as without any initial starting point, or even with a bad starting point, the clustering results would not be well

optimized. Figure A.11 shows the subject exemplars selection during k-means clustering approach.

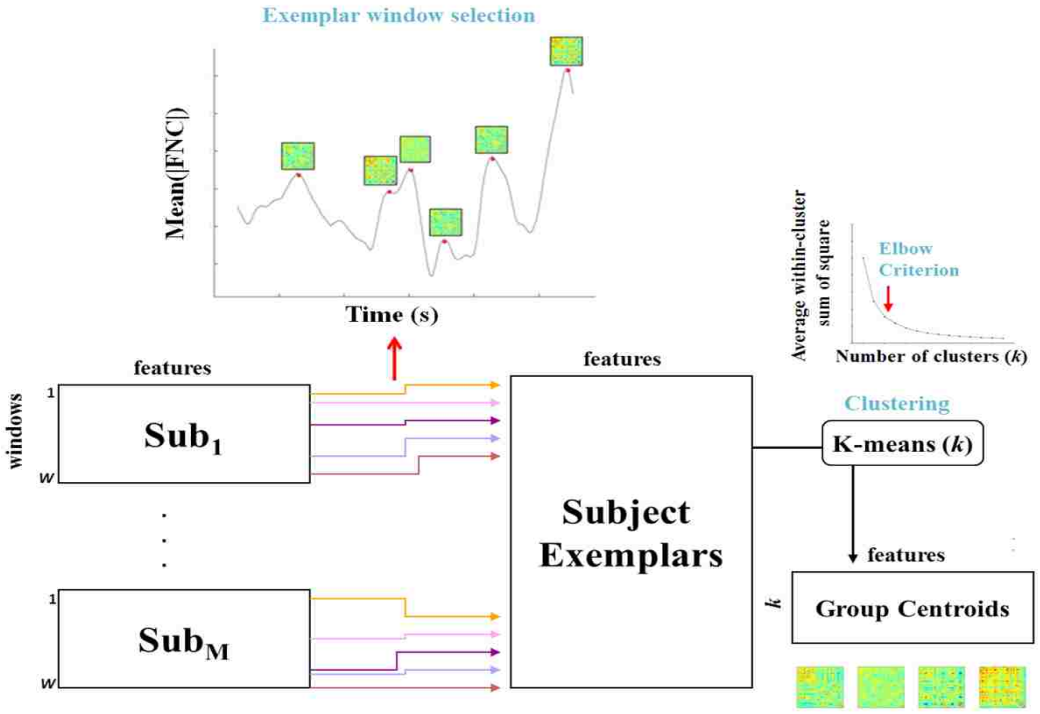

FIGURE A.11: K-means clustering approach and subject exemplars selection (Allen et al., 2012a).

A.7 Validation of dynamic clustering approach

To evaluate whether 'random' or 'spurious' dynamics are a concern in our multivariate clustering approach, we performed simulations where an inconsistent phase randomization in the Fourier domain was applied to original ICN time courses to create new, 'synthetic-like' times courses with a random phase shift. We employed a similar approach as shown in (Handwerker et al., 2012), where we first preserved the important properties of the phase randomized time series, such as power spectrum and autocorrelation, while creating the null model. We then computed dFNC correlation matrices using these phase-randomized time courses for

all subjects. We performed k-means clustering on the dFNC matrices and compared the observed cluster centroids to those obtained using original nonrandomized data. To ensure that the correlation magnitudes (which will be different in the phase-randomized data versus the original data) were not driving the observed structure in cluster centroids, we demeaned the dFNC correlation time series prior to clustering for both original and phase-randomized datasets.

For the multivariate clustering approach, the cluster centroids from k-means clustering of original data (Figure A.12) show structured modular patterns whereas the centroids obtained from dFNC matrices from phase-randomized time courses show no structure. To quantify this apparent difference, we calculated the total distance between centroids (defined as sum of pairwise Euclidean distances between all five k-means cluster centroids) for the cluster centroids derived using phase randomized ICN time courses and for the observed data. As seen in Figure A.13, the observed distance between centroids (red triangle) is much larger and shows no overlap with the null distribution of distances (histogram bar plots), generated by clustering the dFNC matrices of phase-randomized time courses (n = 500 iterations). Note that, the distance between centroids in the original nonrandomized data should be much greater than the null distribution of the distances between centroids, which are expected to be very close to each other.

The phase randomization approach that we applied here for generating the null model is appropriate and attractive since it preserves both the spectral power as well as the temporal autocorrelation of the original timeseries. These simulations suggest that the multivariate clustering approach to detect connectivity dynamics, which is based on patterns of connectivity rather than variability per se, is indeed uncovering effects that are clearly distinguishable from a null.

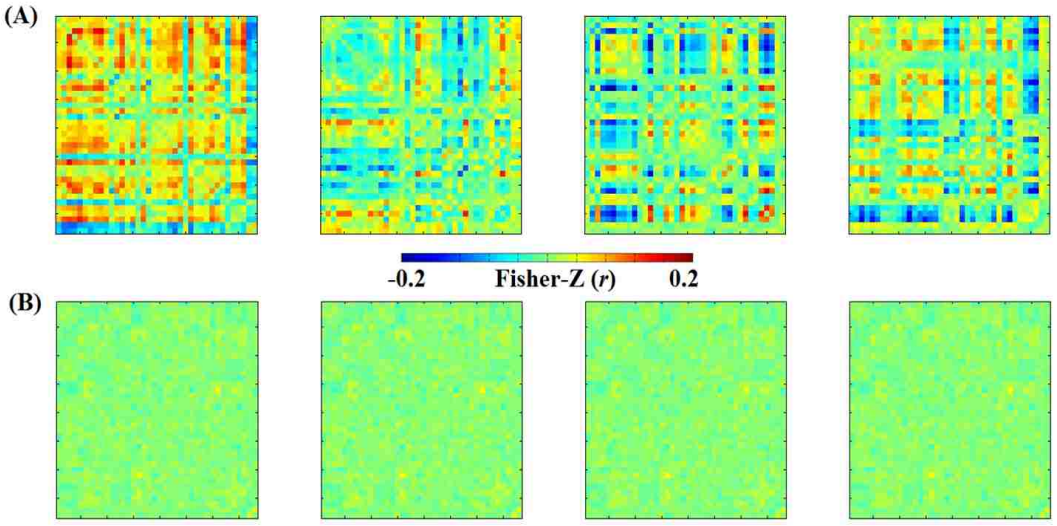

FIGURE A.12: A) Centroids obtained from k-means clustering of demeaned dFNC correlation time courses computed using ICN time courses from 774 subjects. B) Centroids obtained from k-means clustering of the same data as shown in A, except that ICN time courses were phase randomized in the Fourier domain.

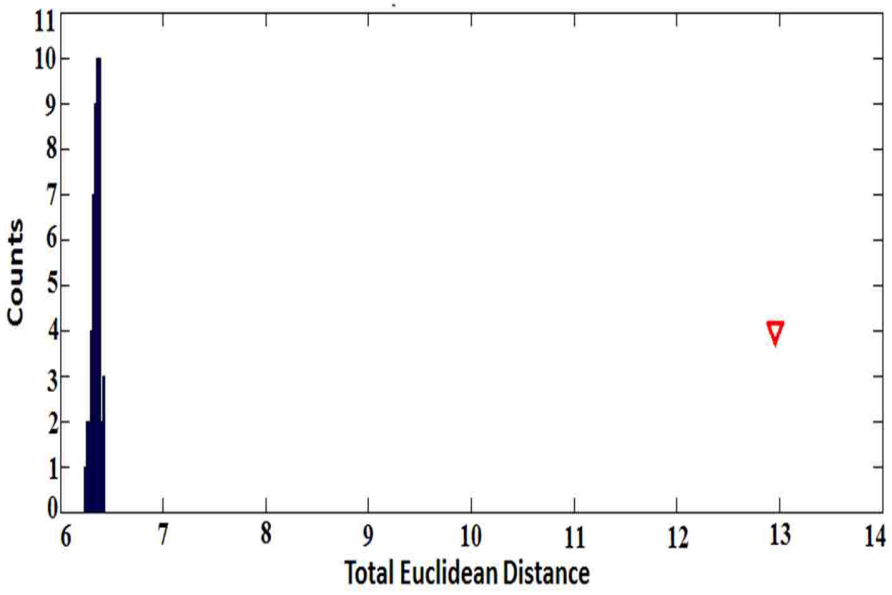

FIGURE A.13: Null distribution of total Euclidean distances (defined as sum of pairwise Euclidean distances between all five k-means cluster centroids) between cluster centroids derived using phase randomized ICN time courses (histogram bar plots) and the actual (un-randomized) data (red triangle).

A.8 Signal-to-fluctuation-noise Ratio (SFNR)

To measure the temporal stability, we computed the signal to fluctuation noise ratio or SFNR (Friedman and Glover, 2006), by using the following equation:

$$SFNR = \frac{\text{average}(\text{average}(S_{\text{object}_{\text{voxel\_intensity}}}))_{\text{time}}}{std_{\text{temporal}}(\text{average}(S_{\text{object}_{\text{voxel\_intensity}}}))} \tag{A.7}$$

Where, ROI: 20x20 voxels at the center of the object (in this case, the brain)

Signal: the average voxel intensity in all the ROIs defined in the object, averaged across time. Fluctuation noise: the (temporal) standard deviation of the (spatial) average in the same ROIs, after the slow drift (quadratic) has been removed from the temporal series.

A.9 Normalization with a study-specific template

We have also performed a sub-analysis for this specific sample, where we first created an age appropriate, study-specific structural template (GenR template) by taking the average of the middle volume of all the subjects, and then re-normalizing the group aggregate maps of the independent components as found by our original group-ICA approach using this study-specific template. We also re-normalized a subset of 50 subjects' data to this study specific template. Using these study-specific normalized data, we performed spatial-temporal regression (STR) analysis and generated back-reconstructed spatial maps and time-courses for those subjects. Finally, we computed the static FNC matrix for these 50 subjects using the STR back-reconstructed time-courses, and compared it with the original static FNC matrix for the same 50 subjects. We found no significant statistical

	Sample=560	**Beta**	**p-value**
Association of MDT and SRS	**State-2**	12.07	0.0003
	State-3	-5.90	0.008
	Sample=208	**Beta**	**p-value**
	State-2	17.92	<2E-10
	State-3	-3.68	0.156

TABLE A.5: Association of MDT and SRS for original sample and restricted-age analysis.

difference between the two static FNC matrices. This is expected and is one of the benefits of using the group ICA approach, which we have shown is relatively robust to spatial variability among subjects (Allen et al., 2012b).

A.10 Analyses of co-linearity between age and SRS effects

In order to verify if there is any co-linearity between the effects of age and those of SRS (even though little/no interaction between age and SRS score was observed), we ran a restricted-age analysis, where we took a sub-group of 8-to-9-year-old subjects (total 208 children). Restricting the age-range in the study limits the potential for residual age-related confounding. We then performed the regression analysis on the MDT of this sub-group and checked if the associations that we observed with full dataset (560 subjects) still hold. In general, in instances of residual confounding, we would expect to see highly attenuated effect estimates and non-significant p-values in a restricted sample such as this. However, results are consistent with the original study, and in some cases even become stronger, suggesting minimal residual age-related confounding. Results in states that showed significant effects in the original study are given in the below Table A.5:

Child Characteristics (n=774)	
Age at MRI	7.99±1.01
Gender (% boy)	52.1
Ethnicity (%)	
Dutch	71.8
Other Western	6.5
Non-Western	21.7
Social Responsiveness Scale weighted total score	0.27±0.31
Age(years) at Social Responsiveness Scale assessment	6.2±0.46
No-verbal IQ	102±14.5

TABLE A.6: Participant characteristics

Cognitive Measures	Full Sample n=774		Confirmed Cases n=19	
	Mean	Range	Mean	Range
Non-verbal intelligence	102	50-140	99	67-122
Language Comprehension Score	22	12-26	22	13-26
Word production 30 months, no of words	244	2-310	230	60-301
Non verbal intelligence was measured using two subsets of the Snijders-Oomen Neit-verbale				

TABLE A.7: Additional participant characteristics

Also, we computed the spearman correlation between age and SRS for the full sample and found no correlation between age and SRS (r=0.03, p-value =0.5248).

ICN Region	Coordinate
Sub-cortical networks	
IC: 37	
Right Putamen	[18 13 -6]
IC: 13	
Left Putamen	[-27 0 3]
Right Putamen	[27 3 3]
IC: 60	
Right Thalamus	[12 -30 9]
Auditory networks	
IC:99	
Left Superior Temporal Gyrus	[-51 -27 9]
Right Superior Temporal Gyrus	[60 -18 9]
Sensorimotor networks	
IC:21	
Left SMA	[-3 6 48]
IC: 51	
Right SupraMarginal Gyrus	[54 -33 27]
IC: 24	
Right SupraMarginal Gyrus	[-58 -24 41]
IC: 3	
Left Precentral Gyrus	[-36 -24 57]
IC: 6	
Right Paracentral Lobule	[6 -30 66]
IC: 8	
Right Postcentral Gyrus	[54 -9 33]
Left Postcentral Gyrus	[-51 -12 33]
Visual networks	
IC: 53	
Right Fusiform Gyrus	[27 -45 -12]
Left Fusiform Gyrus	[-24 -48 -9]
IC: 77	
Left Lingual Gyrus	[-9 -57 0]
IC: 26	
Left Calcarine Gyrus	[-12 -60 18]
IC: 57	
Right Fusiform Gyrus	[30 -78 -6]
IC: 61	
Left Cuneus	[3 -84 24]
IC: 62	
Left Cuneus	[12 -72 36]
IC: 80	
Right Superior Occipital Gyrus	[30 -66 45]
IC: 81	[21 -66 9]
Right Superior Occipital Gyrus	

ICN Region	Coordinate
Cognitive control networks	
Left Superior Medial Gyrus	[-6 55 9]
IC: 47	
Left Middle Frontal Gyrus	[-24 48 25]
IC: 31	
Left Superior Frontal Gyrus	[-18 22 53]
IC: 89	
Right Middle Temporal Gyrus	[45 -60 12]
IC: 67	
Left Middle Temporal Gyrus	[-48 -57 12]
IC: 71	
Right Middle Frontal Gyrus	[42 7 40]
IC: 73	
Right Middle Frontal Gyrus	[33 45 12]
IC: 96	
Left Inferior Frontal Gyrus	[-48 15 27]
IC: 90	
Right Inferior Parietal Lobule	[48 -39 48]
IC: 98	
Right Insula Lobe	[45 3 6]
IC: 83	
Right Middle Temporal Gyrus	[51 -39 6]
IC: 79	
Left Superior Parietal Lobule	[-30 -54 48]
Default-mode networks	
IC: 34	
Right Precuneus	[3 -65 55]
IC: 95	
Right Middle Cingulate Cortex	[6 30 30]
IC: 12	
Left Middle Cingulate Cortex	[0 0 33]
IC: 92	
Right Angular Gyrus	[48 -57 39]
IC: 19	
Left Precuneus	[0 -57 33]
IC: 50	
Left Angular Gyrus	[-45 -60 36]
Cerebellar networks	
IC: 2	
Left Cerebellum	[-33 -66 -42]
IC: 7	
Right Cerebellum	[36 -63 -39]

FIGURE A.14: Table showing peak coordinates of ICN spatial maps.Coordinates = max coordinate (mm) in MNI space, following LPI conversion.

APPENDIX B

APPENDIX B

B.1 Feature selection using DISR method

Figure B.1 shows the information on how many of the 10 cross-validation (CV) runs selected the same features using the double input symmetric relevance (DISR) method (Meyer and Bontempi, 2006) . Note that total number of features that were selected at least once in the 10 CV 124. Here, to be consistent with the number of features used in static FNC classification, we are just showing the counts for top 100 features. Here, first we obtained 100 static featured for each cross-validation iteration. Then we computed how many of the 10 CV runs had these features in common. For convenience, we labeled the 100 features from the first CV run as (feat 1, feat 2, ..., feat 100), and used them as a reference while comparing the features from all other CV runs. Out of those 100 features obtained using DISR method at each CV run, 70 features (feat 1 through feat 70) were consistently found across all 10 CV runs. 9 features (feat 71 through feat 79) were consistent across 9 CV runs. 15 features (feat 80 through feat 94) were

present across 8 CV runs. The remaining 6 features (feat 95 through feat 100) were obtained consistently in 7 CV runs.

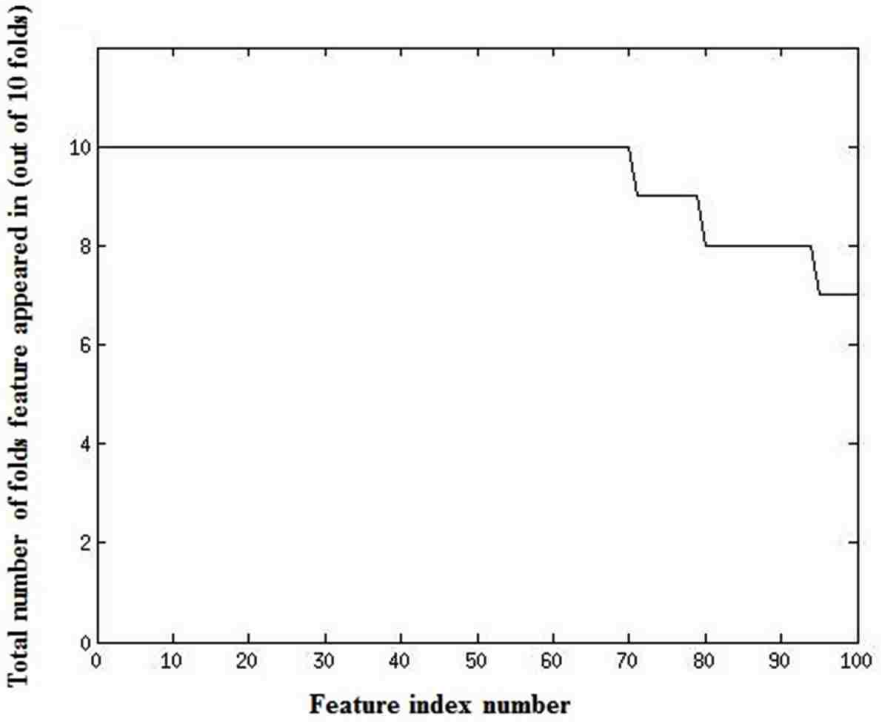

FIGURE B.1: Plot showing features that were consistently selected across different cross-validation runs using DISR method.

Also, as we increased the number of features obtained using DISR method, the number of CV runs with consistent features decreased. For our analysis, we thresholded at minimum of 7 CV folds where features selected by DISR method were commonly found.

B.2 Dynamic FNC feature selection method

Figure B.2 shows an illustration of the dynamic FNC feature selection procedure. For each cross-validation run and for each training subject, the regression analysis was performed at each windowed FNC matrix (using the regression matrix obtained for that CV run using k-means clustering). Then, 15 beta coefficients

or fitness scores were obtained at each of these windows, resulting in 180 $\times$ 15β from all the dynamic windows for each training subject. Once the β coefficients were obtained for all the training subjects across all the dynamic windows, we then computed mean β coefficient across dynamic windows (each subject with 15 β). The classifier finally used these β coefficients as dynamic FNC features.

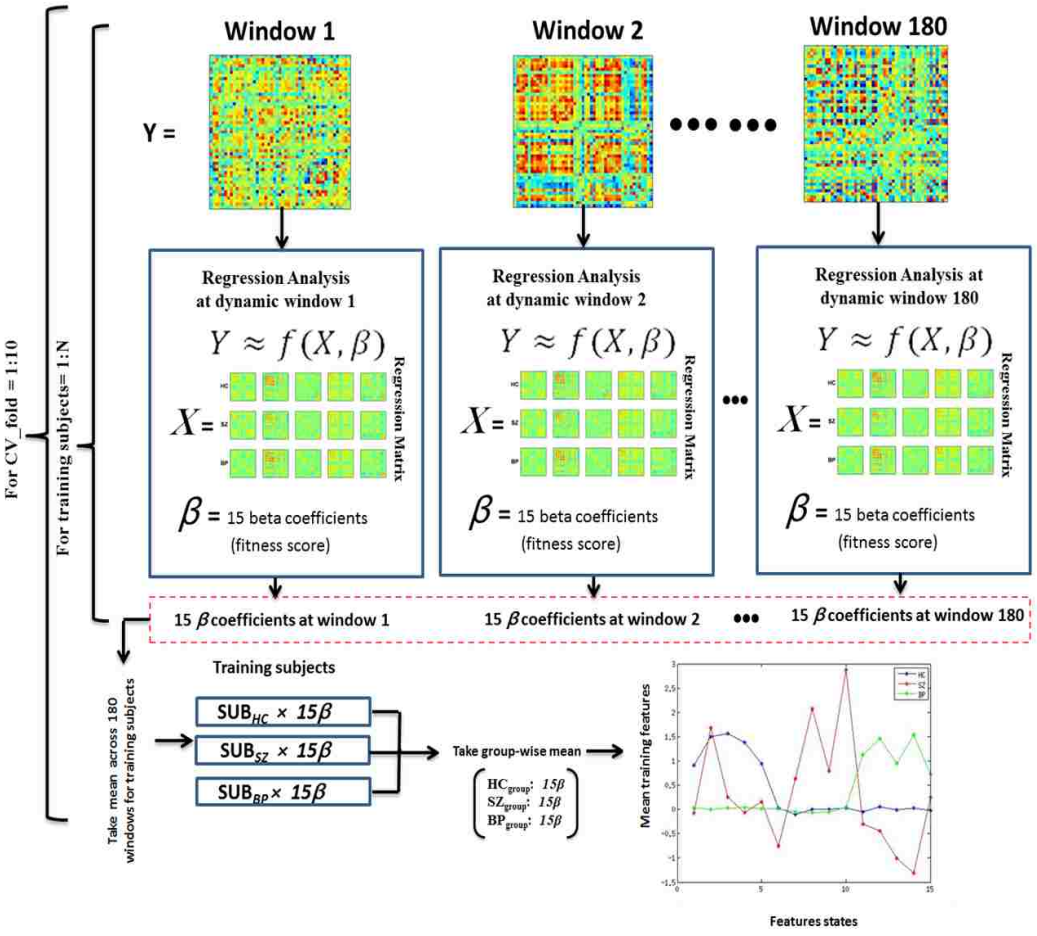

FIGURE B.2: An illustration showing the dynamic FNC feature selection procedure.

B.3 Computation of chance level for classification accuracy

Figure B.3 shows the null distributions of classification accuracy from the empirical tests with 95% confidence intervals for all three classifiers. To determine the chance levels for individual classifier accuracy, we performed 300-run permutation tests. For each permutation run, we randomly shuffled the group labels, and followed the original classification analyses using sFNC, dFNC and combined FNC features. We then recorded the overall accuracy for the classifiers at the end of each permutation run. Our results show that, for classifiers using sFNC, dFNC and combined FNC features, the average accuracy is around 35% (sFNC=34.88%, dFNC=34.56% and Combined=34.82%), with p-value <0.005 for all three chance levels.

Mean correlation ([minimum, maximum])			
Dynamic States	**HC Group**	**SZ Group**	**BP Group**
State 1	0.927 ([0.635 , 0.983])	0.849 ([0.769 , 0.977])	0.735 ([0.56 , 0.927])
State 2	0.981 ([0.941 , 0.992])	0.982 ([0.965 ,0.990])	0.893 ([0.859 , 0.934])
State 3	0.991 ([0.976 , 0.998])	0.957 ([0.887 , 0.993])	0.636 ([0.385 , 0.925])
State 4	0.984 ([0.970 , 0.993])	0.866 ([0.668 , 0.973])	0.959 ([0.882 , 0.998])
State 5	0.969 ([0.896 , 0.993])	0.879 ([0.775 , 0.952])	0.762 ([0.613 , 0.932])

TABLE B.1: Group-wise mean correlation for individual dynamic states

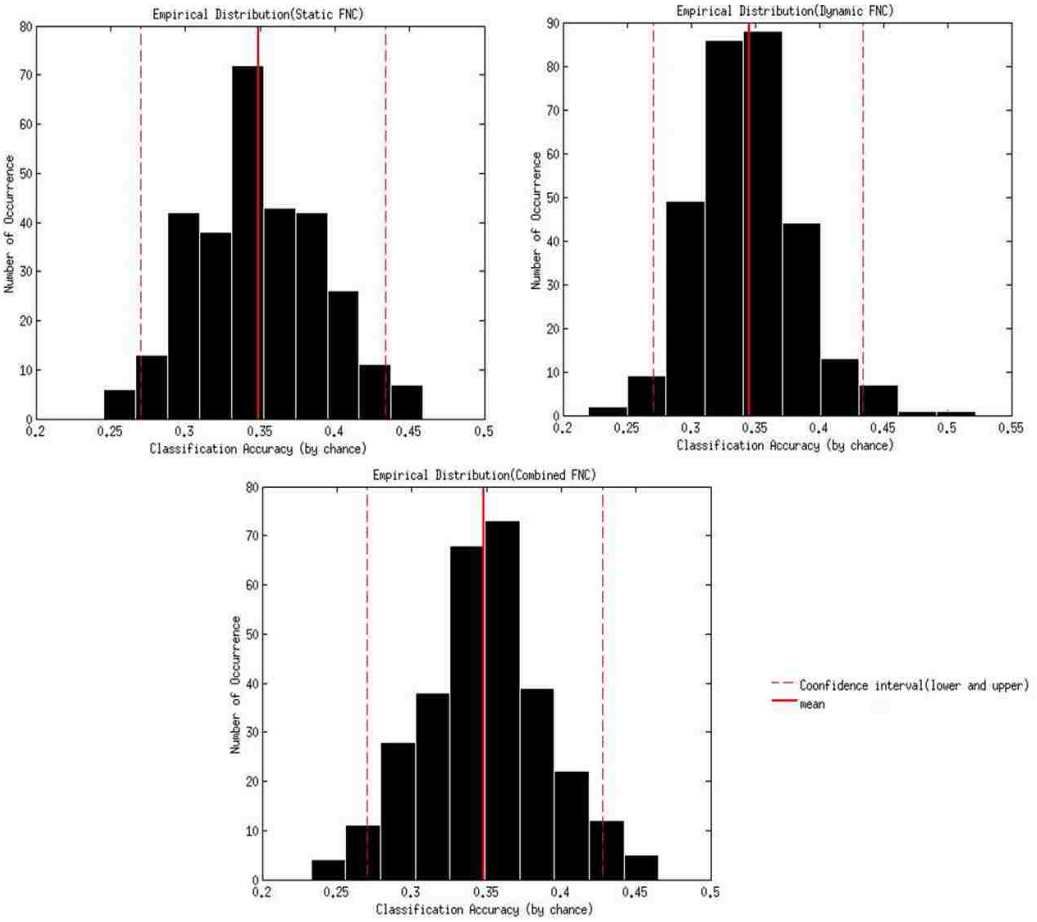

FIGURE B.3: Chance levels for classification accuracy based on the permutation test.

B.4 Details on proportion test

To evaluate the statistical significance across all statistical measures (overall accuracy, sensitivity, specificity, PPV and NPV among all three classifiers, we performed 2-sample test for equality of proportions with 95% confidence level using the built-in R function prop.test ( ). Following parameters were used to perform the proportion tests:

$$\text{prop.test}\left(c(A_{\text{stat\_count}}, B_{\text{stat\_count}}), c(A_{\text{total\_count}}, B_{\text{total\_count}})\right) \tag{B.1}$$

where

$A_{\text{stat\_count}}$= count of group 'G' for a particular statistical measure for classifier 'A'.

$A_{\text{total\_count}}$= total number of subjects in group 'G' for classifier 'A'.

$B_{\text{stat\_count}}$= count of group 'G' for a particular statistical measure for classifier 'B'.

$B_{\text{total\_count}}$= total number of subjects in group 'G' for classifier 'A'.

G = $[HC, SZ, BP]$

TABLE B.2: P-values from the proportion test among all three classification algorithms and all the statistical measures

Groups		SFNC+ DFNC	SFNC + Combined FNC	DFNC+ Combined FNC
	Measure	**P-value**	**P-value**	**P-value**
	Overall Accuracy	3.229ÃŰ10-6	8.653ÃŰ10-8	0.541
HC	**Sensitivity**	0.002264	0.005128	1
	Specificity	0.1989	0.0417	0.591
	PPV	0.08414	0.02074	0.6761
	NPV	0.007462	0.1126	1
SZ	**Sensitivity**	0.03702	0.02039	1
	Specificity	1.387ÃŰ10-5	1.762ÃŰ10-6	0.7816
	PPV	0.0001419	2.364ÃŰ10-5	0.8022
	NPV	0.01376	0.006749	0.982
BP	**Sensitivity**	0.002525	1.045ÃŰ10-6	0.0501
	Specificity	0.1885	0.06773	0.7831
	PPV	0.0297	0.002494	0.5776
	NPV	0.02189	7.26ÃŰ10-5	0.07482

Overall Accuracy (%)			
	Static FNC	**Dynamic FNC**	**Combined FNC**
Classification with all 159 subjects	59.12	84.28	88.68
Classification with 156 subjects	58.97	83.97	87.17
Difference between two classification models	0.15	0.31	1.51

TABLE B.3: Difference in classification accuracy for analyses with 159 subjects and 156 subjects (after removing 3 outliers)

BIBLIOGRAPHY

Abou-Elseoud, A., Starck, T., Remes, J., Nikkinen, J., Tervonen, O., and Kiviniemi, V. (2010). The effect of model order selection in group pica. *Human brain mapping*, 31(8):1207–1216.

Achard, S., Salvador, R., Whitcher, B., Suckling, J., and Bullmore, E. (2006). A resilient, low-frequency, small-world human brain functional network with highly connected association cortical hubs. *The Journal of neuroscience*, 26(1):63–72.

Achim, A. M. and Lepage, M. (2005). Episodic memory-related activation in schizophrenia: meta-analysis. *The British Journal of Psychiatry*, 187(6):500–509.

Aguayo, J. (1990). Auditory hallucinations and smaller superior temporal gyral volume in schizophrenia. *Am. J. Psychiatry*, 147:1457–1462.

Allen, E., Eichele, T., Wu, L., and Calhoun, V. (2013). Eeg signatures of functional connectivity states. *Proceedings of the Human Brain Mapping*.

Allen, E. A., Damaraju, E., Plis, S. M., Erhardt, E. B., Eichele, T., and Calhoun, V. D. (2012a). Tracking whole-brain connectivity dynamics in the resting state. *Cerebral cortex*, page bhs352.

Allen, E. A., Erhardt, E. B., Damaraju, E., Gruner, W., Segall, J. M., Silva, R. F., Havlicek, M., Rachakonda, S., Fries, J., Kalyanam, R., et al. (2011). A baseline for the multivariate comparison of resting-state networks. *Frontiers in systems neuroscience*, 5:2.

Allen, E. A., Erhardt, E. B., Wei, Y., Eichele, T., and Calhoun, V. D. (2012b). Capturing inter-subject variability with group independent component analysis of fmri data: a simulation study. *Neuroimage*, 59(4):4141–4159.

Altshuler, L. L., Bartzokis, G., Grieder, T., Curran, J., Jimenez, T., Leight, K., Wilkins, J., Gerner, R., and Mintz, J. (2000). An mri study of temporal lobe structures in men with bipolar disorder or schizophrenia. *Biological psychiatry*, 48(2):147–162.

Amari, S.-I. (1998). Natural gradient works efficiently in learning. *Neural computation*, 10(2):251–276.

Arbabshirani, M. R., Havlicek, M., Kiehl, K. A., Pearlson, G. D., and Calhoun, V. D. (2013a). Functional network connectivity during rest and task conditions: a comparative study. *Human brain mapping*, 34(11):2959–2971.

Arbabshirani, M. R., Kiehl, K., Pearlson, G., and Calhoun, V. D. (2013b). Classification of schizophrenia patients based on resting-state functional network connectivity. *Frontiers in neuroscience*, 7:133.

Arieli, A., Sterkin, A., Grinvald, A., and Aertsen, A. (1996). Dynamics of ongoing activity: explanation of the large variability in evoked cortical responses. *Science*, 273(5283):1868.

Arribas, J. I., Calhoun, V. D., and Adali, T. (2010). Automatic bayesian classification of healthy controls, bipolar disorder, and schizophrenia using intrinsic connectivity maps from fmri data. *IEEE Transactions on Biomedical Engineering*, 57(12):2850–2860.

Baxter, A., Brugha, T., Erskine, H., Scheurer, R., Vos, T., and Scott, J. (2015). The epidemiology and global burden of autism spectrum disorders. *Psychological medicine*, 45(03):601–613.

Becerril, K. E., Repovs, G., and Barch, D. M. (2011). Error processing network dynamics in schizophrenia. *Neuroimage*, 54(2):1495–1505.

Beckmann, C. F., DeLuca, M., Devlin, J. T., and Smith, S. M. (2005). Investigations into resting-state connectivity using independent component analysis. *Philosophical Transactions of the Royal Society of London B: Biological Sciences*, 360(1457):1001–1013.

Bell, A. J. and Sejnowski, T. J. (1995). An information-maximization approach to blind separation and blind deconvolution. *Neural computation*, 7(6):1129–1159.

Berument, S. K., Rutter, M., Lord, C., Pickles, A., and Bailey, A. (1999). Autism screening questionnaire: diagnostic validity. *The British Journal of Psychiatry*, 175(5):444–451.

Binder, J. R., Desai, R. H., Graves, W. W., and Conant, L. L. (2009). Where is the semantic system? a critical review and meta-analysis of 120 functional neuroimaging studies. *Cerebral Cortex*, 19(12):2767–2796.

Biswal, B., Zerrin Yetkin, F., Haughton, V. M., and Hyde, J. S. (1995). Functional connectivity in the motor cortex of resting human brain using echo-planar mri. *Magnetic resonance in medicine*, 34(4):537–541.

Blanken, L. M., Mous, S. E., Ghassabian, A., Muetzel, R. L., Schoemaker, N. K., El Marroun, H., van der Lugt, A., Jaddoe, V. W., Hofman, A., Verhulst, F. C., et al. (2015). Cortical morphology in 6-to 10-year old children with autistic traits: a population-based neuroimaging study. *American Journal of Psychiatry*, 172(5):479–486.

Bluhm, R. L., Miller, J., Lanius, R. A., Osuch, E. A., Boksman, K., Neufeld, R. W., Théberge, J., Schaefer, B., and Williamson, P. C. (2009). Retrosplenial cortex connectivity in schizophrenia. *Psychiatry Research: Neuroimaging*, 174(1):17–23.

Bokde, A., Lopez-Bayo, P., Meindl, T., Pechler, S., Born, C., Faltraco, F., Teipel, S., Möller, H.-J., and Hampel, H. (2006). Functional connectivity of the fusiform gyrus during a face-matching task in subjects with mild cognitive impairment. *Brain*, 129(5):1113–1124.

Britz, J., Van De Ville, D., and Michel, C. M. (2010). Bold correlates of eeg topography reveal rapid resting-state network dynamics. *Neuroimage*, 52(4):1162–1170.

Buckner, R. L., Andrews-Hanna, J. R., and Schacter, D. L. (2008). The brain's default network. *Annals of the New York Academy of Sciences*, 1124(1):1–38.

Buckner, R. L., Sepulcre, J., Talukdar, T., Krienen, F. M., Liu, H., Hedden, T., Andrews-Hanna, J. R., Sperling, R. A., and Johnson, K. A. (2009). Cortical hubs revealed by intrinsic functional connectivity: mapping, assessment of stability,

and relation to alzheimer's disease. *The Journal of Neuroscience*, 29(6):1860–1873.

Cabeza, R. and Nyberg, L. (2000). Imaging cognition ii: An empirical review of 275 pet and fmri studies. *Journal of cognitive neuroscience*, 12(1):1–47.

Calhoun, V., Adali, T., McGinty, V., Pekar, J., Watson, T., and Pearlson, G. (2001a). fmri activation in a visual-perception task: network of areas detected using the general linear model and independent components analysis. *NeuroImage*, 14(5):1080–1088.

Calhoun, V., Adali, T., Pearlson, G., and Pekar, J. (2001b). Group ica of functional mri data: separability, stationarity, and inference. In *Proc. Int. Conf. on ICA and BSS San Diego, CA. p*, volume 155.

Calhoun, V., Adali, T., Pearlson, G., and Pekar, J. (2001c). A method for making group inferences from functional mri data using independent component analysis. *Human brain mapping*, 14(3):140–151.

Calhoun, V., Adali, T., Pearlson, G., and Pekar, J. (2001d). Spatial and temporal independent component analysis of functional mri data containing a pair of task-related waveforms. *Human brain mapping*, 13(1):43–53.

Calhoun, V. et al. (2004a). Group ica of fmri toolbox (gift). *Online at http://icatb. sourceforge. net*.

Calhoun, V. D. and Adali, T. (2012). Multisubject independent component analysis of fmri: a decade of intrinsic networks, default mode, and neurodiagnostic discovery. *IEEE reviews in biomedical engineering*, 5:60–73.

Calhoun, V. D., Adalı, T., and Pekar, J. J. (2004b). A method for comparing group fmri data using independent component analysis: application to visual, motor and visuomotor tasks. *Magnetic resonance imaging*, 22(9):1181–1191.

Calhoun, V. D., Eichele, T., and Pearlson, G. (2009a). Functional brain networks in schizophrenia: a review. *Frontiers in human neuroscience*, 3:17.

Calhoun, V. D., Kiehl, K. A., and Pearlson, G. D. (2008a). Modulation of temporally coherent brain networks estimated using ica at rest and during cognitive tasks. *Human brain mapping*, 29(7):828–838.

Calhoun, V. D., Liu, J., and Adalı, T. (2009b). A review of group ica for fmri data and ica for joint inference of imaging, genetic, and erp data. *Neuroimage*, 45(1):S163–S172.

Calhoun, V. D., Maciejewski, P. K., Pearlson, G. D., and Kiehl, K. A. (2008b). Temporal lobe and âĂIJdefaultâĂİ hemodynamic brain modes discriminate between schizophrenia and bipolar disorder. *Human brain mapping*, 29(11):1265–1275.

Calhoun, V. D., Miller, R., Pearlson, G., and Adalı, T. (2014). The chronnectome: time-varying connectivity networks as the next frontier in fmri data discovery. *Neuron*, 84(2):262–274.

Calhoun, V. D., Sui, J., Kiehl, K., Turner, J., Allen, E., and Pearlson, G. (2011). Exploring the psychosis functional connectome: aberrant intrinsic networks in schizophrenia and bipolar disorder. *Magnetic resonance imaging of disturbed brain connectivity in psychiatric illness*, page 35.

Camchong, J., MacDonald, A. W., Bell, C., Mueller, B. A., and Lim, K. O. (2011). Altered functional and anatomical connectivity in schizophrenia. *Schizophrenia bulletin*, 37(3):640–650.

Cardoso, J.-F. and Souloumiac, A. (1993). Blind beamforming for non-gaussian signals. In *IEE Proceedings F-Radar and Signal Processing*, volume 140, pages 362–370. IET.

Cavanna, A. E. and Trimble, M. R. (2006). The precuneus: a review of its functional anatomy and behavioural correlates. *Brain*, 129(3):564–583.

Chang, C. and Glover, G. H. (2009). Relationship between respiration, end-tidal co 2, and bold signals in resting-state fmri. *Neuroimage*, 47(4):1381–1393.

Chang, C. and Glover, G. H. (2010). Time–frequency dynamics of resting-state brain connectivity measured with fmri. *Neuroimage*, 50(1):81–98.

Chen, J., Calhoun, V. D., Pearlson, G. D., Ehrlich, S., Turner, J. A., Ho, B.-C., Wassink, T. H., Michael, A. M., and Liu, J. (2012). Multifaceted genomic risk for brain function in schizophrenia. *NeuroImage*, 61(4):866–875.

Chepenik, L. G., Raffo, M., Hampson, M., Lacadie, C., Wang, F., Jones, M. M., Pittman, B., Skudlarski, P., and Blumberg, H. P. (2010). Functional connectivity between ventral prefrontal cortex and amygdala at low frequency in the resting state in bipolar disorder. *Psychiatry Research: Neuroimaging*, 182(3):207–210.

Clos, M., Langner, R., Meyer, M., Oechslin, M. S., Zilles, K., and Eickhoff, S. B. (2014). Effects of prior information on decoding degraded speech: an fmri study. *Human brain mapping*, 35(1):61–74.

Cole, D. M., Smith, S. M., and Beckmann, C. F. (2010). Advances and pitfalls in the analysis and interpretation of resting-state fmri data. *Frontiers in systems neuroscience*, 4:8.

Collin, G., Pol, H. E. H., Haijma, S. V., Cahn, W., Kahn, R. S., and van den Heuvel, M. P. (2011). Impaired cerebellar functional connectivity in schizophrenia patients and their healthy siblings. *Magnetic resonance imaging of disturbed brain connectivity in psychiatric illness*, page 48.

Constantino, J. N., Davis, S. A., Todd, R. D., Schindler, M. K., Gross, M. M., Brophy, S. L., Metzger, L. M., Shoushtari, C. S., Splinter, R., and Reich, W. (2003). Validation of a brief quantitative measure of autistic traits: comparison of the social responsiveness scale with the autism diagnostic interview-revised. *Journal of autism and developmental disorders*, 33(4):427–433.

Constantino, J. N. and Todd, R. D. (2003). Autistic traits in the general population: a twin study. *Archives of general psychiatry*, 60(5):524–530.

Constantino, L. Q., Supekar, K., and Menon, V. (2013). Social responsiveness scale (srs). *Front. Hum. Neurosci.*, 7(458):23–33.

Cordes, D., Haughton, V., Carew, J. D., Arfanakis, K., and Maravilla, K. (2002). Hierarchical clustering to measure connectivity in fmri resting-state data. *Magnetic resonance imaging*, 20(4):305–317.

Cordes, D., Haughton, V. M., Arfanakis, K., Carew, J. D., Turski, P. A., Moritz, C. H., Quigley, M. A., and Meyerand, M. E. (2001). Frequencies contributing to functional connectivity in the cerebral cortex in âĂIJresting-stateâĂİ data. *American Journal of Neuroradiology*, 22(7):1326–1333.

Correa, N., Adalı, T., and Calhoun, V. D. (2007). Performance of blind source separation algorithms for fmri analysis using a group ica method. *Magnetic resonance imaging*, 25(5):684–694.

Costafreda, S. G., Fu, C. H., Picchioni, M., Toulopoulou, T., McDonald, C., Kravariti, E., Walshe, M., Prata, D., Murray, R. M., and McGuire, P. K. (2011). Pattern of neural responses to verbal fluency shows diagnostic specificity for schizophrenia and bipolar disorder. *BMC psychiatry*, 11(1):1.

Cox, R. W. (1996). Afni: software for analysis and visualization of functional magnetic resonance neuroimages. *Computers and Biomedical research*, 29(3):162–173.

Cribben, I., Haraldsdottir, R., Atlas, L. Y., Wager, T. D., and Lindquist, M. A. (2012). Dynamic connectivity regression: determining state-related changes in brain connectivity. *Neuroimage*, 61(4):907–920.

Damaraju, E., Allen, E., Belger, A., Ford, J., McEwen, S., Mathalon, D., Mueller, B., Pearlson, G., Potkin, S., Preda, A., et al. (2014a). Dynamic functional connectivity analysis reveals transient states of dysconnectivity in schizophrenia. *NeuroImage: Clinical*, 5:298–308.

Damaraju, E., Caprihan, A., Lowe, J., Allen, E. A., Calhoun, V. D., and Phillips, J. (2014b). Functional connectivity in the developing brain: a longitudinal study from 4 to 9months of age. *NeuroImage*, 84:169–180.

Damoiseaux, J., Rombouts, S., Barkhof, F., Scheltens, P., Stam, C., Smith, S. M., and Beckmann, C. (2006). Consistent resting-state networks across healthy subjects. *Proceedings of the national academy of sciences*, 103(37):13848–13853.

Di Martino, A., Fair, D. A., Kelly, C., Satterthwaite, T. D., Castellanos, F. X., Thomason, M. E., Craddock, R. C., Luna, B., Leventhal, B. L., Zuo, X.-N., et al. (2014). Unraveling the miswired connectome: a developmental perspective. *Neuron*, 83(6):1335–1353.

Di Martino, A., Ross, K., Uddin, L. Q., Sklar, A. B., Castellanos, F. X., and Milham, M. P. (2009a). Functional brain correlates of social and nonsocial processes in autism spectrum disorders: an activation likelihood estimation meta-analysis. *Biological psychiatry*, 65(1):63–74.

Di Martino, A., Shehzad, Z., Kelly, C., Roy, A. K., Gee, D. G., Uddin, L. Q., Gotimer, K., Klein, D. F., Castellanos, F. X., and Milham, M. P. (2009b). Relationship between cingulo-insular functional connectivity and autistic traits in neurotypical adults. *American Journal of Psychiatry*, 166(8):891–899.

Dosenbach, N. U., Nardos, B., Cohen, A. L., Fair, D. A., Power, J. D., Church, J. A., Nelson, S. M., Wig, G. S., Vogel, A. C., Lessov-Schlaggar, C. N., et al. (2010). Prediction of individual brain maturity using fmri. *Science*, 329(5997):1358–1361.

Erhardt, E. B., Allen, E. A., Damaraju, E., and Calhoun, V. D. (2011a). On network derivation, classification, and visualization: a response to habeck and moeller. *Brain connectivity*, 1(2):105–110.

Erhardt, E. B., Rachakonda, S., Bedrick, E. J., Allen, E. A., Adali, T., and Calhoun, V. D. (2011b). Comparison of multi-subject ica methods for analysis of fmri data. *Human brain mapping*, 32(12):2075–2095.

Fair, D. A., Cohen, A. L., Power, J. D., Dosenbach, N. U., Church, J. A., Miezin, F. M., Schlaggar, B. L., and Petersen, S. E. (2009). Functional brain networks

develop from a âĂIJlocal to distributedâĂİ organization. *PLoS comput biol*, 5(5):e1000381.

Fair, D. A., Dosenbach, N. U., Church, J. A., Cohen, A. L., Brahmbhatt, S., Miezin, F. M., Barch, D. M., Raichle, M. E., Petersen, S. E., and Schlaggar, B. L. (2007). Development of distinct control networks through segregation and integration. *Proceedings of the National Academy of Sciences*, 104(33):13507–13512.

Ferreira, L. K., Diniz, B. S., Forlenza, O. V., Busatto, G. F., and Zanetti, M. V. (2011). Neurostructural predictors of alzheimer's disease: a meta-analysis of vbm studies. *Neurobiology of aging*, 32(10):1733–1741.

First, M. B., Gibbon, M., Spitzer, R. L., and Benjamin, L. S. (1997). *User's guide for the structured clinical interview for DSM-IV axis II personality disorders: SCID-II*. American Psychiatric Pub.

Ford, J., Shen, L., Makedon, F., Flashman, L. A., and Saykin, A. J. (2002a). A combined structural-functional classification of schizophrenia using hippocampal volume plus fmri activation. In *Engineering in Medicine and Biology, 2002. 24th Annual Conference and the Annual Fall Meeting of the Biomedical Engineering Society EMBS/BMES Conference, 2002. Proceedings of the Second Joint*, volume 1, pages 48–49. IEEE.

Ford, J. M., Mathalon, D. H., Whitfield, S., Faustman, W. O., and Roth, W. T. (2002b). Reduced communication between frontal and temporal lobes during talking in schizophrenia. *Biological psychiatry*, 51(6):485–492.

Fox, M. D. and Greicius, M. (2010). Clinical applications of resting state functional connectivity. *Frontiers in systems neuroscience*, 4:19.

Fox, M. D. and Raichle, M. E. (2007). Spontaneous fluctuations in brain activity observed with functional magnetic resonance imaging. *Nature Reviews Neuroscience*, 8(9):700–711.

Franco, A. R., Pritchard, A., Calhoun, V. D., and Mayer, A. R. (2009). Interrater and intermethod reliability of default mode network selection. *Human brain mapping*, 30(7):2293–2303.

Fransson, P., Skiöld, B., Horsch, S., Nordell, A., Blennow, M., Lagercrantz, H., and Åden, U. (2007). Resting-state networks in the infant brain. *Proceedings of the National Academy of Sciences*, 104(39):15531–15536.

Freire, L. and Mangin, J.-F. (2001). Motion correction algorithms may create spurious brain activations in the absence of subject motion. *NeuroImage*, 14(3):709–722.

Freire, L., Roche, A., and Mangin, J.-F. (2002). What is the best similarity measure for motion correction in fmri time series? *IEEE transactions on medical imaging*, 21(5):470–484.

Friedman, J., Hastie, T., and Tibshirani, R. (2008). Sparse inverse covariance estimation with the graphical lasso. *Biostatistics*, 9(3):432–441.

Friedman, L. and Glover, G. H. (2006). Report on a multicenter fmri quality assurance protocol. *Journal of Magnetic Resonance Imaging*, 23(6):827–839.

Friston, K., Frith, C., Liddle, P., and Frackowiak, R. (1993). Functional connectivity: the principal-component analysis of large (pet) data sets. *Journal of Cerebral Blood Flow & Metabolism*, 13(1):5–14.

Friston, K. J. (2002). Dysfunctional connectivity in schizophrenia. *World Psychiatry*, 1(2):66–71.

Friston, K. J. (2011). Functional and effective connectivity: a review. *Brain connectivity*, 1(1):13–36.

Friston, K. J. and Frith, C. D. (1995). Schizophrenia: a disconnection syndrome. *Clin Neurosci*, 3(2):89–97.

Fukunaga, M., Horovitz, S. G., van Gelderen, P., de Zwart, J. A., Jansma, J. M., Ikonomidou, V. N., Chu, R., Deckers, R. H., Leopold, D. A., and Duyn, J. H. (2006). Large-amplitude, spatially correlated fluctuations in bold fmri signals during extended rest and early sleep stages. *Magnetic resonance imaging*, 24(8):979–992.

Fusar-Poli, P., Borgwardt, S., Crescini, A., Deste, G., Kempton, M. J., Lawrie, S., Mc Guire, P., and Sacchetti, E. (2011). Neuroanatomy of vulnerability to psychosis: a voxel-based meta-analysis. *Neuroscience & Biobehavioral Reviews*, 35(5):1175–1185.

Gao, W., Gilmore, J. H., Giovanello, K. S., Smith, J. K., Shen, D., Zhu, H., and Lin, W. (2011). Temporal and spatial evolution of brain network topology during the first two years of life. *PloS one*, 6(9):e25278.

Garrity, A. G., Pearlson, G. D., McKiernan, K., Lloyd, D., Kiehl, K. A., and Calhoun, V. D. (2007). Aberrant âĂIJdefault modeâĂİ functional connectivity in schizophrenia. *American journal of psychiatry*, 164(3):450–457.

Georgiev, P. and Cichocki, A. (2001). Blind source separation via symmetric eigenvalue decomposition. In *Signal Processing and its Applications, Sixth International, Symposium on. 2001*, volume 1, pages 17–20. IEEE.

Geschwind, D. H. and Levitt, P. (2007). Autism spectrum disorders: developmental disconnection syndromes. *Current opinion in neurobiology*, 17(1):103–111.

Gibbs, R. A., Belmont, J. W., Hardenbol, P., Willis, T. D., Yu, F., Yang, H., Ch'ang, L.-Y., Huang, W., Liu, B., Shen, Y., et al. (2003). The international hapmap project. *Nature*, 426(6968):789–796.

Gilbert, S. J., Spengler, S., Simons, J. S., Steele, J. D., Lawrie, S. M., Frith, C. D., and Burgess, P. W. (2006). Functional specialization within rostral prefrontal cortex (area 10): a meta-analysis. *Journal of cognitive neuroscience*, 18(6):932–948.

Gonzalo, D., Shallice, T., and Dolan, R. (2000). Brain activity during memory encoding: the influence of imagery and semantic relatedness. *NeuroImage*, 11(5):S389.

Greicius, M. (2008). Resting-state functional connectivity in neuropsychiatric disorders. *Current opinion in neurology*, 21(4):424–430.

Greicius, M. D., Krasnow, B., Reiss, A. L., and Menon, V. (2003). Functional connectivity in the resting brain: a network analysis of the default mode hypothesis. *Proceedings of the National Academy of Sciences*, 100(1):253–258.

Greicius, M. D., Srivastava, G., Reiss, A. L., and Menon, V. (2004). Default-mode network activity distinguishes alzheimer's disease from healthy aging: evidence from functional mri. *Proceedings of the National Academy of Sciences of the United States of America*, 101(13):4637–4642.

Hall, D. A., Fussell, C., and Summerfield, A. Q. (2005). Reading fluent speech from talking faces: typical brain networks and individual differences. *Journal of Cognitive Neuroscience*, 17(6):939–953.

Handwerker, D. A., Roopchansingh, V., Gonzalez-Castillo, J., and Bandettini, P. A. (2012). Periodic changes in fmri connectivity. *Neuroimage*, 63(3):1712–1719.

Harrison, B. J., Pujol, J., López-Solà, M., Hernández-Ribas, R., Deus, J., Ortiz, H., Soriano-Mas, C., Yücel, M., Pantelis, C., and Cardoner, N. (2008). Consistency and functional specialization in the default mode brain network. *Proceedings of the National Academy of Sciences*, 105(28):9781–9786.

Hasson, U., Avidan, G., Gelbard, H., Vallines, I., Harel, M., Minshew, N., and Behrmann, M. (2009). Shared and idiosyncratic cortical activation patterns in autism revealed under continuous real-life viewing conditions. *Autism Research*, 2(4):220–231.

Heinrichs, R. W. and Zakzanis, K. K. (1998). Neurocognitive deficit in schizophrenia: a quantitative review of the evidence. *Neuropsychology*, 12(3):426.

Hernandez, L. M., Rudie, J. D., Green, S. A., Bookheimer, S., and Dapretto, M. (2015). Neural signatures of autism spectrum disorders: insights into brain network dynamics. *Neuropsychopharmacology*, 40(1):171–189.

Himberg, J. and Hyvarinen, A. (2003). Icasso: software for investigating the reliability of ica estimates by clustering and visualization. In *Neural Networks for Signal Processing, 2003. NNSP'03. 2003 IEEE 13th Workshop on*, pages 259–268. IEEE.

Himberg, J., Hyvärinen, A., and Esposito, F. (2004). Validating the independent components of neuroimaging time series via clustering and visualization. *Neuroimage*, 22(3):1214–1222.

Hoffman, R. E., Fernandez, T., Pittman, B., and Hampson, M. (2011). Elevated functional connectivity along a corticostriatal loop and the mechanism of auditory/verbal hallucinations in patients with schizophrenia. *Biological psychiatry*, 69(5):407–414.

Hoffman, R. E. and Hampson, M. (2012). Functional connectivity studies of patients with auditory verbal hallucinations. *Front. Hum. Neurosci*, 6(6).

Honey, G. D., Pomarol-Clotet, E., Corlett, P. R., Honey, R. A., Mckenna, P. J., Bullmore, E. T., and Fletcher, P. C. (2005). Functional dysconnectivity in schizophrenia associated with attentional modulation of motor function. *Brain*, 128(11):2597–2611.

Huang, X.-Q., Lui, S., Deng, W., Chan, R. C., Wu, Q.-Z., Jiang, L.-J., Zhang, J.-R., Jia, Z.-Y., Li, X.-L., Li, F., et al. (2010). Localization of cerebral functional deficits in treatment-naive, first-episode schizophrenia using resting-state fmri. *Neuroimage*, 49(4):2901–2906.

Hutchison, R. M. and Morton, J. B. (2015). Tracking the brain's functional coupling dynamics over development. *The Journal of Neuroscience*, 35(17):6849–6859.

Hutchison, R. M., Womelsdorf, T., Allen, E. A., Bandettini, P. A., Calhoun, V. D., Corbetta, M., Della Penna, S., Duyn, J. H., Glover, G. H., Gonzalez-Castillo, J., et al. (2013a). Dynamic functional connectivity: promise, issues, and interpretations. *Neuroimage*, 80:360–378.

Hutchison, R. M., Womelsdorf, T., Gati, J. S., Everling, S., and Menon, R. S. (2013b). Resting-state networks show dynamic functional connectivity in awake humans and anesthetized macaques. *Human brain mapping*, 34(9):2154–2177.

Hyvärinen, A. and Oja, E. (1997). A fast fixed-point algorithm for independent component analysis. *Neural computation*, 9(7):1483–1492.

Hyvärinen, A. and Oja, E. (2000). Independent component analysis: algorithms and applications. *Neural networks*, 13(4):411–430.

Jaddoe, V. W., van Duijn, C. M., Franco, O. H., van der Heijden, A. J., van IIzendoorn, M. H., de Jongste, J. C., van der Lugt, A., Mackenbach, J. P., Moll, H. A., Raat, H., et al. (2012). The generation r study: design and cohort update 2012. *European journal of epidemiology*, 27(9):739–756.

Jafri, M. J., Pearlson, G. D., Stevens, M., and Calhoun, V. D. (2008). A method for functional network connectivity among spatially independent resting-state components in schizophrenia. *Neuroimage*, 39(4):1666–1681.

Jagannathan, K., Calhoun, V. D., Gelernter, J., Stevens, M. C., Liu, J., Bolognani, F., Windemuth, A., Ruaño, G., Assaf, M., and Pearlson, G. D. (2010). Genetic associations of brain structural networks in schizophrenia: a preliminary study. *Biological psychiatry*, 68(7):657–666.

Jamadar, S., Powers, N., Meda, S., Gelernter, J., Gruen, J., and Pearlson, G. (2011). Genetic influences of cortical gray matter in language-related regions in healthy controls and schizophrenia. *Schizophrenia research*, 129(2):141–148.

Jann, K., Dierks, T., Boesch, C., Kottlow, M., Strik, W., and Koenig, T. (2009). Bold correlates of eeg alpha phase-locking and the fmri default mode network. *Neuroimage*, 45(3):903–916.

Jeong, B., Wible, C. G., Hashimoto, R.-I., and Kubicki, M. (2009). Functional and anatomical connectivity abnormalities in left inferior frontal gyrus in schizophrenia. *Human brain mapping*, 30(12):4138–4151.

Johnstone, E. C., Owens, D., Crow, T. J., Frith, C., Alexandropolis, K., Bydder, G., and Colter, N. (1989). Temporal lobe structure as determined by nuclear magnetic resonance in schizophrenia and bipolar affective disorder. *Journal of Neurology, Neurosurgery & Psychiatry*, 52(6):736–741.

Jung, M., Kosaka, H., Saito, D. N., Ishitobi, M., Morita, T., Inohara, K., Asano, M., Arai, S., Munesue, T., Tomoda, A., et al. (2014). Default mode network in young male adults with autism spectrum disorder: relationship with autism spectrum traits. *Molecular autism*, 5(1):1.

Kandel, E. R., Schwartz, J. H., Jessell, T. M., Siegelbaum, S. A., and Hudspeth, A. (2000). *Principles of neural science*, volume 4. McGraw-hill New York.

Kennedy, D. P., Redcay, E., and Courchesne, E. (2006). Failing to deactivate: resting functional abnormalities in autism. *Proceedings of the National Academy of Sciences*, 103(21):8275–8280.

Keshavan, M. S., Clementz, B. A., Pearlson, G. D., Sweeney, J. A., and Tamminga, C. A. (2013). Reimagining psychoses: an agnostic approach to diagnosis. *Schizophrenia research*, 146(1):10–16.

Khadka, S., Meda, S. A., Stevens, M. C., Glahn, D. C., Calhoun, V. D., Sweeney, J. A., Tamminga, C. A., Keshavan, M. S., OâĂŹNeil, K., Schretlen, D., et al. (2013). Is aberrant functional connectivity a psychosis endophenotype? a resting state functional magnetic resonance imaging study. *Biological psychiatry*, 74(6):458–466.

Kim, D. I., Manoach, D. S., Mathalon, D. H., Turner, J. A., Mannell, M., Brown, G. G., Ford, J. M., Gollub, R. L., White, T., Wible, C., et al. (2009). Dysregulation of working memory and default-mode networks in schizophrenia using

independent component analysis, an fbirn and mcic study. *Human brain mapping*, 30(11):3795–3811.

Kiviniemi, V., Starck, T., Remes, J., Long, X., Nikkinen, J., Haapea, M., Veijola, J., Moilanen, I., Isohanni, M., Zang, Y.-F., et al. (2009). Functional segmentation of the brain cortex using high model order group pica. *Human brain mapping*, 30(12):3865–3886.

Kodinariya, T. M. and Makwana, P. R. (2013). Review on determining number of cluster in k-means clustering. *International Journal*, 1(6):90–95.

Kubicki, M., McCarley, R., Westin, C.-F., Park, H.-J., Maier, S., Kikinis, R., Jolesz, F. A., and Shenton, M. E. (2007). A review of diffusion tensor imaging studies in schizophrenia. *Journal of psychiatric research*, 41(1):15–30.

Laird, A. R., Eickhoff, S. B., Li, K., Robin, D. A., Glahn, D. C., and Fox, P. T. (2009). Investigating the functional heterogeneity of the default mode network using coordinate-based meta-analytic modeling. *The Journal of Neuroscience*, 29(46):14496–14505.

Langen, C. D., White, T., Ikram, M. A., Vernooij, M. W., and Niessen, W. J. (2015). Integrated analysis and visualization of group differences in structural and functional brain connectivity: Applications in typical ageing and schizophrenia. *PloS one*, 10(9):e0137484.

Larson-Prior, L. J., Power, J. D., Vincent, J. L., Nolan, T. S., Coalson, R. S., Zempel, J., Snyder, A. Z., Schlaggar, B. L., Raichle, M. E., and Petersen, S. E. (2011). Modulation of the brain's functional network architecture in the transition from wake to sleep. *Progress in brain research*, 193.

Lenroot, R. K. and Giedd, J. N. (2006). Brain development in children and adolescents: insights from anatomical magnetic resonance imaging. *Neuroscience & Biobehavioral Reviews*, 30(6):718–729.

Liu, J. and Calhoun, V. (2007). Parallel independent component analysis for multimodal analysis: application to fmri and eeg data. In *2007 4th IEEE International Symposium on Biomedical Imaging: From Nano to Macro*, pages 1028–1031. IEEE.

Liu, J. and Calhoun, V. D. (2000). A review of multivariate analyses in imaging genetics.

Liu, J., Pearlson, G., Windemuth, A., Ruano, G., Perrone-Bizzozero, N. I., and Calhoun, V. (2009). Combining fmri and snp data to investigate connections between brain function and genetics using parallel ica. *Human brain mapping*, 30(1):241–255.

Lohmann, G., Margulies, D. S., Horstmann, A., Pleger, B., Lepsien, J., Goldhahn, D., Schloegl, H., Stumvoll, M., Villringer, A., and Turner, R. (2010). Eigenvector centrality mapping for analyzing connectivity patterns in fmri data of the human brain. *PloS one*, 5(4):e10232.

Lui, S., Li, T., Deng, W., Jiang, L., Wu, Q., Tang, H., Yue, Q., Huang, X., Chan, R. C., Collier, D. A., et al. (2010). Short-term effects of antipsychotic treatment on cerebral function in drug-naive first-episode schizophrenia revealed by âĂIJresting stateâĂİ functional magnetic resonance imaging. *Archives of general psychiatry*, 67(8):783–792.

Ma, S., Calhoun, V. D., Phlypo, R., and Adalı, T. (2014). Dynamic changes of spatial functional network connectivity in healthy individuals and schizophrenia patients using independent vector analysis. *Neuroimage*, 90:196–206.

Makeig, S., Debener, S., Onton, J., and Delorme, A. (2004). Mining event-related brain dynamics. *Trends in cognitive sciences*, 8(5):204–210.

McKeown, M. J., Makeig, S., Brown, G. G., Jung, T.-P., Kindermann, S. S., Bell, A. J., and Sejnowski, T. J. (1997). Analysis of fmri data by blind separation into independent spatial components. Technical report, DTIC Document.

McKeown, M. J., Varadarajan, V., Huettel, S., and McCarthy, G. (2002). Deterministic and stochastic features of fmri data: implications for analysis of event-related experiments. *Journal of neuroscience methods*, 118(2):103–113.

Meda, S. A., Gill, A., Stevens, M. C., Lorenzoni, R. P., Glahn, D. C., Calhoun, V. D., Sweeney, J. A., Tamminga, C. A., Keshavan, M. S., Thaker, G., et al. (2012). Differences in resting-state functional magnetic resonance imaging functional network connectivity between schizophrenia and psychotic bipolar probands and their unaffected first-degree relatives. *Biological psychiatry*, 71(10):881–889.

Meda, S. A., Jagannathan, K., Gelernter, J., Calhoun, V. D., Liu, J., Stevens, M. C., and Pearlson, G. D. (2010). A pilot multivariate parallel ica study to investigate differential linkage between neural networks and genetic profiles in schizophrenia. *Neuroimage*, 53(3):1007–1015.

Meyer, P. E. and Bontempi, G. (2006). On the use of variable complementarity for feature selection in cancer classification. In *Workshops on Applications of Evolutionary Computation*, pages 91–102. Springer.

Meyer-Lindenberg, A., Poline, J.-B., Kohn, P. D., Holt, J. L., Egan, M. F., Weinberger, D. R., and Berman, K. F. (2001). Evidence for abnormal cortical functional connectivity during working memory in schizophrenia. *American Journal of Psychiatry*, 158(11):1809–1817.

Meyer-Lindenberg, A. and Weinberger, D. R. (2006). Intermediate phenotypes and genetic mechanisms of psychiatric disorders. *Nature Reviews Neuroscience*, 7(10):818–827.

Minzenberg, M. J., Laird, A. R., Thelen, S., Carter, C. S., and Glahn, D. C. (2009). Meta-analysis of 41 functional neuroimaging studies of executive function in schizophrenia. *Archives of general psychiatry*, 66(8):811–822.

Mohamed, S., Paulsen, J. S., O'Leary, D., Arndt, S., and Andreasen, N. (1999). Generalized cognitive deficits in schizophrenia: a study of first-episode patients. *Archives of General Psychiatry*, 56(8):749–754.

Müller, V. I., Cieslik, E. C., Laird, A. R., Fox, P. T., and Eickhoff, S. B. (2013). Dysregulated left inferior parietal activity in schizophrenia and depression: functional connectivity and characterization.

Musso, F., Brinkmeyer, J., Mobascher, A., Warbrick, T., and Winterer, G. (2010). Spontaneous brain activity and eeg microstates. a novel eeg/fmri analysis approach to explore resting-state networks. *Neuroimage*, 52(4):1149–1161.

Norman, K. A., Polyn, S. M., Detre, G. J., and Haxby, J. V. (2006). Beyond mind-reading: multi-voxel pattern analysis of fmri data. *Trends in cognitive sciences*, 10(9):424–430.

Ogawa, S., Lee, T.-M., Kay, A. R., and Tank, D. W. (1990a). Brain magnetic resonance imaging with contrast dependent on blood oxygenation. *Proceedings of the National Academy of Sciences*, 87(24):9868–9872.

Ogawa, S., Lee, T.-M., Nayak, A. S., and Glynn, P. (1990b). Oxygenation-sensitive contrast in magnetic resonance image of rodent brain at high magnetic fields. *Magnetic resonance in medicine*, 14(1):68–78.

Ogawa, S., Menon, R., Tank, D., Kim, S., Merkle, H., Ellermann, J., and Ugurbil, K. (1993). Functional brain mapping by blood oxygenation level-dependent contrast magnetic resonance imaging. a comparison of signal characteristics with a biophysical model. *Biophysical journal*, 64(3):803.

Öngür, D., Lundy, M., Greenhouse, I., Shinn, A. K., Menon, V., Cohen, B. M., and Renshaw, P. F. (2010). Default mode network abnormalities in bipolar disorder and schizophrenia. *Psychiatry Research: Neuroimaging*, 183(1):59–68.

Park, I. H., Kim, J.-J., Chun, J., Jung, Y. C., Seok, J. H., Park, H.-J., and Lee, J. D. (2009). Medial prefrontal default-mode hypoactivity affecting trait physical anhedonia in schizophrenia. *Psychiatry Research: Neuroimaging*, 171(3):155–165.

Pearlson, G. D. (1997). Superior temporal gyrus and planum temporale in schizophrenia: a selective review. *Progress in Neuro-Psychopharmacology and Biological Psychiatry*, 21(8):1203–1229.

Pomarol-Clotet, E., Canales-Rodriguez, E. J., Salvador, R., Sarró, S., Gomar, J. J., Vila, F., Ortiz-Gil, J., Iturria-Medina, Y., Capdevila, A., and McKenna, P. J. (2010). Medial prefrontal cortex pathology in schizophrenia as revealed by

convergent findings from multimodal imaging. *Molecular psychiatry*, 15(8):823–830.

Power, J. D., Barnes, K. A., Snyder, A. Z., Schlaggar, B. L., and Petersen, S. E. (2012). Spurious but systematic correlations in functional connectivity mri networks arise from subject motion. *Neuroimage*, 59(3):2142–2154.

Price, C. J. (2010). The anatomy of language: a review of 100 fmri studies published in 2009. *Annals of the New York Academy of Sciences*, 1191(1):62–88.

Purcell, S., Neale, B., Todd-Brown, K., Thomas, L., Ferreira, M. A., Bender, D., Maller, J., Sklar, P., De Bakker, P. I., Daly, M. J., et al. (2007). Plink: a tool set for whole-genome association and population-based linkage analyses. *The American Journal of Human Genetics*, 81(3):559–575.

Ragland, J. D., Laird, A. R., Ranganath, C., Blumenfeld, R. S., Gonzales, S. M., and Glahn, D. C. (2009). Prefrontal activation deficits during episodic memory in schizophrenia. *American Journal of Psychiatry*, 166(8):863–874.

Rashid, B., Arbabshirani, M. R., Damaraju, E., Cetin, M. S., Miller, R., Pearlson, G. D., and Calhoun, V. D. (2015). Classification of schizophrenia and bipolar patients using static and time-varying resting-state fmri brain connectivity. In *2015 IEEE 12th International Symposium on Biomedical Imaging (ISBI)*, pages 251–254. IEEE.

Rashid, B., Arbabshirani, M. R., Damaraju, E., Cetin, M. S., Miller, R., Pearlson, G. D., and Calhoun, V. D. (2016a). Classification of schizophrenia and bipolar patients using static and dynamic resting-state fmri brain connectivity. *NeuroImage*, 134:645–657.

Rashid, B., Blanken, L., Muetzel, R., Miller, R., Damaraju, E., Arbabshirani, M., Erhardt, E., Verhulst, F., van der Lugt, A., Jaddoe, V., Tiemeier, H., White, T., and Calhoun, V. (2016b). A pediatric population-based resting state study of connectivity dynamics in typical development. In *22nd annual meeting of the Organization of Human Brain Mapping, 2016*, pages June26–30. OHBM.

Rashid, B., Chen, J., Rashid, I., Liu, Jingyu andDamaraju, E., Miller, R., and Calhoun, V. (2016c). Exploring the genetics of the dynamic functional network connectivity in schizophrenia. In *International Imaging Genetics Conference, 2016,January*, pages 26–30. UC Irvine,CA,USA.

Rashid, B., Damaraju, E., Pearlson, G. D., and Calhoun, V. D. (2014). Dynamic connectivity states estimated from resting fmri identify differences among schizophrenia, bipolar disorder, and healthy control subjects. *Frontiers in human neuroscience*, 8:897.

Repovs, G., Csernansky, J. G., and Barch, D. M. (2011). Brain network connectivity in individuals with schizophrenia and their siblings. *Biological psychiatry*, 69(10):967–973.

Robinson, S., Basso, G., Soldati, N., Sailer, U., Jovicich, J., Bruzzone, L., Kryspin-Exner, I., Bauer, H., and Moser, E. (2009). A resting state network in the motor control circuit of the basal ganglia. *BMC neuroscience*, 10(1):1.

Rose, E. J. and Donohoe, G. (2013). Brain vs behavior: an effect size comparison of neuroimaging and cognitive studies of genetic risk for schizophrenia. *Schizophrenia bulletin*, 39(3):518–526.

Rotarska-Jagiela, A., Oertel-Knoechel, V., DeMartino, F., van de Ven, V., Formisano, E., Roebroeck, A., Rami, A., Schoenmeyer, R., Haenschel, C.,

Hendler, T., et al. (2009). Anatomical brain connectivity and positive symptoms of schizophrenia: a diffusion tensor imaging study. *Psychiatry Research: Neuroimaging*, 174(1):9–16.

Rotarska-Jagiela, A., Schönmeyer, R., Oertel, V., Haenschel, C., Vogeley, K., and Linden, D. E. (2008). The corpus callosum in schizophrenia-volume and connectivity changes affect specific regions. *Neuroimage*, 39(4):1522–1532.

Roy, C. S. and Sherrington, C. S. (1890). On the regulation of the blood-supply of the brain. *The Journal of physiology*, 11(1-2):85.

Rubinov, M. and Sporns, O. (2010). Complex network measures of brain connectivity: uses and interpretations. *Neuroimage*, 52(3):1059–1069.

Rugg, M. D. and Henson, R. N. (2002). Episodic memory retrieval: an (event-related) functional neuroimaging perspective. *The cognitive neuroscience of memory encoding and retrieval*, pages 3–37.

Saad, Z. S., Reynolds, R. C., Argall, B., Japee, S., and Cox, R. W. (2004). Suma: an interface for surface-based intra-and inter-subject analysis with afni. In *Biomedical Imaging: Nano to Macro, 2004. IEEE International Symposium on*, pages 1510–1513. IEEE.

Sakoğlu, Ü., Pearlson, G. D., Kiehl, K. A., Wang, Y. M., Michael, A. M., and Calhoun, V. D. (2010). A method for evaluating dynamic functional network connectivity and task-modulation: application to schizophrenia. *Magnetic Resonance Materials in Physics, Biology and Medicine*, 23(5-6):351–366.

Salgado-Pineda, P., Fakra, E., Delaveau, P., McKenna, P., Pomarol-Clotet, E., and Blin, O. (2011). Correlated structural and functional brain abnormalities

in the default mode network in schizophrenia patients. *Schizophrenia research*, 125(2):101–109.

Sambataro, F., Blasi, G., Fazio, L., Caforio, G., Taurisano, P., Romano, R., Di Giorgio, A., Gelao, B., Bianco, L. L., Papazacharias, A., et al. (2010). Treatment with olanzapine is associated with modulation of the default mode network in patients with schizophrenia. *Neuropsychopharmacology*, 35(4):904–912.

Scharinger, C., Rabl, U., Sitte, H. H., and Pezawas, L. (2010). Imaging genetics of mood disorders. *Neuroimage*, 53(3):810–821.

Schmahmann, J. D. and Caplan, D. (2006). Cognition, emotion and the cerebellum. *Brain*, 129(2):290–292.

Shallice, T., Fletcher, P., Frith, C., Grasby, P., Frackowiak, R., and Dolan, R. (1994). Brain regions associated with acquisition and retrieval of verbal episodic memory. *Nature*, 368(6472):633–635.

Shen, H., Wang, L., Liu, Y., and Hu, D. (2010). Discriminative analysis of resting-state functional connectivity patterns of schizophrenia using low dimensional embedding of fmri. *Neuroimage*, 49(4):3110–3121.

Shenton, M. E., Dickey, C. C., Frumin, M., and McCarley, R. W. (2001). A review of mri findings in schizophrenia. *Schizophrenia research*, 49(1):1–52.

Shinkareva, S. V., Ombao, H. C., Sutton, B. P., Mohanty, A., and Miller, G. A. (2006). Classification of functional brain images with a spatio-temporal dissimilarity map. *NeuroImage*, 33(1):63–71.

Silva, R. F., Castro, E., Gupta, C. N., Cetin, M., Arbabshirani, M., Potluru, V. K., Plis, S. M., and Calhoun, V. D. (2014). The tenth annual mlsp competition:

schizophrenia classification challenge. In *2014 IEEE International Workshop on Machine Learning for Signal Processing (MLSP)*, pages 1–6. IEEE.

Simmonds, D. J., Hallquist, M. N., Asato, M., and Luna, B. (2014). Developmental stages and sex differences of white matter and behavioral development through adolescence: a longitudinal diffusion tensor imaging (dti) study. *Neuroimage*, 92:356–368.

Skudlarski, P., Jagannathan, K., Anderson, K., Stevens, M. C., Calhoun, V. D., Skudlarska, B. A., and Pearlson, G. (2010). Brain connectivity is not only lower but different in schizophrenia: a combined anatomical and functional approach. *Biological psychiatry*, 68(1):61–69.

Smith, S. M., Fox, P. T., Miller, K. L., Glahn, D. C., Fox, P. M., Mackay, C. E., Filippini, N., Watkins, K. E., Toro, R., Laird, A. R., et al. (2009). Correspondence of the brain's functional architecture during activation and rest. *Proceedings of the National Academy of Sciences*, 106(31):13040–13045.

Smith, S. M., Miller, K. L., Salimi-Khorshidi, G., Webster, M., Beckmann, C. F., Nichols, T. E., Ramsey, J. D., and Woolrich, M. W. (2011). Network modelling methods for fmri. *Neuroimage*, 54(2):875–891.

Sorg, C., Manoliu, A., Neufang, S., Myers, N., Peters, H., Schwerthöffer, D., Scherr, M., Mühlau, M., Zimmer, C., Drzezga, A., et al. (2013). Increased intrinsic brain activity in the striatum reflects symptom dimensions in schizophrenia. *Schizophrenia bulletin*, 39(2):387–395.

Sorg, C., Riedl, V., Mühlau, M., Calhoun, V. D., Eichele, T., Läer, L., Drzezga, A., Förstl, H., Kurz, A., Zimmer, C., et al. (2007). Selective changes of resting-state networks in individuals at risk for alzheimer's disease. *Proceedings of the National Academy of Sciences*, 104(47):18760–18765.

Spoletini, I., Cherubini, A., Di Paola, M., Banfi, G., Rüsch, N., Martinotti, G., Bria, P., Rubino, I. A., Siracusano, A., Caltagirone, C., et al. (2009). Reduced fronto-temporal connectivity is associated with frontal gray matter density reduction and neuropsychological deficit in schizophrenia. *Schizophrenia research*, 108(1):57–68.

Spoormaker, V. I., Schröter, M. S., Gleiser, P. M., Andrade, K. C., Dresler, M., Wehrle, R., Sämann, P. G., and Czisch, M. (2010). Development of a large-scale functional brain network during human non-rapid eye movement sleep. *The Journal of neuroscience*, 30(34):11379–11387.

Starck, T., Nikkinen, J., Rahko, J., Remes, J., Hurtig, T., Haapsamo, H., Jussila, K., Kuusikko-Gauffin, S., Mattila, M.-L., Jansson-Verkasalo, E., et al. (2013). Resting state fmri reveals a default mode dissociation between retrosplenial and medial prefrontal subnetworks in asd despite motion scrubbing.

Stigler, K. A., McDonald, B. C., Anand, A., Saykin, A. J., and McDougle, C. J. (2011). Structural and functional magnetic resonance imaging of autism spectrum disorders. *Brain research*, 1380:146–161.

Su, L., Wang, L., Shen, H., Feng, G., and Hu, D. (2013). Discriminative analysis of non-linear brain connectivity in schizophrenia: an fmri study. *Frontiers in human neuroscience*, 7:702.

Sui, J., Pearlson, G., Caprihan, A., Adali, T., Kiehl, K. A., Liu, J., Yamamoto, J., and Calhoun, V. D. (2011). Discriminating schizophrenia and bipolar disorder by fusing fmri and dti in a multimodal cca+ joint ica model. *Neuroimage*, 57(3):839–855.

Sullivan, P. F. (2010). The psychiatric gwas consortium: big science comes to psychiatry. *Neuron*, 68(2):182–186.

Sullivan, P. F., Neale, M. C., and Kendler, K. S. (2000). Genetic epidemiology of major depression: review and meta-analysis. *American Journal of Psychiatry*, 157(10):1552–1562.

Swerdlow, N. R. (2010). Integrative circuit models and their implications for the pathophysiologies and treatments of the schizophrenias. In *Behavioral Neurobiology of Schizophrenia and Its Treatment*, pages 555–583. Springer.

Tong, L., Soon, V., Huang, Y., and Liu, R. (1990). Amuse: a new blind identification algorithm. In *Circuits and Systems, 1990., IEEE International Symposium on*, pages 1784–1787. IEEE.

Tononi, G., Edelman, G. M., and Sporns, O. (1998). Complexity and coherency: integrating information in the brain. *Trends in cognitive sciences*, 2(12):474–484.

Tu, P.-C., Hsieh, J.-C., Li, C.-T., Bai, Y.-M., and Su, T.-P. (2012). Cortico-striatal disconnection within the cingulo-opercular network in schizophrenia revealed by intrinsic functional connectivity analysis: a resting fmri study. *Neuroimage*, 59(1):238–247.

Uddin, L. Q., Supekar, K., Lynch, C. J., Khouzam, A., Phillips, J., Feinstein, C., Ryali, S., and Menon, V. (2013a). Salience network–based classification

and prediction of symptom severity in children with autism. *JAMA psychiatry*, 70(8):869–879.

Uddin, L. Q., Supekar, K., and Menon, V. (2013b). Reconceptualizing functional brain connectivity in autism from a developmental perspective. *Front. Hum. Neurosci.*, 7(458):23–33.

Uhlhaas, P. J. and Singer, W. (2006). Neural synchrony in brain disorders: relevance for cognitive dysfunctions and pathophysiology. *Neuron*, 52(1):155–168.

Van Snellenberg, J. X., Torres, I. J., and Thornton, A. E. (2006). Functional neuroimaging of working memory in schizophrenia: task performance as a moderating variable. *Neuropsychology*, 20(5):497.

Varoquaux, G., Baronnet, F., Kleinschmidt, A., Fillard, P., and Thirion, B. (2010). Detection of brain functional-connectivity difference in post-stroke patients using group-level covariance modeling. In *International Conference on Medical Image Computing and Computer-Assisted Intervention*, pages 200–208. Springer.

Vincent, J., Patel, G., Fox, M., Snyder, A., Baker, J., Van Essen, D., Zempel, J., Snyder, L., Corbetta, M., and Raichle, M. (2007). Intrinsic functional architecture in the anaesthetized monkey brain. *Nature*, 447(7140):83–86.

Wang, F., Kalmar, J. H., He, Y., Jackowski, M., Chepenik, L. G., Edmiston, E. E., Tie, K., Gong, G., Shah, M. P., Jones, M., et al. (2009). Functional and structural connectivity between the perigenual anterior cingulate and amygdala in bipolar disorder. *Biological psychiatry*, 66(5):516–521.

Wang, L., Metzak, P. D., and Woodward, T. S. (2011). Aberrant connectivity during self–other source monitoring in schizophrenia. *Schizophrenia research*, 125(2):136–142.

White, T., El Marroun, H., Nijs, I., Schmidt, M., van der Lugt, A., Wielopolki, P. A., Jaddoe, V. W., Hofman, A., Krestin, G. P., Tiemeier, H., et al. (2013). Pediatric population-based neuroimaging and the generation r study: the intersection of developmental neuroscience and epidemiology. *European journal of epidemiology*, 28(1):99–111.

White, T., Muetzel, R., Schmidt, M., Langeslag, S. J., Jaddoe, V., Hofman, A., Calhoun, V. D., Verhulst, F. C., and Tiemeier, H. (2014). Time of acquisition and network stability in pediatric resting-state functional magnetic resonance imaging. *Brain connectivity*, 4(6):417–427.

Wilson, E. B. (1927). Probable inference, the law of succession, and statistical inference. *Journal of the American Statistical Association*, 22(158):209–212.

Wise, R. G., Ide, K., Poulin, M. J., and Tracey, I. (2004). Resting fluctuations in arterial carbon dioxide induce significant low frequency variations in bold signal. *Neuroimage*, 21(4):1652–1664.

Wolf, D. H., Gur, R. C., Valdez, J. N., Loughead, J., Elliott, M. A., Gur, R. E., and Ragland, J. D. (2007). Alterations of fronto-temporal connectivity during word encoding in schizophrenia. *Psychiatry Research: Neuroimaging*, 154(3):221–232.

Wu, L., Eichele, T., and Calhoun, V. D. (2010). Reactivity of hemodynamic responses and functional connectivity to different states of alpha synchrony: a concurrent eeg-fmri study. *Neuroimage*, 52(4):1252–1260.

Xiong, J., Parsons, L. M., Gao, J.-H., and Fox, P. T. (1999). Interregional connectivity to primary motor cortex revealed using mri resting state images. *Human brain mapping*, 8(2-3):151–156.

Yaesoubi, M., Allen, E. A., Miller, R. L., and Calhoun, V. D. (2015). Dynamic coherence analysis of resting fmri data to jointly capture state-based phase, frequency, and time-domain information. *NeuroImage*, 120:133–142.

Yan, C.-G., Cheung, B., Kelly, C., Colcombe, S., Craddock, R. C., Di Martino, A., Li, Q., Zuo, X.-N., Castellanos, F. X., and Milham, M. P. (2013). A comprehensive assessment of regional variation in the impact of head micromovements on functional connectomics. *Neuroimage*, 76:183–201.

Yang, H., Liu, J., Sui, J., Pearlson, G., and Calhoun, V. D. (2010). A hybrid machine learning method for fusing fmri and genetic data: combining both improves classification of schizophrenia. *Frontiers in human neuroscience*, 4:192.

Ylipaavalniemi, J. and Vigário, R. (2008). Analyzing consistency of independent components: An fmri illustration. *NeuroImage*, 39(1):169–180.

Yuan, H., Zotev, V., Phillips, R., Drevets, W. C., and Bodurka, J. (2012). Spatiotemporal dynamics of the brain at restâĂŤexploring eeg microstates as electrophysiological signatures of bold resting state networks. *Neuroimage*, 60(4):2062–2072.

Zeng, L.-L., Shen, H., Liu, L., Wang, L., Li, B., Fang, P., Zhou, Z., Li, Y., and Hu, D. (2012). Identifying major depression using whole-brain functional connectivity: a multivariate pattern analysis. *Brain*, 135(5):1498–1507.

Zhou, Y., Liang, M., Tian, L., Wang, K., Hao, Y., Liu, H., Liu, Z., and Jiang, T. (2007). Functional disintegration in paranoid schizophrenia using resting-state fmri. *Schizophrenia research*, 97(1):194–205.

Zhou, Y., Shu, N., Liu, Y., Song, M., Hao, Y., Liu, H., Yu, C., Liu, Z., and Jiang, T. (2008). Altered resting-state functional connectivity and anatomical connectivity of hippocampus in schizophrenia. *Schizophrenia research*, 100(1):120–132.

Zhu, F., Kapitan, J., Tranter, G. E., Pudney, P. D., Isaacs, N. W., Hecht, L., and Barron, L. D. (2008). Residual structure in disordered peptides and unfolded proteins from multivariate analysis and ab initio simulation of raman optical activity data. *Proteins: Structure, Function, and Bioinformatics*, 70(3):823–833.